The hERG1 PAS Domain: an Antiarrhythmic Drug Target and Master Regulator of I_{Kr}

by

Chiamaka Ugochi Ukachukwu

A dissertation submitted in partial fulfillment
of the requirements for the degree of
Doctor of Philosophy
(Pharmacology)
in the University of Michigan
2023

Doctoral Committee:

Assistant Professor David K. Jones, Chair
Professor Henry Colecraft, Columbia University
Professor Santhi Ganesh
Professor Lori Isom
Professor Leslie Satin

Chiamaka U. Ukachukwu

ugochi@umich.edu

ORCID iD: 0000-0002-7752-4123

© Chiamaka U. Ukachukwu 2023

Dedication

I dedicate this dissertation to my mother, Dr. Victoria Chikaodili Ukachukwu. Thank you for paving the way, leading by example, and being your truth. The strength, courage, and grace that you've reflected throughout your life has created an unshakeable foundation for me and generations to come. I am blessed to be your daughter and grateful for your Presence. I love you from the place where nothing exists and everything is born.

Acknowledgements

I can easily write another dissertation to thank everyone who has supported me throughout this process. First, I want to thank my mother, Dr. Victoria Ukachukwu, for normalizing (Black) excellence in our home. I recognize how special it is for a Black woman to earn a PhD in science, let alone in organic chemistry, and how fortunate I am to be raised by you! Your example created an unshakeable confidence in my ability to earn this degree. I am grateful that I was able to lean on you throughout this process and look to you as my role model. Thank you to my grandmother, for fiercely paving the way for my mother.

Thank you, Uncle Emmy. I love you more x infinity! Your Presence in my life is one of my greatest blessings. Thank you for always reminding me that I always deserve the absolute best and for rooting fiercely for me every step of the way. You are a part of my heart forever and I carry you with me always. With the greatest love, Maximus. To my sister, Nkiruka, I am so happy I get to share life with you and have you as my sister. Thank you for sharing your light and being a source of joy, laughter, and admiration. My future will always be bright with you in it.

To my Georgia Tech family – Dr. Carrie Shepler, Dr. Raquel Lieberman, and Dr. Adegboyega Oyelere – thank you for pouring into me and helping me get into graduate school! You all believed and invested in me before any institution recognized my potential and I am eternally grateful for your support. Dr. Lieberman, joining your lab was one of the best decisions I have ever made. Thank you for your advice, mentorship, and the phenomenal scientific training I received in your lab. Joining your lab helped me build a strong foundation as a research scientist and critical thinker which helped me excel in graduate school effortlessly.

Thank you to the Rackham Bridges Program in Molecular, Cellular, and Developmental Biology (MCDB) for the opportunity to earn my MS in MCDB with full funding, tuition, health insurance, and a living stipend. Student loan debt disproportionately impacts Black households, with Black women holding the highest percentage of educational loan debt. As a Black scholar with undergraduate loan debt, completing an MS without accumulating additional debt was truly lifechanging for me.

Thank you to the Chapman Empire and my MS advisor, Dr. Matthew Chapman. I am thankful to have you all as my family. Thank you to Dr. Maggie Gardner for being a phenomenal mentor, friend, and example of a fierce and brilliant scientist. You inspire me. To my MS thesis committee Dr. Ann Miller and Dr. Anuj Kumar, thank you for your guidance and ensuring I had the best possible experience in MCDB.

I found my way to Michigan Pharmacology thanks to Lisa Garber who introduced me to the Program in Biomedical Sciences (PIBS). I had no intention of pursuing a PhD in Pharmacology and I am so glad you connected me with the Department and recognized that Pharmacology would be the perfect fit for me. Thank you to Dr. Lori Isom and Dr. Donna Shewach who were enthusiastic about meeting with me to discuss the Pharmacology PhD. Even though I was not admitted the first time I applied, they continued to provide guidance when I asked for support. I will always appreciate and remember that.

Dr. Colleen Carpenter and Dr. Nnamdi Edokobi, your mentorship and friendship truly fueled me through this program. Thank you for supporting me, helping me course correct, and holding me to the highest standards. Seeing myself reflected through you encouraged me throughout my training. Colleen, I remember the first day I met you after you had served on a PIBS panel and I thought, “I want to be just like her.” Honored to be part of the PhD club with you

two now. To the Michigan Pharmacology community – my cohort, faculty mentors, and friends – thank you for creating a warm and intellectually rigorous environment. To Dr. Carole Parent, one of the most stylish and brilliant scientists I know, thank you for your support and care. Dr. Paul Jenkins, I am grateful for our many unplanned conversations and banter. Dr. Emily Jutkiewicz and Dr. Jorge A. Iñiguez-Lluhí, thank you for being incredible professors and showing unending patience and grace. Thank you for helping me with statistical analyses for my work.

Thank you to the Michigan Pharmacology DEI committee for helping plan and bring Nnamdi's brainchild, Pharmacology in Color, to life! This was the perfect way to spend my last day in the Department.

To my PhD advisor, Dr. David Jones, thank you for pouring your all into us, the lab, and your work. I appreciate your guidance and support, even when we disagreed, and the fact that you always have our best interest at heart. Thank you for pushing me to be my best, even if did so begrudgingly at times. I am a better scientist and person for completing my PhD with you and I would choose your lab every time. To the Jones Lab, I feel so lucky that I got to do exciting research in a supportive and welcoming environment. It has been an absolute joy doing the coolest science and answering exciting research questions with you all. Thank you to Dr. Eric Jiménez-Vázquez for helping me further develop my electrophysiology and patch clamp expertise. Thank you for helping me deepen my understanding of ion channel biophysics. Abhilasha Jain, thank you for your friendship and support throughout the years. You have been a pillar in my research projects, and I appreciate the time and effort you poured into supporting this work. To Dr. Francisco Sanchez-Conde and Diamond Thomas, thanks for being the best lab mates turned friends. I am grateful for sharing the late-night patching and snack parties that lasted well beyond

midnight and on the weekends with you. I hope to never do that again but will always have fond memories of sharing that space with you.

Thank you to Dr. Cherie Dotson for reminding me of my strength and spirit. Your guidance has been so transformative. I have to thank the OGPS office for the career and professional development. I secured my internship at Merck and my literal dream job at Eli Lilly thanks to the programming centered on resume editing, interview prep, etc. You deserve all of the flowers. It is one thing to complete a PhD and another task to market those skills and turn them into something fruitful. You all helped me achieve my dreams!

A special shoutout to some of the phenomenal Black women I met at Michigan: Dr. Nkemka Anyiwo, Dr. Ramona Perry, Dr. Joy Obayemi, Dr. Nathalie Momplaisir, Dr. Korie Grayson, Dr. Lydia Mensah, Ifeoluwa Owolabi, Dr. Sierra Nance, and Dr. Naomi Wilson. Thank you for lifting me up during the joyful and challenging times. Thank you for carrying me, being a safe space, reminding me to eat and drink water, laughing with me, grieving with me, celebrating with me, and of course, stunting with me. You all are my inspiration, my sisters, and I love you all dearly.

Dr. Jade Diaz, I am so proud of us for finding our way! Thank you for always being there for me, sharing my love for food, and cheering for me as if my wins are your own (they are). To the Smith family, Aisha Folkes, and Dr. Adaeze Eneli thank you for feeding me while I was dissertating. You have no idea how much I needed that support. My (legwork) family, Professor Kweku Abimbola and Dr. Adaeze Eneli, I will forever appreciate sharing our enjoyment on the dance floor. Thank you for covering me in love and support and always showing up for me, even before I know I need the support.

To my ABCJ crew, Jennifer Onyewuenyi, Alexandria Skeete, and Dr. Biola Ogunfuyi. Thank you for being a space for laughter, enjoyment, self-reflection, and spiritual growth. Y'all have carried me through so much and I thank God for your friendship.

Thank you to Randall Wilson, Moliehi Mokoroane, and Orezi Aki, my dearest friends who always show up and pour into me. To my brother, Warren Johnson, you are one of the greatest beings I know. Your friendship and family are a blessing.

To My Fulbright Noir Muvas, Desirée Daring, Hannah Menelas, and Dr. Sonita Moss, you all are the epitome of Black Girl Magic. Thank you for your continued friendship and laughter. Dr. Olugbenga Joseph, thanks for always expecting and demanding the best for and of me. Thank you for celebrating (with) me. My life is infinitely better with you in it, to be clear. I am so grateful that Fulbright connected us all.

To Ayo from Ohio, the actual GOAT (pun intended). I love you. You are one of the best things about Michigan and in my life. Dr. Oluwatobi Eboda, thank you for holding me down throughout the years. I am so grateful we got to share our MS and PhD journeys together and live abroad as international scientists. I am so proud of us for making our dreams come true!

Dr. Ijeoma Anunobi, my sis! We made it. Thank you for being the best friend and role model. Niccole Marcial, I am so grateful for your friendship. Sharing our truths and self-reflecting together is a Divine gift. I am honored to call you my friend. Dr. Shruti Patel, I am so glad we met at Merck! Thank you for being such a great friend and a kind soul. Dr. Sean Schnarr, thanks for always being there for me and answering my random questions throughout the years. I am proud of you and grateful for your friendship. We made it!

To the Enjoyment Crew and my NiteWriters family, thank you for the enjoyment and accountability. Your support was essential for me completing this degree as my full self and

chopping life well well! Dancing in the freezing cold, making s'mores around bonfires, tubing on the lake, brinners, dancing with Jael at the Do-Over, and battling at JerkxJollof™ and AfrobeatsxTrap carried me through. Thank you for the scholarship and joy. I love y'all!

To every single person who has rooted for me, cheered me on loudly or silently, thank you. I appreciate you and my gratitude is boundless. Thank you for being a part of my village.

Last but not least, I have to thank myself for showing up, doing the work, and giving my best every day. I thank myself for remembering that this degree reflects and can never define me. I am proud of myself for staying centered, being flexible, asking for help, listening to guidance, and always honoring myself. I have been pushed to grow in some of the most challenging and difficult ways and I thank God that I rose to the occasion every time and kept moving forward. This journey has shown me that I can achieve anything. Whatever comes my way, I will prevail. I am thankful for every season, lesson, win, and redirection because it helped me evolve into the best version of myself. I thank myself for committing to love myself through this journey. My younger self would be so proud of and inspired by the woman that I am today. I accomplished my dreams and then some and this is just the beginning.

Table of Contents

List of Tables

List of Figures

Abstract

The hERG1 potassium channel conducts the cardiac repolarizing current I_{Kr}. It is one of the first currents to appear in the heart and its disruption is associated with cardiac disorders. hERG1 channels comprise at least two subunits, hERG1a and hERG1b. hERG1a channels contain an N-terminal Per-Arnt-Sim (PAS) domain that interacts with the C-terminal cyclic nucleotide binding homology domain (CNBHD) to regulate channel gating. hERG1b is identical to hERG1a except for its unique N-terminus which is much shorter and has no PAS domain. Shifts in the relative abundance of hERG1a and hERG1b alter I_{Kr} gating and repolarization which modulates cardiac function. The goal of this dissertation was to identify a novel hERG1 antiarrhythmic drug target and elucidate the role of hERG1 subunit abundance in cardiac development and pathophysiology.

In Chapter 1 we tested the antiarrhythmic capacity of a single chain variable fragment antibody, scFv2.10, in a model of long QT syndrome (LQTS). scFv2.10 selectively binds the hERG1a PAS domain and disrupts its interaction with the CNBHD. This causes a two-fold increase in the time course of hERG1 deactivation, inactivation recovery, and increases hERG1 current in HEK293 cells. In human induced pluripotent stem cell-derived cardiomyocytes (hiPSC-CMs), scFv2.10 increases I_{Kr} and shortens action potential (AP) duration. We hypothesized that the hERG1 PAS domain could represent a novel therapeutic target for diseases of impaired cardiac repolarization. To test this, we recorded cardiac currents and APs from an hiPSC-CM line derived from a patient with Jervell and Lange Nielsen syndrome (JLN), a severe form of LQTS. Compared to hiPSC-CMs derived from a healthy patient, JLN hiPSC-CMs display hallmarks of

proarrhythmia including prolonged AP duration (APD), increased AP variability, and early after depolarizations (EADs). scFv2.10 expression shortened APD and reduced AP variability and the incidence of EADs in JLN hiPSC-CMs, compared to GFP controls. Thus, disabling the PAS domain may be a viable approach for treating disrupted cardiac excitability.

In Chapter 2 we investigated the role of hERG1 subunit abundance in early cardiac physiology. hERG1 variants are linked with intrauterine fetal death and sudden infant death syndrome (SIDS), yet little is known about hERG1's role in developing cardiomyocytes. We used substrate-mediated hiPSC-CM maturation model immature and matured cardiomyocytes to determine how maturation impacts hERG1 function and subunit abundance. Immature hiPSC-CMs had reduced hERG1a mRNA and protein levels and elevated hERG1b mRNA and protein levels compared to matured hiPSC-CMs. This apparent shift in subunit abundance coincided with reduced I_{Kr} density in immature hiPSC-CMs. Extracellular acidosis, which is proposed to promote SIDS, inhibits hERG1 channels and has a greater inhibitory effect on hERG1b. We hypothesized that acidosis preferentially inhibits I_{Kr} of the immature myocardium where hERG1b is upregulated, which could promote arrhythmia and SIDS. We screened the impact of extracellular acidosis on native I_{Kr} at pH 6.3 and pH 7.4. Acidic extracellular pH significantly reduced I_{Kr} magnitude in immature and matured hiPSC-CMs and the magnitude of I_{Kr} inhibition was significantly greater in immature hiPSC-CMs compared to matured hiPSC-CMs. PAS expression, which effectively converts hERG1b to hERG1a channels, reduced the magnitude of I_{Kr} inhibition. These data demonstrate that hERG1 subunit abundance modulates I_{Kr} sensitivity to acidosis and may be a contributing factor to SIDS.

Together, these findings highlight the crucial role of the PAS domain as a potential antiarrhythmic target and structural determinant for the onset of SIDS.

Chapter 1 Targeting the Voltage-Gated Potassium Channel, hERG1, to Repair Disrupted Cardiac Repolarization

Introduction

KCNH2 encodes hERG1, a voltage-gated potassium channel that is essential for healthy cardiac repolarization. hERG1 conducts I_{Kr}, which is critical for phase 3 repolarization of the cardiac action potential [1-5]. Loss-of-function *KCNH2* variants or off-target pharmacological hERG1 block that reduce or abolish I_{Kr} slow repolarization and prolong the cardiac action potential duration (APD). Consequently, disrupting hERG1 function promotes the onset of lethal arrhythmias such as *torsades de pointes*, long QT syndrome type 2 (LQTS 2), and is implicated in intrauterine fetal death, sudden infant death syndrome, and other diseases of cardiac excitability [2, 6-11].

The QT interval of a surface ECG reflects the time between ventricular depolarization and repolarization. QT prolongation reflects delayed ventricular repolarization, which is caused by ventricles taking longer to recover from excitation. The perturbation of synchronized electrical activity and ventricular function can fatally impair cardiac function. [12, 13].

Impaired cardiac repolarization is a major arrhythmogenic trigger in several disease states, including heart failure and LQTS. Thus, there is considerable interest in developing therapies to restore normal electrical excitability when repolarization is impaired. To this end, hERG1 activators are being tested for their ability to restore disrupted repolarization by increasing I_{Kr}. [14-16]. In this review, I will discuss the role of hERG1 in cardiac dysfunction, hERG1 modulators

and their challenges with off-target effects, and a new strategy for selectively targeting hERG1 to protect against arrhythmic events caused by cardiac electrical dysfunction.

The structure and composition of hERG1

hERG1 is structurally homologous to other voltage-gated potassium channels. hERG1 channels are tetrameric, where each subunit has six helical transmembrane domains termed S1 through S6. The S1-S4 helices of each subunit form a voltage sensing domain, whereas the S5 and S6 from each subunit combine to form the ion conducting pore (Figure 1.1). [17-22].

hERG1 activation is much slower than hERG1 inactivation [23]. As channels activate, they are almost immediately inactivated, such that current is largely suppressed at depolarized potentials [24]. During action potential repolarization, particularly in phase 3, hERG1 channels rapidly recovery from their inactivated state but are slow to close [23]. Thus, hERG1 channels produce a resurgent current at the tail of the action potential that drives phase 3 repolarization and protects against premature excitation [25].

At least two distinct hERG1 subunits, hERG1a and hERG1b, combine *in vivo* to conduct native I_{Kr} in cardiac tissue. hERG1a and hERG1b are produced from alternate *KCNH2* transcripts. Both subunits are identical except for their N-terminal domains [26]. The *hERG1a* transcript encodes a 398 amino acid N-terminal domain that includes a Per-Arnt-Sim (PAS) domain (residues 1-135) [17, 26, 27]. The PAS domain interacts directly with the C-terminal cyclic nucleotide binding homology domain (CNBHD) and voltage sensing domain of the neighboring subunit to regulate channel gating [28, 29]. Typically, PAS domains bind with ligands such as heme groups, flavin nucleotides, and metal ions to regulate protein function [30]. However, no such endogenous ligand has been identified for hERG1 [31].

The *hERG1b* transcript encodes a shorter and unique 36 amino acid N-terminal domain that lacks a PAS domain [26, 32]. The absence of a PAS domain in hERG1b causes a two-fold increase in the time course of activation, deactivation, and recovery from inactivation. Consequently, heteromeric hERG1a/1b channels conduct roughly twice as much current during a ventricular action potential wave form compared to homomeric hERG1a channels [33].

Off-target pharmacological hERG block is a major concern in drug development

Drug-induced QT prolongation leading to polymorphic ventricular tachycardia is a major challenge in the pharmaceutical industry. Unforeseen hERG1 liability has cost the pharmaceutical industry billions of dollars in development [34, 35]. Between 1953-2013, ~30% of drugs were with withdrawn post market due to QT prolongation and sudden cardiac death caused by off-target hERG1 block [36-39]. Consequently, the FDA mandates that all drugs be counter-screened against hERG1 prior to approval [40]. While pore block is the primary cause of drug-induced QT prolongation, disrupted hERG1 trafficking also causes QT prolongation and torsadogenic risk and is the primary cause of congenital LQTS type 2 [41].

Mechanisms of hERG1 drug block

While the mechanism of drug-binding is not always fully defined, there is consensus that most hERG1 blockers act through a state-dependent mechanism. hERG1 activation opens the intracellular pore to allow drugs to bind in the central cavity and inhibit K^+ flux [42]. hERG1 inactivation at the selectivity filter stabilizes binding of several drugs including cisapride, dofetilide, terfenadine, and astemizole [43]. Interestingly, EAG channels, which are structurally

homologous to hERG1 channels, display no sensitivity to many hERG1 blockers. EAG channels activate more quickly than hERG1 channels, display little to no inactivation, and therefore lack inward rectification that is a defining feature of hERG1 channels. Introducing a 15-residue segment of the hERG1 pore domain into EAG channels enables EAG channels to rapidly inactivate and display inward rectification. Accordingly, imparting inactivation upon EAG channels confers sensitivity to many but not all hERG1 blockers [44-46].

hERG1 mutations that disrupt inactivation also alter drug sensitivity, however, these mutations also impact other channel properties that could influence drug binding such as deactivation and permeation [47, 48]. Relatedly, previous studies show that hERG1 block can occur independent of inactivation. Thus, it cannot be concluded that inactivation alone is always required for hERG1 block [48, 49].

Several amino acid residues within the pore domain are critical for hERG1 drug block. Mutating residues in the pore domain (Phe557, Thr623, Ser624, Val625, Gly648 Tyr652, Phe656) have been repeatedly shown to significantly increase the hERG IC_{50} of many drugs such as MK-499, cisapride, and terfenadine (Figure 1.2, Figure 1.3) [42, 50-52]. Tyr652 and Phe656 form a hydrophobic binding pocket and are proposed to be primary determinants of hERG1's binding promiscuity, as other voltage-gated potassium channels have non-polar, non-aromatic residues at analogous positions (Ile/Phe) [50]. The aromaticity of Tyr652, but not the phenol group, is required for drug sensitivity and changing either residue significantly impacts hERG1 sensitivity to certain drugs [50]. As mutations in the pore domain yield different effects on hERG1 sensitivity to drug block, it is likely that there are multiple binding modes. For example, mutating Phe656 and Tyr652 differentially impact hERG1 block by propafenone and moxifloxacin. Phe656 is critical for propafenone mediated block, whereas Tyr652 is critical for moxifloxacin mediated block [53, 54].

The first cryo-EM structure of hERG1 bound to an inhibitor provided important insights about the mechanism of hERG1 block (Figure 1.2) [41]. In this study, Astemizole is bound to hERG1 in the open conformation and forms nine hydrophobic interactions with Thr623, Ser624, Val625, Gly648, Ser649, Tyr652, and Phe656, a π-π stacking interaction with Tyr652, hydrogen bonding with the carbonyl group of Ser624 and the benzimidazole ring of astemizole, and likely has electrotactic interactions between the ionizable 4-aminopiperdine group of astemizole and the presumed electronegative cavity.

The above binding model agrees with previous work proposing that Phe646, Thr623, and Tyr652 form hydrophobic, hydrogen bonding, and π-π stacking interactions with a drug's hydrophobic, carbonyl, and aromatic groups, respectively [55]. These studies also support π-π stacking with Tyr652 and not cation-π stacking as previously proposed [50, 56]. While key residues for hERG1 block have been identified, the mechanism of hERG1 block is complex.

Mechanisms of hERG1 activation

hERG1 activators are classified into four types based on their primary mode of action on hERG1 channel gating. Type 1 activators bind the intracellular side of the pore and slow deactivation. These compounds prevent closure of the intracellular activation gate formed by S6 α-helices [57]. Type 2 activators are proposed to bind the extracellular side of the selectivity filter. Type 2 activators enhance current by slowing the onset of inactivation, promoting the conducting conformation, and causing a rightward shift in the voltage dependence of inactivation. Type 3 activators bind the inner cavity and cause a leftward shift in the voltage dependence of activation. Type 4 activators increase single channel open probability without affecting voltage dependence or gating kinetics. [47, 58-60].

Proposed residues that modulate hERG1 activator-mediated channel opening include those in S1, S4, and S5-S6. Nearly all hERG1 activators interact with overlapping residues within drug-binding sites for hERG1 blockers such as Phe557, Tyr652, Phe656, and Ser624 (Figure 1.2, Figure 1.3). For example, type 2 hERG1 activators ICA-105574 and AZSMO23 both form interactions Tyr652 and Phe656. The mutation Y652A converts AZSMO-23 into a blocker but reduces hERG1 sensitivity to canonical hERG1 blockers like terfenadine and cisapride [61-64]. Readers should consult a recently published review that extensively details key residues and the mechanism of activation of hERG1 activators [65].

Current therapies for disrupted repolarization

The standard of care for LQTS management is not intended to correct the source of cardiac electrical dysfunction. For example, β-blockers remain a first line of therapy for LQTS management with the goal of reducing and/or eliminating the risk of cardiac triggers [66]. Mexiletine is an antiarrhythmic drug that is only recommended for use for life-threatening events as it has major side effects such as teratogenicity in pregnant women [67, 68]. The simplest remedy for drug induced LQTS is to stop treatment with hERG1 blocking drugs. Lifestyle changes, such as reducing rigorous physical activity, to prevent activation of the sympathetic nervous system are also encouraged [69]. If β-blockers therapy fails, implantable cardioverter defibrillators can be used to shock the heart back into a normal rhythm during arrhythmia [70].

Successes and Challenges with hERG1 activation as a therapeutic strategy for LQTS

The challenge with using hERG1 activators as a therapeutic agent stems from their tendency to exhibit off-target and proarrhythmic effects, despite their ability to shorten the QT interval and APD [71]. In guinea pigs, the hERG1 activator NS3623 reduced drug induced QT prolongation but increased heart rate that persisted throughout the study [72]. Similar effects were observed with the hERG1 activator ICA-105574 in dogs [62]. Mallotoxin, a naturally occurring hERG1 activator, induced ventricular tachycardia and fibrillation in isolated rabbit hearts [71]. Although these activators have been shown to increase I_{Kr}, the risk for potentially lethal adverse cardiac events limits their potential therapeutic benefit.

NS1643, a structural analogue of NS3623, reduced premature ventricular complexes, ectopic beats, and shortened the QT interval in a rabbit model of *torsades de pointes* induced by ventricular bradypacing with three-week atrioventricular block or acquired LQTS using the hERG1 blocker dofetilide. However, NS1643 was ineffective at high concentrations of dofetilide, likely due to reduced availability of hERG1 channels for activation [73]. A later study found that NS1643 increased ventricular fibrillation in a transgenic LQTS type 1 rabbit model despite shortening the QT interval and APD. It was proposed that NS1643 may have overcorrected the APD as the transgenic rabbit model did not display a significantly prolonged APD compared to control rabbits [15, 71].

Schewe et al. identified a negatively charged activating (NCA) pharmacophore present in some potassium channel activators that non-selectively activate hERG1, large conductance calcium activated (BK_{Ca}), and TREK two pore domain ($TREK_{2P}$), channels. Among these molecules included hERG1 activators NS3623 and PD-110857, previously classified as hERG1 selective [14]. Although not included in this study, NS1643 contains the NCA pharmacophore and

is structurally similar to NS3623. Thus, it is possible that off-target activation of additional potassium channels contributed to the arrhythmic events.

In addition to small molecule hERG1 activators, there are two natural products that activate hERG1 channels, ginsenoside RG3 and mallotoxin, isolated from the plant species *Panax ginseng* and the *Mailotus philippensis*, respectively. These natural products also display complex polypharmacology [74-76].

Lumacaftor, an FDA approved drug for the treatment of cystic fibrosis, has been shown to rescue hERG1 trafficking defective mutants to the membrane and increase I_{Kr} magnitude [16, 77]. Paradoxically, the rescue of certain hERG1 trafficking mutants by Lumacaftor caused APD prolongation due to dominant-negative effects. The mechanism of Lumacaftor is not known but is proposed to bind unfolded protein to exert its chaperone effect [78]. While there is potential for Lumacaftor to be repurposed for LQTS treatment, more studies need to be done to understand its mechanism of action and to ensure targeted hERG1 rescue will be clinically therapeutic [16].

Overall, these findings highlight the complexities of hERG1 activation and the need to explore new therapeutic approaches to selectively increase I_{Kr} [79].

Single chain variable fragment antibodies as hERG activators

To better understand hERG1 modulation, Harley et al. generated a library of single chain variable fragment (scFv) antibodies that selectively bind the hERG1 PAS domain. They identified and characterized two novel hERG1 activators, scFv2.10 and scFv2.12, that disable the PAS-CNBHD interaction by binding within the PAS-Cap (residues 1-25) and PAS globular domain (residues 26-135), respectively. Compared to scFv2.12, scFv2.10 displayed ~10-fold higher

binding affinity to the PAS domain with a K_d = 0.254 nM, but both were highly selective for hERG1 [31].

The PAS domain regulates channel gating through interactions with the cytosolic S4-S5 linker in the VSD and the CNBHD. Disrupting the PAS-CNBDH interaction alters VSD relaxation and accelerates channel closing [80]. scFv2.12 is proposed to bind to the open conformation of hERG1 and scFv2.10 is predicted to bind independent of the channel's conformation [81].

At physiological temperature, scFv2.10 and scFv2.12 caused a rightward shift in the voltage dependence of inactivation and increased hERG1 current by different molecular mechanisms. scFv2.10 slowed the onset of inactivation, whereas scFv2.12 accelerated inactivation recovery. In hiPSC-CMs, scFv2.10 and scFv2.12 increased I_{Kr} magnitude and shortened APD [31, 33].

We recently measured the antiarrhythmic capacity of scFv2.10 in a novel hiPSC-CM line derived from a patient with Jervell and Lange Nielsen syndrome (JLN). JLN syndrome is a severe form of LQTS Type 1 characterized by increased APD and incidence of both cardiac arrhythmia and sudden cardiac death [82]. Compared to hiPSC-CMs derived from a healthy genetic background, JLN hiPSC-CMs display hallmarks of proarrhythmia including AP prolongation, increased AP variability, and early after depolarizations (EADs). scFv2.10 reduced APD, AP variability, and the incidence of EADs in JLN hiPSC-CMs, compared to GFP controls (unpublished).

These data suggest that the hERG1 PAS domain could be a potential therapeutic target to treat disorders of electrical excitability. Furthermore, scFvs constitute a new class of hERG1 activators as they are the first modulators designed to enhance I_{Kr} by targeting the PAS domain.

While hERG1 activators have been primarily tested for their therapeutic effects in LQTS, they may also be useful in other diseased states that disrupt I_{Kr} such as heart failure.

Conclusion

hERG1 is a master regulator of cardiac repolarization. Genetic mutations, pharmacological inhibition, or diseased states that reduce I_{Kr} dramatically increase arrhythmogenic potential. [1, 3]. Promiscuous drug binding in hERG1's central cavity poses a major challenge in pharmaceutical development due to the risk of *torsades de pointes* and sudden cardiac death [83]. Although the mechanism of hERG1 block is not fully understood, significant progress has been made in identifying important structural determinants of hERG1 drug sensitivity [41, 83].

Challenges with selective targeting, translating therapeutic effects into *in vivo* models, and interspecies differences, make it difficult to predict how hERG1 modulators will translate clinically [15, 73, 84, 85]. To date, no hERG1 activators have advanced to preclinical development [79]. With further optimization, highly selective hERG1 activators have the potential to mitigate disrupted cardiac repolarization.

Figures

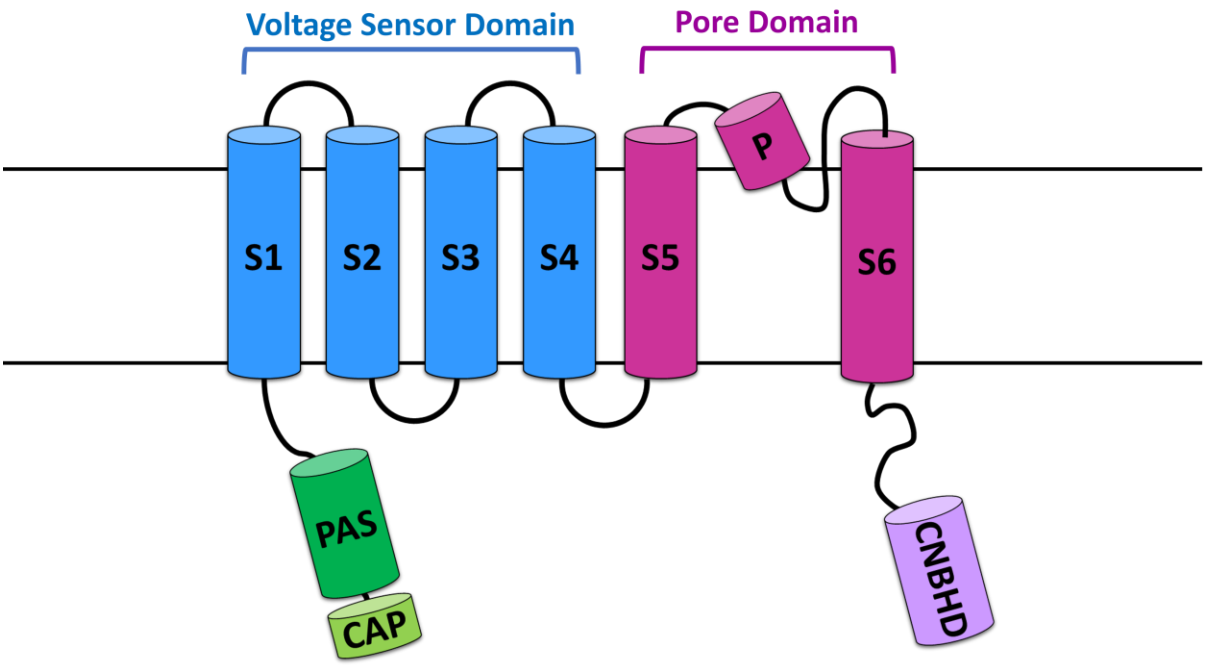

Figure 1.1 hERG1 structure

Cartoon representation of the hERG1 channel. PAS = PAS Domain. CAP = PAS-Cap region. CNBHD = cyclic nucleotide binding homology domain. S1-S6 = Segments 1- 6.

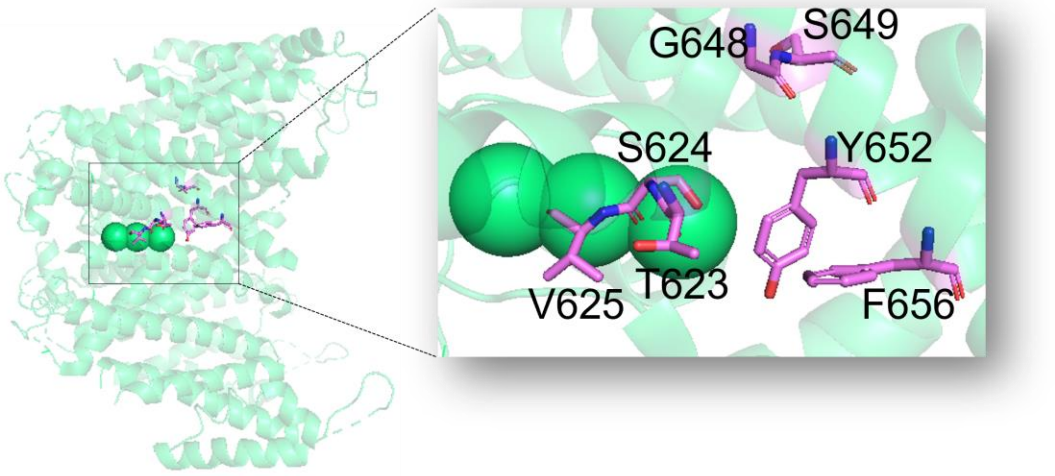

Figure 1.2 Astemizole interactions with hERG1

Cryo-EM structure of Astemizole bound to hERG1. hERG1 residues that form key interactions that facilitate Astemizole binding. Residues within the hERG1 pore domain (Thr623, Ser624, Val625, Gly648, Tyr652, Phe656) that dictate IC_{50} of hERG1 blockers are labeled (PDB ID 7CN1)[41].

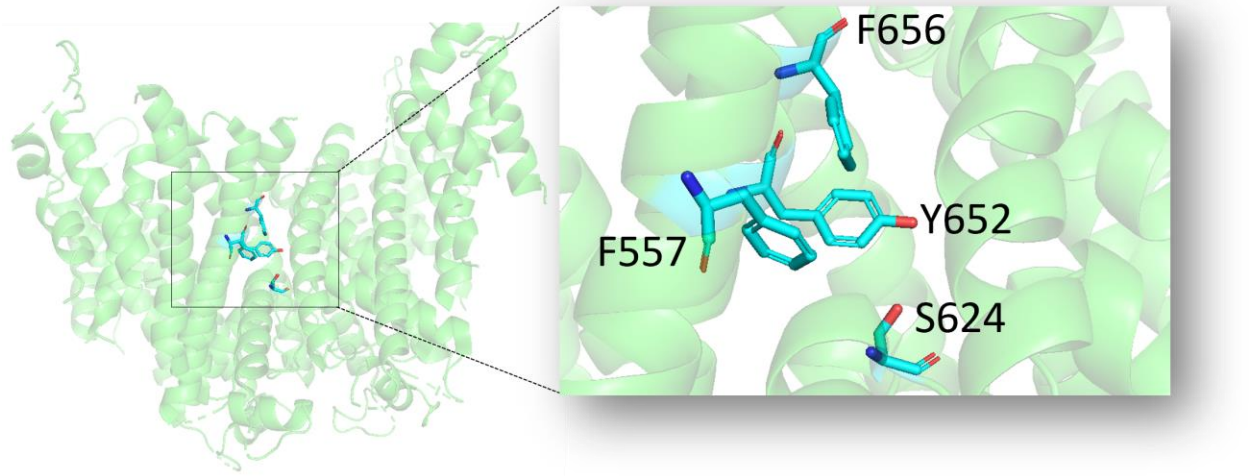

Figure 1.3 Key hERG1 residues that interact with hERG1 activators and blockers

Shared molecular determinants of between hERG1 activators and hERG1 blockers. A few overlapping residues (Phe557, Ser624, Tyr652, Phe656) within the hERG1 pore domain that are critical for both small molecule hERG1 activator and blocker mechanism of action (PDB ID 7CN1)[41]

Chapter 2 A PAS-Targeting hERG1 Activator Reduces Arrhythmic Events in JLN Patient-Derived hiPSC-CMs

Chiamaka U. Ukachukwu[1], Shreya Salawi[1], Matt Goodrich[1], Francisco Sanchez-Conde[1], Abhilasha Jain[1], Eric N. Jimenez-Vazquez[1], David K. Jones[1,2]
[1]Department of Pharmacology, University of Michigan Medical School
[2]Department of Internal Medicine, University of Michigan Medical School

Corresponding Author:
David K. Jones
Department of Pharmacology
University of Michigan Medical School
Ann Arbor, MI 48109 USA
734-936-8639
davekj@umich.edu

Author contributions

C. U. U. and D. K. J. conceptualization; C. U. U., E. N. J.-V., S. S., M. G., and A.J. formal analysis; C. U. U., E. N. J.-V., and A. J. investigation; C. U. U., E. N. J.-V., D. K. J. writing–original draft; C. U. U., E. N. J.-V., and D. K. J. writing–review & editing.

Summary

Targeting the hERG1 PAS domain with a single chain variable fragment antibody increases I_{Kr} magnitude, shortens action potential duration, and reduces early after depolarizations in stem-cell cardiomyocytes derived from a patient with Jervell and Lange Nielsen syndrome.

Abstract

The hERG1 potassium channel, encoded by *KCNH2*, conducts I_{Kr}, the rapid delayed rectifier current that regulates cardiac function and action potential (AP) morphology. Given its role mediating electrical excitability, hERG1 has emerged as a potential therapeutic target for cardiac

diseases marked by prolonged AP duration (APD). Unfortunately, many hERG1 activators display unexpected off-target and sometimes pro-arrhythmic effects that limit their therapeutic potential. A Per-Arnt-Sim (PAS) domain in the hERG1 N-terminus slows channel activation and promotes inactivation, thereby reducing I_{Kr} magnitude during phase 2 and 3 of the AP. Disrupting PAS activity increases I_{Kr} magnitude and shortens the AP in cardiomyocytes differentiated from healthy human induced pluripotent stem cells (hiPSC-CMs). We hypothesized that selectively targeting the hERG1 PAS domain could represent a therapeutic strategy to accelerate repolarization and reduce arrhythmogenic potential in a long QT syndrome (LQTS) background. To test this, we measured the antiarrhythmic capacity of a selective PAS-disabling single chain variable fragment antibody, scFv2.10, in a novel hiPSC-CM line derived from a patient with Jervell and Lange Nielsen syndrome (JLN). JLN is a severe form of LQTS type 1 characterized by prolonged APD, and increased risk of cardiac arrhythmia and sudden cardiac death. JLN hiPSC-CMs displayed prolonged APD, AP beat-to-beat variability, and incidence of early after depolarizations (EADs) compared to healthy control hiPSC-CMs. Disrupting PAS activity in JLN hiPSC-CMs with scFv2.10 increased I_{Kr}, shortened APs, and reduced both AP variability and the incidence of EADs compared to GFP-transduced JLN hiPSC-CMs. These data demonstrate that the hERG1 PAS domain could serve as a therapeutic target to treat disorders of cardiac electrical dysfunction.

Introduction

KCNH2 encodes the voltage-gated potassium channel (hERG1/Kv11.1) that conducts the rapid delayed rectifier potassium current, I_{Kr} [1, 24]. hERG1 activation is a promising avenue to treat diseases of electrical excitability [15, 86]; however current small molecule hERG1 agonists lack sufficient specificity and were shown to increase arrhythmogenesis despite increasing I_{Kr} [14, 15]. Further work is needed to create novel, targeted agonists that modulate hERG1 with a high level of specificity.

hERG1 channels in human cardiomyocytes are composed of at least two subunits, hERG1a and hERG1b, that are identical except for their N-termini [26, 33, 87-89]. The hERG1a N-terminal domain contains a Per-Arnt-Sim (PAS) domain that regulates channel gating through a direct interaction with the channel's C-terminal cyclic nucleotide binding homology domain (CNBHD) [90, 91]. hERG1b has a unique and shorter N-terminus that lacks a PAS domain. hERG1 channels containing hERG1b display faster deactivation, activation, and inactivation recovery compared to homomeric hERG1a channels [29, 33]. Consequently, heteromeric hERG1a/1b channels display larger current amplitudes than homomeric hERG1a channels [33, 92].

Previous work identified a single chain variable fragment antibody, scFv2.10 - a novel hERG1 activator that works by selectively binding the PAS domain to disrupt the PAS-CNBHD interaction [31]. In HEK293 cells stably expressing hERG1a, intracellular delivery of purified scFv2.10 accelerated the time course of deactivation, slowed the onset of inactivation, and increased hERG1 current magnitude. In cardiomyocytes differentiated from healthy human induced pluripotent stem cells (hiPSC-CMs), intracellular scFv2.10 delivery increased I_{Kr} magnitude and shortened APD [31]. Based on these findings, we hypothesized that the PAS domain could represent a novel antiarrhythmic drug target.

We tested the antiarrhythmic capacity of disrupting PAS action in a hiPSC-CM line derived from a patient with Jervell and Lange-Nielsen (JLN) syndrome. JLN is a severe form of long QT syndrome (LQTS) type 1, where loss-of-function *KCNQ1* variants abolish the slowed delayed rectifier potassium current, I_{Ks}. JLN is characterized by QT prolongation, syncope, congenital deafness, and increased risk for arrhythmia and sudden cardiac death [93]. JLN hiPSC-CMs displayed prolonged APs, and increased AP variability and incidence of early after depolarizations (EADs) compared to control hiPSC-CMs derived from a healthy patient background. Disrupting PAS activity in JLN hiPSC-CMs by overexpressing scFv2.10 increased I_{Kr}, shortened APs, and reduced both AP variability and the incidence of EADs compared to GFP-transduced controls. These data demonstrate that disabling PAS activity could be a viable strategy for enhancing hERG1 current and treating diseases of impaired cardiac repolarization.

Results

JLN hiPSC-CMs display markers of proarrhythmia.

To create an *in vitro* model of impaired cardiac repolarization, we differentiated JLN patient-derived hiPSCs into ventricular cardiomyocytes using a GiWi protocol, as described [94, 95]. We then cultured differentiated hiPSC-CMs on Matrigel-coated polydimethylsiloxane (PDMS) coverslips to promote cardiac maturation [95, 96]. JLN hiPSC-CMs carry a *KCNQ1* compound heterozygous mutation that produces a premature stop codon and an exon 3 deletion (Δ3) that were predicted to collectively abolish *KCNQ1* expression and currents. Thus, we expect JLN hiPSC-CMs to lack I_{Ks} and display proarrhythmic action potentials.

To verify the appropriate molecular and electrophysiological phenotype of JLN hiPSC-CMs, we measured ion channel-specific immunofluorescence, ionic currents, and APs from

healthy control (df19.9.11, WiCell) and JLN hiPSC-CMs (Figure 2.1, 2.3). Control hiPSC-CMs displayed robust hERG1 and KCNQ1 immunofluorescence (Figure 2.1) and conducted voltage-dependent I_{Ca} and chromonal-293b and E-4031-sensitive currents, indicative of I_{Ks} and I_{Kr}, respectively (Figure 2.1, 2.3, 2.6). JLN hiPSC-CMs displayed a hERG1 immunofluorescent signal, I_{Ca} and I_{Kr} currents, but did not display KCNQ1 immunofluorescence or I_{Ks} currents (Figure 2.1, 2.3, 2.6). Notably, JLN hiPSC-CMs showed a ~two-fold reduction in hERG1 immunofluorescent signal compared to control hiPSC-CMs, which comports with previous findings that KCNQ1 knockdown reduces hERG1 surface expression [97]. Lastly, JLN hiPSC-CMs also displayed a substantially prolonged APD at 90% repolarization (APD_{90}) (739 ± 609 ms, APD_{90} ± st dev, n=14) compared to control hiPSC-CMs (264 ± 71 ms, APD_{90} ± st dev, n=7) (Figure 2.2). These data demonstrate that the JLN patient-derived hiPSC-CMs display the appropriate markers of LQTS1.

scFv2.10 overexpression increases I_{Kr} magnitude in JLN hiPSC-CMs.

Deactivation is a reliable proxy of PAS activity in hERG1a, where accelerated correlates with decreased or impaired PAS action [98]. Purified scFv2.10 delivered through the recording pipette accelerates hERG1 deactivation, indicating that scFv2.10 is properly folded and bind to the hERG1a PAS domain [31]. To confirm that lentiviral scFv2.10 expression can generate sufficient levels of active scFv2.10 polypeptide to modulate hERG1 gating, we measured hERG1 current deactivation from HEK293 cells stably expressing hERG1a transduced with either scFv2.10 or GFP. hERG1 deactivation recorded from scFv2.10-transduced cells was significantly accelerated compared to GFP-transduced controls (Figure 2.7).

To determine the antiarrhythmic capacity of disabling the hERG1a PAS domain, we transduced JLN hiPSC-CMs with lentiviral particles encoding the scFv2.10 polypeptide and measured their

corresponding cardiac currents and APs. In JLN hiPSC-CMs, scFv2.10 transduction increased steady-state and tail I_{Kr} by ~two-fold compared to GFP-transduced cells. Increased tail I_{Kr} is a proxy for increased channel trafficking to the membrane, thus, these data suggest that scFv2.10 expression increases hERG1 abundance at the surface membrane (Figure 2.4). Surprisingly, scFv2.10 transduction slowed the time course of deactivation in JLN hiPSC-CMs, suggesting that PAS activity is increased in the scFv2.10-transduced JLN hiPSC-CMs (Figure 2.4). Notably, scFv2.10 did not affect voltage-dependent I_{Ca} in JLN hiPSC-CMs supporting that scFv2.10 is hERG1-selective, as previously shown [31] (Figure 2.6).

scFv expression selectively increases hERG1a abundance in JLN hiPSC-CMs.

Increasing the relative abundance of the hERG1a PAS domain slows the time course of deactivation and stabilizes inactivation [33, 98, 99]. Transducing JLN hiPSC-CMs with the PAS-targeting scFv2.10 slowed the time course of deactivation, which could indicate that scFv2.10 is promoting hERG1a subunit expression over hERG1b (Figure 2.4).

To test if scFv2.10-mediated PAS disruption alters hERG1 subunit abundance, we measured hERG1a and hERG1b-specific immunofluorescence in JLN hiPSC-CMs transduced with either scFv2.10 or GFP. hERG1a immunofluorescence was significantly increased, and hERG1b significantly decreased in scFv2.10-transduced JLN hiPSC-CMs compared to GFP-transduced controls (Figure 2.4). These data demonstrate that lentiviral scFv2.10 expression alters heteromeric channel assembly and explain the slowing of I_{Kr} deactivation in the presence of scFv2.10.

scFv2.10 reduces arrhythmic events in JLN hiPSC-CMs.

Our data demonstrate that lentiviral scFv2.10 expression to disable the hERG1 PAS domain increases I_{Kr} magnitude. To test if scFv2.10-mediated PAS disruption mitigates perturbed repolarization in the absence of I_{Ks}, we measured APD_{90} paced at 1 Hz in JLN hiPSC-CMs transduced with scFv2.10 or a GFP control (Figure 2.5, Table 2.2). We assessed three markers of proarrhythmia: APD_{90}, beat-to-beat APD variability, and the incidence of early after depolarizations (EADs). AP beat-to-beat variability is a more reliable predictor of arrhythmogenic potential than AP prolongation alone [100], and EADs are a cellular manifestation of arrhythmia [101]. scFv2.10 transduction shortened APD_{90} by ~200 ms and reduced both beat-to-beat AP variability and the incidence of EADs compared to GFP-transduced controls (Figure 2.5). These data demonstrate that disabling the PAS domain with scFv2.10 is antiarrhythmic in JLN hiPSC-CMs and suggest that targeting the hERG1a PAS domain could be a viable therapeutic target for diseases of impaired cardiac repolarization.

Discussion

The present study investigated the antiarrhythmic potential of disrupting the hERG1a PAS domain by overexpressing the PAS-targeting hERG1 activator, scFv2.10, in JLN hiPSC-CMs [31]. Our data demonstrate that scFv2.10 selectively enhances I_{Kr} magnitude, shortens APD, and reduces beat-to-beat AP variability and EAD incidence in JLN hiPSC-CMs. These data highlight the therapeutic potential of targeting the hERG1a PAS domain.

Classical hERG1 activators

Though it is well-established that targeted enhancement of I_{Kr} shortens APD, hERG1 activators display off-target and/or proarrhythmic effects [102]. For example, in a rabbit model of LQTS 1, NS1643 shortened APD and QT interval but also increased ventricular fibrillation. NS1643 also contains a pharmacophore that non-selectively activates BK_{Ca} and K_{2P} channels [14, 15, 102]. NS3623, a structural analog of NS1643, impaired conduction velocity and prolonged the QRS interval in guinea pig hearts [103]. ICA-105574 reduced arrhythmic events in guinea pig hearts but increased susceptibility for arrhythmia at higher concentrations [102]. Mallotoxin, a naturally occurring hERG1 activator, also promotes ventricular fibrillation in rabbit hearts [104]. These data highlight the shortcomings of current hERG1 agonists and the need to develop new, selective hERG1 activators.

Targeting the hERG1a PAS domain

PAS domains comprise a diverse group of proteins that detect input stimuli, like changes in redox potential or light exposure, and regulate wide-ranging processes like circadian rhythm and ion channel gating. PAS domains can be activated by binding to co-factors such as ions or nucleotides, but the majority lack identified co-factors [17, 105-107]. There are no reported hERG1 PAS ligands or PAS-targeting small molecule modulators [90, 108]. To our knowledge, we are the first to show that a PAS-targeting hERG1 activator reduces arrhythmic susceptibility in a LQTS background. The PAS domain is an underexplored antiarrhythmic drug target, and our work highlights its therapeutic potential.

Differential scFv activity

The original characterization of scFv2.10 in HEK293 cells stably expressing hERG1a and demonstrated that scFv2.10 slowed the onset of inactivation recovery and accelerated the time course of deactivation. In hiPSC-CMs, the same study demonstrated that scFv2.10 increased steady-state current density with no effects on gating kinetics reported. Follow up studies showed that scFv2.10 accelerated deactivation at 37°C and disrupted the interaction between PAS and CNBHD HEK293 cells [31, 80, 81].

In our hands, lentiviral scFv2.10 expression accelerates deactivation and reduces steady-state and tail current density in HEK293 cells at RT (Figure 2.7). Surprisingly, scFv2.10 expression slows the time course of deactivation and increases steady-state and tail I_{Kr} in JLN hiPSC-CMs. In agreement with these data, scFv2.10 increases hERG1a and reduces hERG1b abundance at the surface membrane. The shift in hERG1a and hERG1b subunit abundance could account for the slowed gating we observed in this study, but the molecular mechanism by which this shift occurs is unclear.

The differences observed in our studies may be attributed to chronically expressing scFv2.10 with lentiviral delivery in lieu of acute intracellular delivery through the recording pipette. hERG1b contains an endoplasmic reticulum retention signal (RXR) in its N-terminus that is masked by the hERG1a N-terminus. In the absence of hERG1a, the majority of hERG1b subunits are retained in the endoplasmic reticulum and degraded [109]. In this study, we used lentiviral particles to establish stable long-term scFv2.10 overexpression. It is possible that chronic scFv2.10 expression via lentivirus alters inter hERG1 subunit interactions and exposes the hERG1b RXR signal. It is also plausible that scFv2.10 binding of the nascent hERG1a N-terminus similarly disrupts hERG1a/1b heteromerization at the ribosome, further promoting hERG1b

retention and degradation. Conversely, scFv2.10 delivery through the patch clamp recording pipette would act on assembled hERG1a/1b channels at the surface membrane and would likely not impact hERG1 channel assembly and forward trafficking.

hERG-specific blockers, such as E-4031, can act as chemical chaperones by stabilizing hERG1 abundance at the surface membrane [110]. Similarly, the I_{Na} blocker pilsicainide increases hERG1 abundance at the surface membrane. This stabilizing effect, like that of E-4031, is only observed with chronic pilsicainide treatment whereas acute drug treatment has no effect [111]. scFv2.10 may act in a similar manner – but through the N-terminal domain rather than the pore domain like most hERG1 blockers – where chronic scFv2.10 expression stabilizes hERG1 folding to promote forward trafficking and enhance hERG1 abundance at the surface membrane.

KCNQ1 knockdown reduces hERG1 expression [97, 112]. Consistent with these reports, we found that I_{Kr} density in JLN hiPSC-CMs was nearly half that of control hiPSC-CMs. Remarkably, scFv2.10 expression restores I_{Kr} magnitude to levels comparable to control hiPSC-CMs. In JLN hiPSC-CMs, scFv2.10 may act as a substitute chaperone for KCNQ1 and induce a conformational change in hERG1a that promotes forward trafficking.

hERG1 deficiency may be required for scFv2.10 transduction to increase I_{Kr} through enhanced hERG1 trafficking as we only observed this effect in JLN hiPSC-CMs and not control hiPSC-CMs (Figure 2.1, Figure 2.3). It is possible that hiPSC-CMs may have a compensatory mechanism to maintain a steady-state level of hERG1 channels at the surface membrane. Regardless, our data support that scFv2.10 may selectively target diseased cells where hERG1 function is impaired which could be promising for future clinical development.

Limitations

Off-target hERG1 block is a major liability in drug development due to torsadogenic risk, thus, pharmaceutical industries may be hesitant to invest in a hERG1-targeting therapy [37]. There are at least two FDA approved lentiviral gene therapies but the short half-life of scFvs poses concern for drug-potency [86, 113, 114]. Viral delivery systems (i.e. adeno-associated virus (AAV), lentivirus) can illicit immune responses that cause rapid degradation and clearance of the virus. Therefore, it is worth exploring alternative gene-therapy delivery systems such as exosome-AAVs, where exosomes enhance AAV stability by protecting them from immunogenic responses. *In-vitro* transcribed mRNA enclosed in a lipid-based nanoparticle could also serve as an alternative delivery system, which would transfer scFv2.10 production inside the body [115, 116].

Translating between model systems can yield drastically different results and mechanisms of action for potential therapeutics. Although scFv2.10 appears to be selective for hERG1 and we demonstrate its antiarrhythmic potential, it must be tested in multicellular systems and animal models to ensure its proposed therapeutic effects will translate. We have preliminary data showing that scFv2.10 shortens APD in cardiac monolayers derived from a healthy patient control. However, this needs to be repeated to confirm the effect is reproducible (Figure 2.9).

Controlling for dose will also be critical for assessing the risk for AP overcorrection and the onset of short QT syndrome. Strategies for targeting specific cardiac cells should also be considered as hERG1 is expressed throughout the body including the brain, kidney, and liver [117]. Relatedly, one must consider how AP repolarization will be affected in other cardiac cell types as hERG1 is expressed throughout the heart.

Although culturing hiPSC-CMs on PDMS promotes maturation, it does not accurately represent the adult myocardium as some cells still displayed spontaneous activity, a prominent

marker of immaturity [94, 118]. We attempted to test the effects of isoproterenol on JLN hiPSC-CMs as β-adrenergic stimulation increases the risk for arrhythmic events in a LQTS1 background [69]. Unfortunately, our results are inconclusive because we could not pace cells treated with isoproterenol due to the increased firing frequency. Thus, we exclusively recorded APs from spontaneously contracting hiPSC-CMs. Due to their uncontrolled electrical behavior, the experimental set up was insufficient for testing the effects of isoproterenol (Figure 2.8).

Additionally, we did not create an isogenic control for the JLN hiPSC-CMs because the JLN mutation includes an exon deletion. One work-around is to create the JLN mutation in healthy control hiPSC-CMs (df 19.9.11) and repeat the above experiments to test if the effects are reproducible. Relatedly, cardiac ion channel expression can vary greatly amongst different cardiac differentiations. Although we conducted these experiments with multiple biological replicates to ensure the reproducibility of our data, additional JLN human iPS clones should be tested given that we only used one clone for differentiations. [119]. Regardless, our data highlight a novel approach for hERG1 activation to treat cardiac electrical disorders.

Materials and Methods

HEK293 Cell Culture

We maintained cells at 37C and 5% CO2 in a Heracell incubator (Thermo Fisher). We cultured HEK293 cells in minimum essential medium (MEM, Invitrogen, Cat. No 11095080) supplemented with 10% fetal bovine serum (Thermo Fisher, Cat No. SH30070.03) and split cells once they reached 80% confluency every 5 days.

Stem Cell Culture and Cardiac Differentiation

Two human iPS cell lines were used for this study; the df19.9.11 iPS cell line served as a healthy control (WiCell, Madison) and the JLN iPS cell line derived from a Jervell and Lange-Nielsen Syndrome patient which was graciously provided by Timothy J. Kamp from the University of Wisconsin-Madison. As previously described, human iPS cells were cultured and differentiated into cardimyocytes using the GiWi protocol [94]. Briefly, stem cells were seeded on Matrigel-coated plastic plates in iPS-brew medium (Miltenyi Biotec, USA). Cells were checked daily to remove spontaneous differentiation and passed at 80% confluence. For cardiac directed differentiation, ~80,000 cells were plated into each well of a 6-well plate and cultured to ~100% confluency. Cells were first treated with GSK3 inhibitor (day 0) to induce mesodermal differentiation, followed by a Wnt inhibitor (day 2) to induce formation of the cardiac mesoderm. On day 4, the Wnt inhibitor was removed to direct cells into cardiac progenitor cells. After 8-10 days, cardiac monolayers began spontaneously contracting and cultured to day 20 and subsequently purified using the human iPS-derived cardiomyocyte isolation kit, (Miltenyi Biotec, USA) following the manufacturer's protocol. Purified cardiomyocytes were plated as a monolayer

into a Matrigel-coated PDMS 6-well plate (~200e3 cells/well) for 7 days and then trypsinized and replated as single cells (~8000 cells/well). Patch-clamping experiments were completed at least 7 days after replating.

Lentiviral Constructs and Transduction

Lentiviral particles were produced using the lentiviral generating plasmid pLentiLox 3.7 (pLL 3.7), which contains a U6 promoter for shRNA expression and a CMV promoter for GFP expression downstream of the U6-siRNA expression cassette. scFv2.10-GFP was subcloned into the pLL 3.7 *Nhe*I-*Bsr*GI restriction sites. Empty pLL 3.7 vectors expressing GFP were used as controls. Lentiviral constructs and particles used in this study were generated by and purchased from the University of Michigan's Vector Core. Cells were transduced at an MOI of 100. Transduction efficiency was assessed by observing GFP fluorescence 48-72h post transduction.

Lentiviral Production and Determination of Lentiviral Titer Unit

HEK293T cells were grown to 50% confluency and transfected with a pLL 3.7 plasmid. Media was changed 6 hours post transfection and incubated for 48-72 hours at 37°C. Viral supernatant was harvested 48-72 hours post transfection and stored at -80°C. HEK 293T cells were transduced with 1X lentivirus and fluorescence was analyzed at 72 hours. Titer was calculated as follows:

$$\textit{Equation 1:} \quad Titer\ (\frac{TU}{mL}) = \left[\frac{\%\ fluorescent\ positive\ cells * cell\ count}{dilution\ factor * volume\ of\ virus}\right]$$

Immunocytochemistry

hiPSC-CMs were seeded on PDMS and fixed with 4% paraformaldehyde/PBS for 15 min, then washed for 5 min with PBS followed by incubation with blocking buffer (PBS + 1% BSA + 0.5% Triton X + 10% Goat Serum) for 1h. Cells were incubated with primary antibodies in blocking buffer (*sans* Triton X) overnight at 4°C. The next day, cells were washed with PBS (3 × 5 min) and incubated with secondary antibodies in blocking buffer (*sans* Triton X) for 1 h at RT in the dark. Cells were washed with PBS (3 × 5 min) and mounted with ProLong Gold antifade reagent (ThermoFisher) on a coverslip.

Differentiated cardiac lines were validated using immunocytochemistry targeting actin (phalloidin, cat#A12379 ThermoFisher) to confirm the presence of cardiac sarcomeric organization, and patch clamp electrophysiology measuring cardiac I_{Kr}, indicative of hERG1 expression, and I_{Ca}. hiPSC-CMs were immunolabeled for hERG1a (#ALX-215-050-R100, Enzo Life Sciences), hERG1b (#ALX-215-051-R100, Enzo Life Sciences), or hERG1 p-loop (#ALX-804-652-R300, Enzo Life Sciences) using a 1:200 dilution of the primary antibodies followed by a 1:250 dilution of secondary antibody goat anti-rabbit Alexa Fluor 647 (#4050-31, Southern Biotec). KCNQ1 was labeled using a 1:100 dilution of the primary antibody (#ab84819, abcam) followed by a 1:250 dilution of secondary antibody goat anti-mouse Alex Fluor 568 (#A11004, Invitrogen). Actin filaments were labeled using phalloidin (#A12379 ThermoFisher) to confirm the presence of sarcomere structure that is specific to cardiomyocytes. Nuclei were labeled using 1:1000 dilution of DAPI (1µg/mL) for 15 minutes (#2248, ThermoScientific). Immunostained preparations were analyzed using a confocal microscope (Zeiss 880) to determine protein abundance.

Electrophysiology

All ionic currents (I_{Kr}, I_{Ks}, I_{Ca}) currents were recorded at physiological temperature (37 ± 1°C) using whole-cell patch clamp with an IPA® Integrated Patch Amplifier run by SutterPatch® (Sutter Instrument) and Igor Pro 8 (Wavemetrics). Borosilicate glass recording pipettes (2–5 MΩ) were backfilled with intracellular solution containing: 5 mM NaCl, 150 mM KCl, 2 mM CaCl2, 5 mM EGTA, 10 mM HEPES, 5 mM MgATP, and adjusted to pH 7.2 with KOH. Cells were perfused at a rate of ~2 mL/min with extracellular solution that consisted of 150 mM NaCl, 5.4 mM KCl, 1.8 mM $CaCl_2$, 1 mM $MgCl_2$, 15 mM glucose, 10 mM HEPES, 1 mM Na-pyruvate, pH 7.4 adjusted with NaOH. I_{Kr} and I_{Ks} were reported as an E-4031 and chromonal-293b sensitive currents by calculating the difference in current magnitude before and after 2 μM E-4031 and 50 μM chromonal-293b extracellular perfusion, respectively. Series resistance for whole-cell recordings ranged from 3–15MΩ. A 100-ms step to -50 mV was applied prior to I_{Kr} and I_{Ks} recordings to inactivate sodium currents. Voltage was then stepped to a 3 second pulse from -50 to +50 mV in 10 mV increments followed by a 10 second pulse at -40 mV. Data were sampled at 5 kHz and low-pass filtered at 1 kHz. Steady-state I_{Kr} and I_{Ks} density were calculated as the 5-ms mean at the end of each pre-pulse normalized to capacitance as a function of pre-pulse potential. I_{Ca} density was calculated as the peak I_{Ca} normalized to capacitance as a function of pre-pulse potential. Tail I_{Kr} density was calculated as peak tail I_{Kr} normalized to capacitance as a function of pre-pulse potential and fitted with the following Boltzmann equation.

$$\textit{Equation 1:} \quad y = \left[\frac{A_1 - A_2}{1 + e^{(V - V_0)/k}}\right] + A_2,$$

where A_1 and A_2 represent the maximum and minimums of the fit, respectively, V is the membrane potential, V_0 is the midpoint, and k is the slope factor. The time course of I_{Kr} deactivation was

calculated by fitting current decay during the 3 second pulse at +20 mV with a double exponential function:

$$\textit{Equation 2:} \quad y = Y_0 + A_1 e^{-t/\tau_1} + A_2 e^{-t/\tau_2},$$

where Y_0 is the asymptote, A_1 and A_2 are the relative components of the fast and slow time constants τ_1 and τ_2, respectively.

APs were recorded using perforated patch with amphotericin B (0.3 mg/mL) in current clamp as previously described [120]. Borosilicate glass recording pipettes (2-5MΩ) were backfilled with intracellular solution supplemented with amphotericin B. Cardiomyocytes were paced at 1 Hz following perforation which was observed as a rapid hyperpolarization of the resting membrane potential that stabilized within 60 seconds. Series resistance for perforated patch AP recordings were between 22-100MΩ. The time to 90% of action potential repolarization (APD_{90}) and APD_{90} variability were calculated from the average of 20 successive paced APs within a cell. Cells that could not be paced at 1 Hz were not included in AP analyses.

Statistical Analysis

Data were analyzed using IgorPro and GraphPad Prism. We evaluated data for normality and outliers (Shapiro-Wilk test) before statistical evaluation in GraphPad Prism. Data were considered outliers if they fell outside the average ± two times the standard deviation. All data are reported as mean ± SEM. APD and deactivation data were compared using a parametric (normal distribution) or non-parametric (non-normal distribution) student's t-test. We ran the Mann-Whitney or Kolmogorov-Smirnov non-parametric test when groups showed similar or unequal

variances, respectively. We considered variance unequal if there was a two-fold or greater change in the standard deviation. Steady-state and tail I_{Kr} and I_{Ca} were analyzed using two-way ANOVA (mixed methods) with a Šidák post hoc test. I_{Ca} recordings with a calculated voltage error > 6 were excluded from analysis. Only I_{Kr} and I_{Ks} subtractions yielding positive current densities are reported. Statistical significance was taken at $p < 0.05$.

Figures

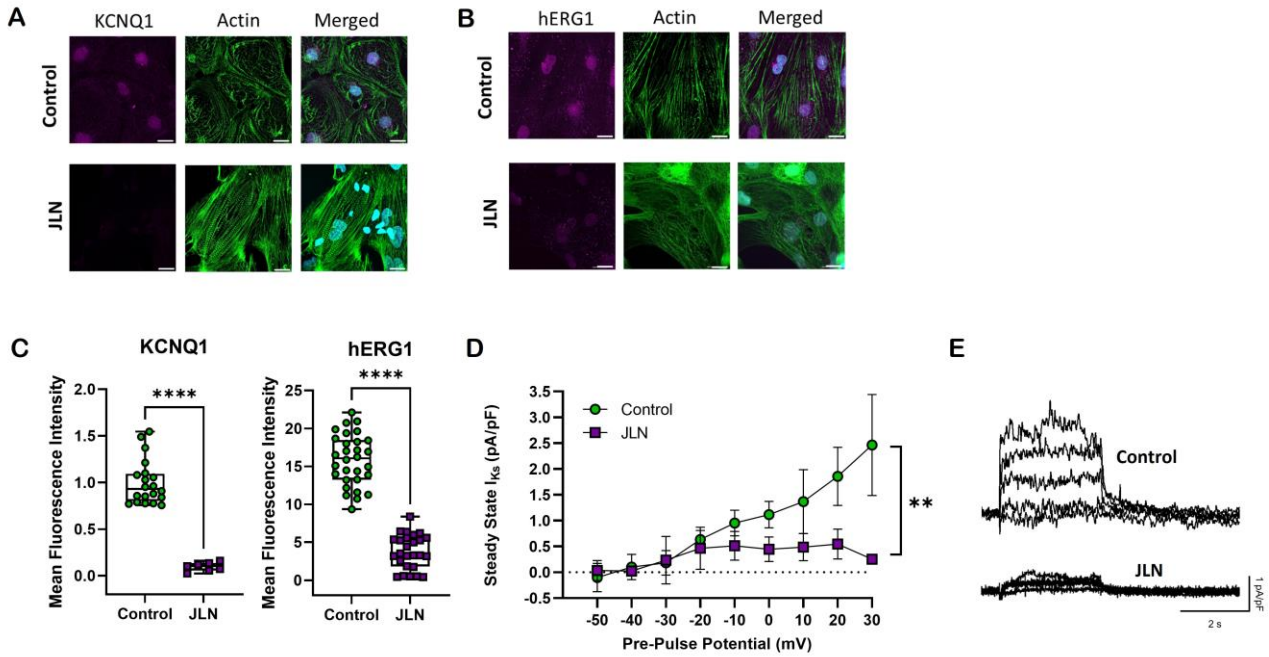

Figure 2.1 Validation of JLN hiPSC-CMs.

(A) Control and JLN hiPSC-CMs immunolabeled for KCNQ1 (magenta), phalloidin (green), and DAPI (cyan). (B) Control and JLN hiPSC-CMs immunolabeled for hERG1 (magenta), phalloidin (green), and DAPI (cyan). (C) Mean fluorescence quantified from images as shown in A and B. (D) Steady-state I_{Ks} density plotted as a function of pre-pulse potential for control (green) and JLN (magenta) hiPSC-CMs. Sample traces are shown in (E). P values were determined by unpaired, two-tailed Student t-test, or ordinary two-way ANOVA (mixed methods) with multiple comparisons and Šidák post hoc test. ****P < 0.0001 **P<0.001. Scale bar, 20μM. [KCNQ1 mean fluorescence intensity, N=3, control n=20, JLN n=7; hERG1 mean fluorescence intensity, N=3, control n=30, JLN n=26; I_{Ks}, N=2, JLN n=6, control, n=4).

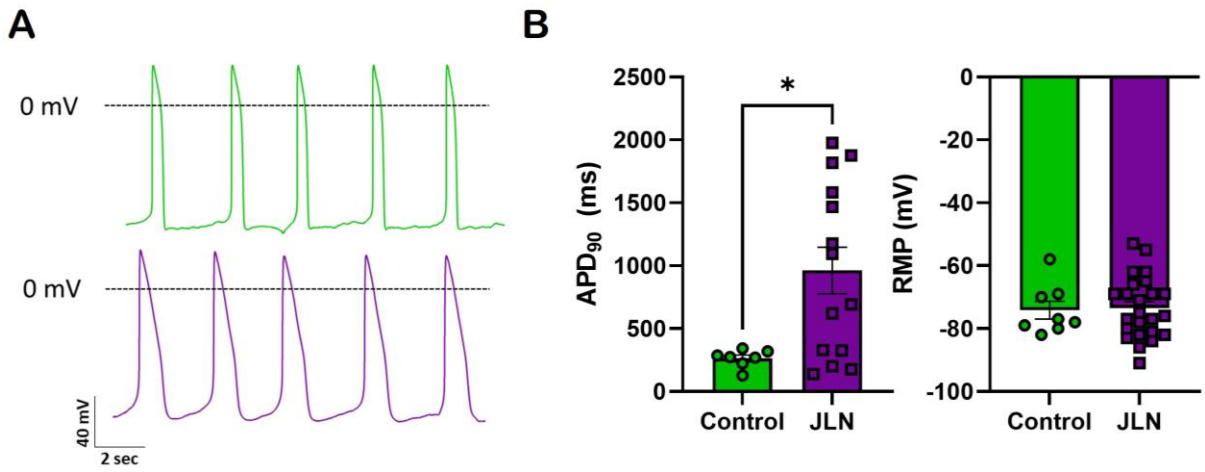

Figure 2.2 JLN hiPSC-CMs are proarrhythmic.

(A) APD_{90} and resting membrane potential recorded from control and JLN hiPSC-CMs. (B) Representative AP traces from control (green) and JLN (purple) hiPSC-CMs. *P* values were determined by unpaired, two-tailed Student *t*-test. *$P < 0.05$ [APD_{90} control N=2, n = 7; JLN N=3, n = 14. Resting membrane potential, control N=2, n = 8; JLN N=3, n=14]. Data are presented as mean ± SD.

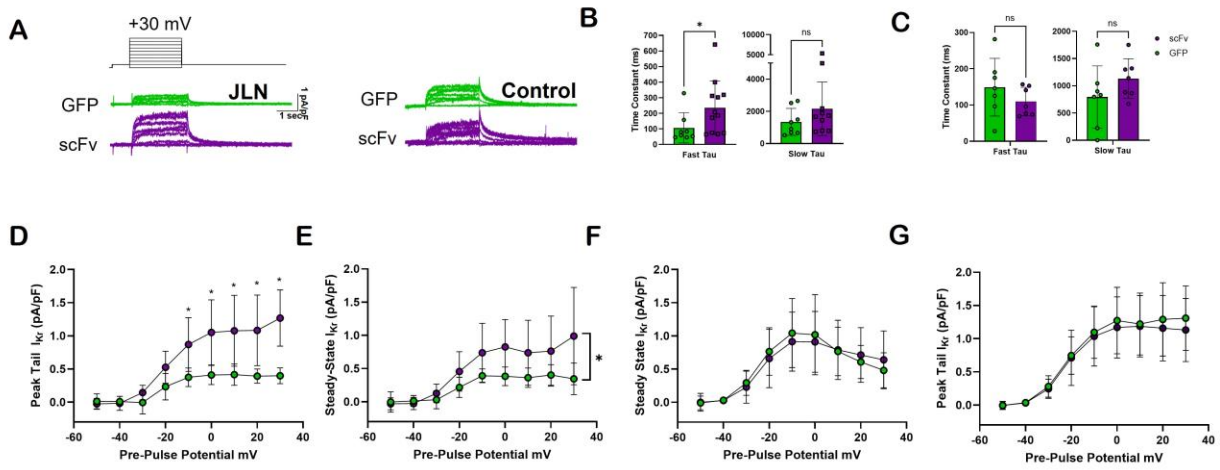

Figure 2.3 scFv2.10 transduction selectively increases I_{Kr} density in JLN hiPSC-CMs

(A) Representative I_{Kr} traces from JLN hiPSC-CMs transduced with GFP (green) or scFv2.10 (purple) elicited by the pulse protocol shown above. (B Fast and slow deactivation time constants recorded from JLN hiPSC-CMs at +20 mV. (D) Peak tail I_{Kr} and plotted as a function of pre-pulse potential from JLN hiPSC-CMs. (E) Steady-state I_{Kr} plotted as a function of pre-pulse potential from JLN hiPSC-CMs. (F) Peak tail I_{Kr} and plotted as a function of pre-pulse potential from JLN hiPSC-CMs. (G) Steady-state I_{Kr} plotted as a function of pre-pulse potential from JLN hiPSC-CMs. P values were determined by unpaired, two-tailed Student t-test, or ordinary two-way ANOVA (mixed methods) with multiple comparisons and Šidák post hoc test. **P* <0.05 [JLN N =3, n = 7, Control N=2, n ≥ 7). Data are presented as mean ± SD.

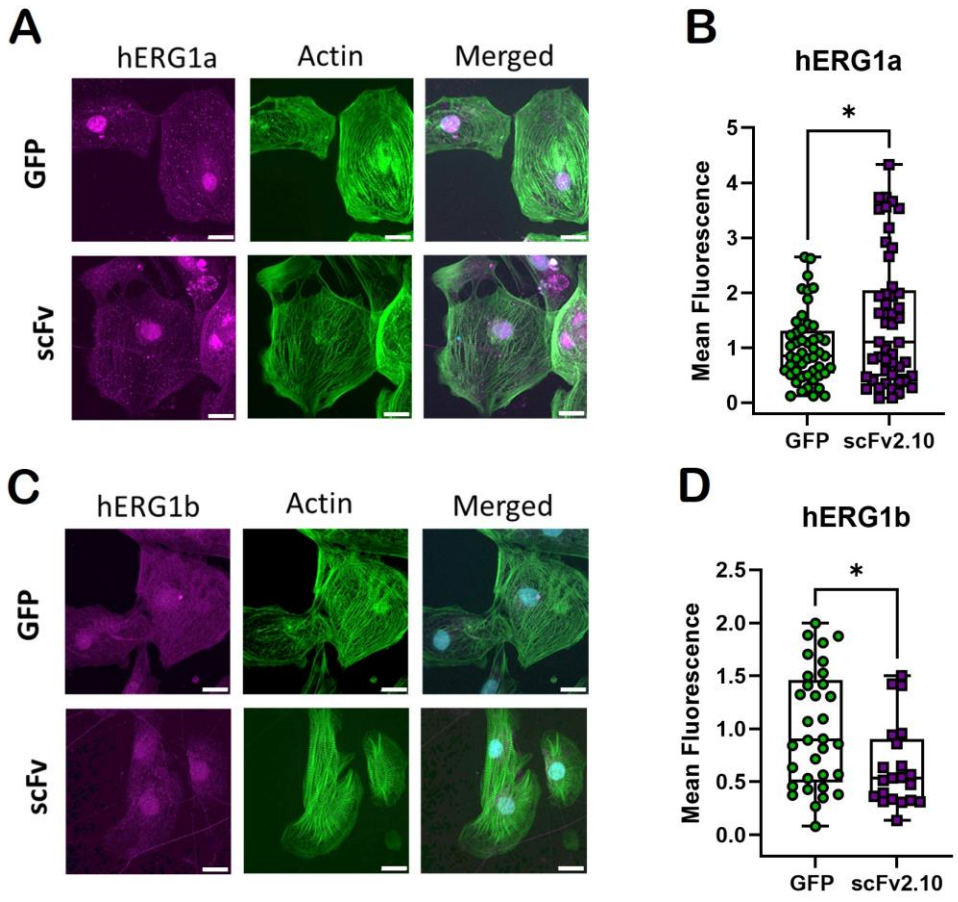

Figure 2.4 scFv2.10 transduction increases hERG1a abundance in JLN hiPSC-CMs

scFv2.10 transduction increases hERG1a abundance in JLN hiPSC-CMs. (A) JLN hiPSC CMs immunolabeled for hERG1a (magenta), phalloidin (green), and DAPI (cyan). (B) Mean fluorescence intensity quantified from images shown in A. (C) JLN hiPSC-CMs immunolabeled for hERG1b (magenta), phalloidin (green), and DAPI (cyan). (D) Mean fluorescent intensity quantified from images shown in C. P values were determined by unpaired, two-tailed Student t-test. *$P < 0.05$. Scale bar, 20 µM. [hERG1a mean fluorescence intensity N=3, GFP n=49; scFv2.10 n=49. hERG1b mean fluorescence intensity N=3, GFP n = 33; scFv2.10 n=21].

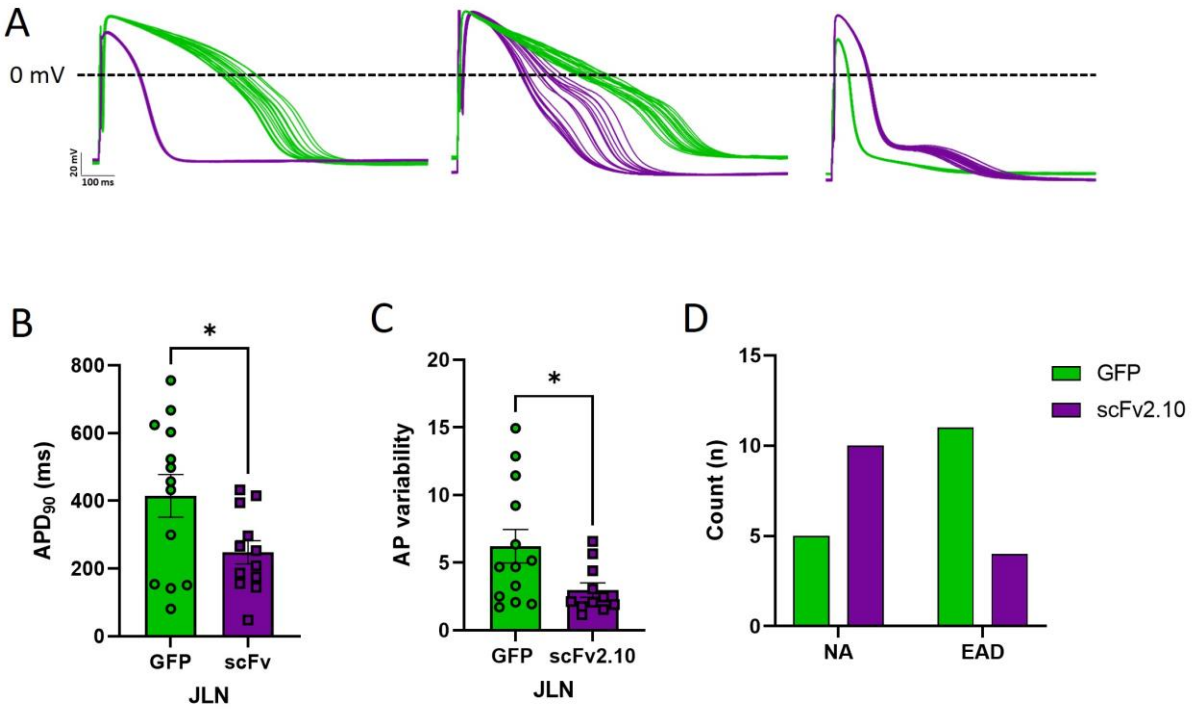

Figure 2.5 scFv2.10 expression is anti-arrhythmic in JLN hiPSC-CMs

(A) Representative AP recordings from JLN hiPSC-CMs transduced with GFP (green) or scFv2.10 (purple). Left, Non-arrhythmic (NA), Center, phase 2 EAD. Right, phase 3 EAD. (B) APD_{90} and (C) AP beat-to-beat variability calculated from AP recordings as shown in A. (D) EAD count recorded from JLN hiPSC-CMs transduced with GFP or scFv2.10. P values were determined by unpaired, Two-tailed Student t-test. $*P < 0.05$. [APD_{90} N=3, GFP n = 13; scFv2.10 =12. AP variability N=3, GFP n =13; scFv2.10 n =11. EAD N=3, GFP n=15, scFv2.10 n=15]. Data are presented as mean ± SD.

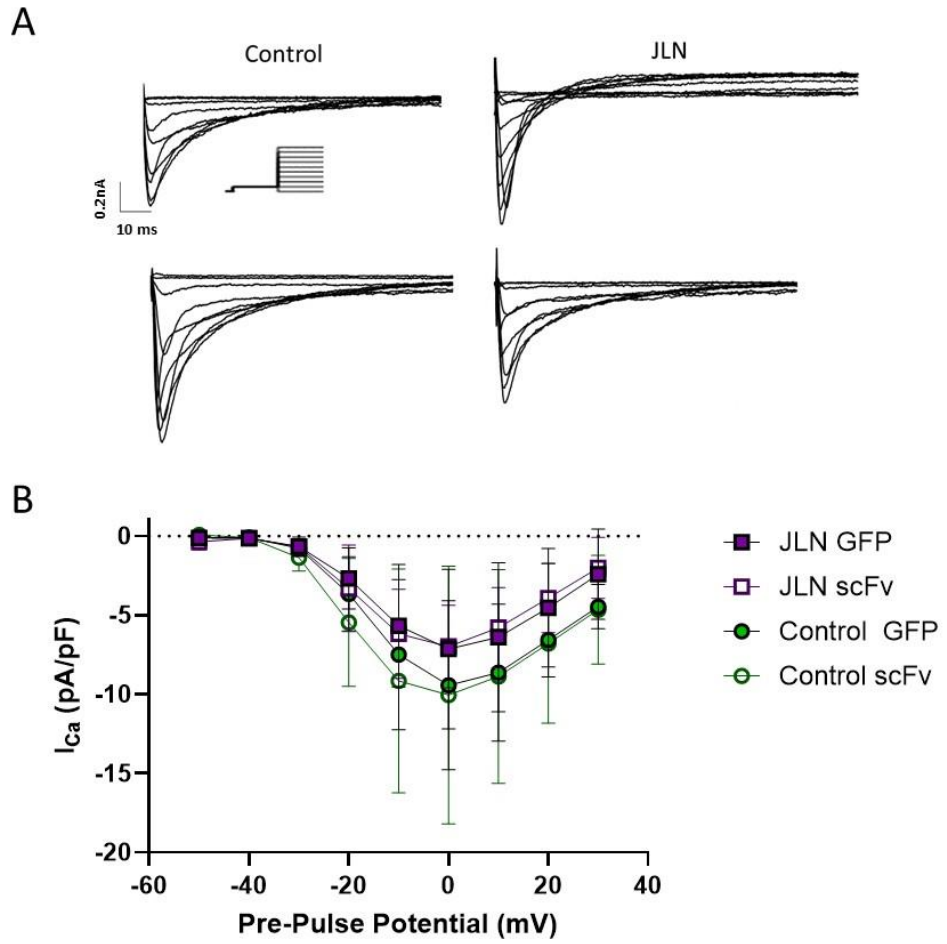

Figure 2.6 I_{Ca} density in control and JLN hiPSC-CMs transduced with scFv2.10 or GFP

(A) Representative I_{Ca} traces from control or JLN hiPSC-CMs transduced with GFP (top) or scFv2.10 (bottom). Voltage protocol shown in the inset. (B) Peak I_{Ca} density recorded from control and JLN hiPSC-CMs transduced with GFP or scFv2.10 and plotted as a function of pre-pulse. [JLN N =3, n = 9, Control N=2, n ≥ 9). Data are presented as mean ± SD.

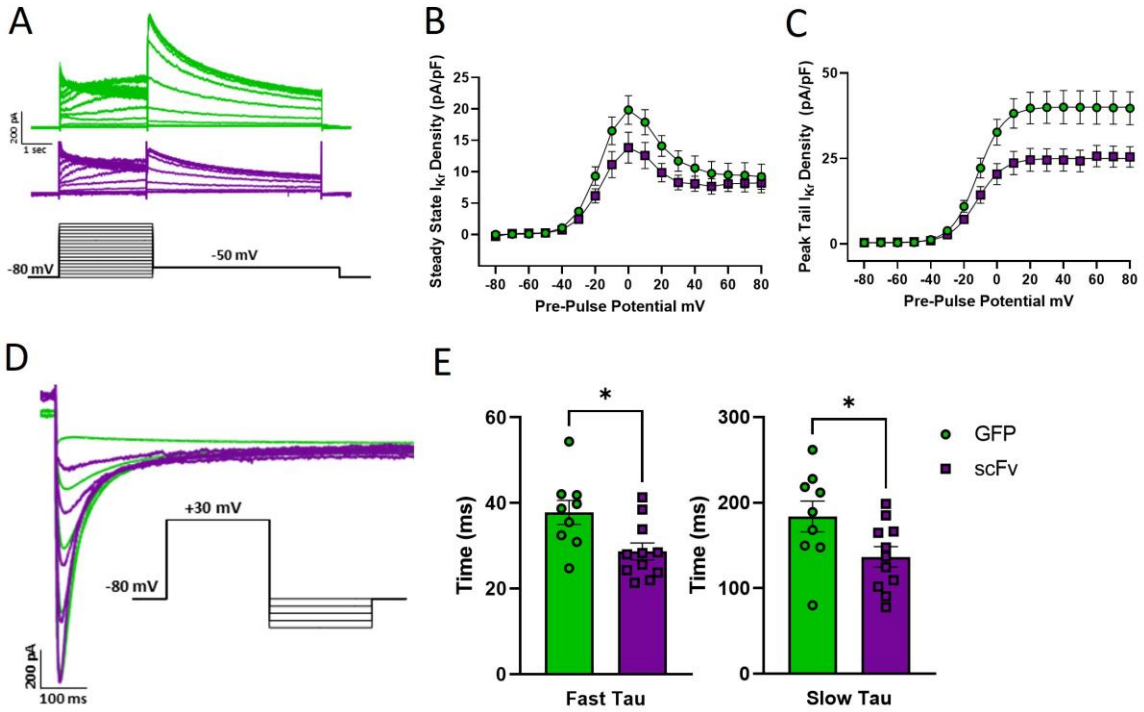

Figure 2.7 scFv2.10 transduction reduces I_{Kr} density and accelerates gating in HEK293 cells stably expressing hERG1a at RT.

(A) Representative traces from HEK293 cells stably expressing hERG1a transduced with GFP control (green) or scFv2.10 (purple) at RT. Pulse protocol for steady-state and tail hERG1 current shown below. (B) Steady-State I_{Kr} plotted as a function of pre-pulse potential. (C) Peak tail I_{Kr} density plotted as a function of pre-pulse potential. (D) Representative traces as described in "A". Pulse protocol for hERG1 deactivation shown below. (E) Fast and slow time constants of deactivation at -110 mV. P values were determined by unpaired, two-tailed Student t-test, or ordinary two-way ANOVA (mixed methods) with multiple comparisons and Šidák post hoc test. *P < 0.05. [Fast and Slow Tau N=2, GFP n = 9; scFv2.10 n = 11. Steady-state and Peak tail I_{Kr} N=2, n= 17]. Data are presented as mean ± SD.

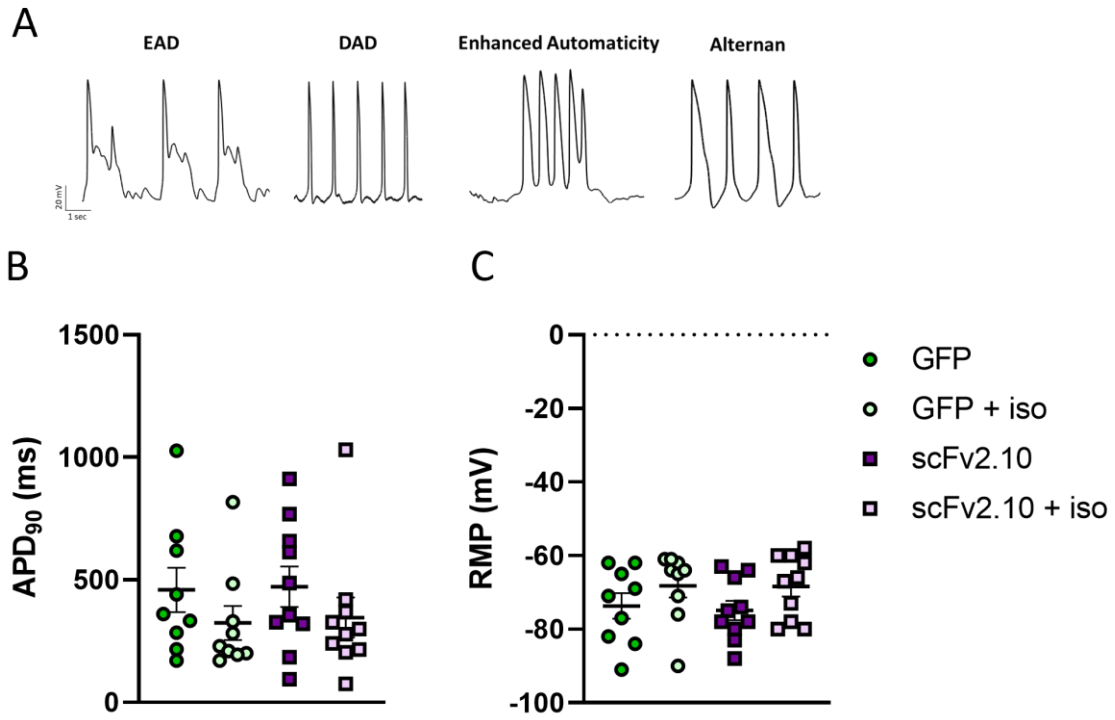

Figure 2.8 Effects of isoproterenol on spontaneously contracting JLN hiPSC-CMs

(A) Representative traces of arrhythmic events classified into four groups. (B) APD_{90} and (C) resting membrane potential of spontaneously contracting JLN hiPSC-CMs transduced with either GFP or scFv2.10 treated with isoproterenol.

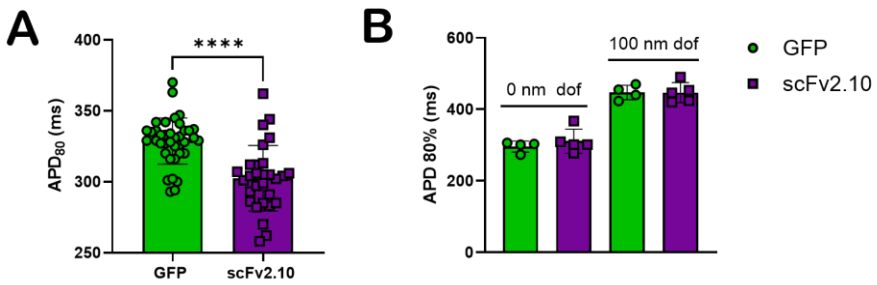

Figure 2.9 Optical mapping with control hiPSC-CM monolayers

(A) APD measured at 80% repolarization repolarization from cardiac monolayers derived from a healthy patient control. (B) APD_{80} as described in (A) +/- dofetilide (dof).

Tables

AP Parameters (Spontaneous)	Control	n	SD	JLN	n	SD
APD_{90} (ms)	264*	7	71	739*	24	609
RMP (mV)	-74	8	8	-73	24	8
JLN AP Parameters (1Hz)	**GFP**	**n**	**SD**	**scFv2.10**	**n**	**SD**
APD_{90} (ms)	414.50*	13	226.92	247.80*	12	119.12
RMP (mV)	-76.84	13	7.43	-73.22	13	13.50

P values determined using Two-tailed Student *t*-test. *$P<0.05$ N=3.

Table 2.1 AP Parameters of Control and JLN hiPSC-CMs

Current Parameter		Control	n	SD	JLN	n	SD
Steady-state I_{Ks} at +10 mV (pA/pF)	GFP	1.37*	4	0.62	0.488*	4	0.26
Steady-state I_{Kr} at -10 mV (pA/pF)	GFP	1.04	7	0.52	0.39	7	0.11
	scFv2.10	0.91	7	0.44	0.74*	10	0.44
Peak tail I_{Kr} at -10 mV (pA/pF)	GFP	1.27	7	0.39	0.37*	7	0.14
	scFv2.10	1.17	7	0.45	0.87*	10	0.41
Fast Tau at +20 mV (ms)	GFP	149.06	7	79.55	107.11*	8	96.91
	scFv2.10	76.65	7	39.43	235.28*	12	171.94
Slow Tau at +20 mV (ms)	GFP	793.38	7	571.36	1345.04	8	834.75
	scFv2.10	1140.70	7	364.82	2158.02	10	1662.49
Peak I_{Ca} at 0 mV (pA/pF)	GFP	-9.44	6	5.34	-7.15	9	5.01
	scFv2.10	-10.05	7	8.14	-6.99	8	2.57

P values determined using a Two-way ANOVA. N = 3. *$P < 0.05$.

Table 2.2 Electrophysiological Parameters of GFP and scFv2.10-GFP transduced hiPSC-CMs

Chapter 3 hERG1 Channel Subunit Composition Mediates Proton Inhibition of Rapid Delayed Rectifier Potassium Current (I_{Kr}) in Cardiomyocytes Derived from hiPSCs

This chapter was published in the Journal of Biological Chemistry in 2022.

* Indicates shared first authorship.

Chiamaka U. Ukachukwu*[1], Eric N. Jimenez-Vazquez*[1], Abhilasha Jain[1], David K. Jones[1,2]
[1]Department of Pharmacology, University of Michigan Medical School
[2]Department of Internal Medicine, University of Michigan Medical School

Author contributions

C. U. U., E. N. J.-V., and D. K. J. conceptualization; C. U. U., E. N. J.-V., and A .J. formal analysis; C. U. U., E. N. J.-V., and A. J. investigation; C. U. U., E. N. J.-V., A. J., D. K. J. writing–original draft; C. U. U., E. N. J.-V., A. J., and D. K. J. writing–review & editing.

Summary

Substrate-mediated maturation of human stem cell-derived cardiomyocytes promotes changes in hERG1 subunit transcription, altering both I_{Kr} magnitude and kinetics *in vitro*. Additionally, hERG1 channel subunits differentially impact the magnitude of native I_{Kr} inhibition by extracellular protons.

Abstract

Voltage-gated Channel hERG1 conducts rapid delayed rectifier potassium current (I_{Kr}) and is critical for repolarization of the human heart. Reduced I_{Kr} causes long QT syndrome and increases the risk for cardiac arrhythmia and sudden cardiac death. At least two subunits combine to form

functional hERG1 channels, hERG1a and hERG1b. Changes in hERG 1a/1b subunit abundance modulate I_{Kr} kinetics, magnitude, and drug sensitivity. Studies from native cardiac tissue have suggested that hERG1 subunit abundance is dynamically regulated, but the impact of altered subunit abundance on I_{Kr} and its response to external stressors is not well understood. Here, we used a substrate-driven hiPSC-CM maturation model to investigate how changes in relative hERG1a/1b subunit abundance impact the response of native I_{Kr} to extracellular acidosis, a known component of ischemic heart disease and sudden infant death syndrome. I_{Kr} recorded from immature hiPSC-CMs displays a two-fold greater inhibition by extracellular acidosis (pH 6.3) compared to matured hiPSC-CMs. qRT-PCR and immunocytochemistry demonstrated that hERG1a subunit mRNA and protein were upregulated, and hERG1b subunit mRNA and protein were downregulated in matured hiPSC-CMs compared to immature hiPSC-CMs. The shift in subunit abundance in matured hiPSC-CMs was accompanied by increased I_{Kr} density. Silencing the impact of hERG1b on native I_{Kr} kinetics by overexpressing a polypeptide identical to the hERG1a N-terminal Per-Arnt-Sim (PAS) domain reduced the magnitude of I_{Kr} proton inhibition in immature hiPSC-CMs to levels comparable to those observed in matured hiPSC-CMs. These data demonstrate hERG1 subunit abundance is dynamically regulated and determines I_{Kr} sensitivity to protons in hiPSC-CMs.

Introduction

hERG1, encoded by *KCNH2*, is the voltage-gated potassium channel that conducts the rapid delayed rectifier potassium current (I_{Kr}). Reduced I_{Kr} from either off-target pharmacological block or loss-of-function *KCNH2* variants causes the cardiac disorder long QT syndrome and increases the risk for cardiac arrhythmia, syncope, and sudden cardiac death [1, 5]. Long QT syndrome is

the leading cause of arrhythmic death in children and accounts for 5–10% of sudden infant death syndrome (SIDS) and intrauterine fetal death cases [7, 10, 11, 121-123]. Furthermore, multiple LQTS-associated *KCNH2* variants have been linked with intrauterine fetal death and SIDS, underscoring the importance of hERG1 in the young heart [7, 8, 124-127].

At least two hERG1 subunits comprise native hERG1 channels, hERG1a and hERG1b [26, 88, 89, 128, 129]. Mutations in both subunits promote/cause cardiac electrical dysfunction [6, 7, 130, 131]. hERG1a subunits contain an N-terminal Per-Arnt-Sim (PAS) domain that regulates channel gating through interactions with the C-terminal cyclic nucleotide binding homology domain (CNBHD) and the cytoplasmic S4-S5 linker [91, 98, 99, 131, 132]. hERG1b has a much shorter and unique N-terminus that lacks a PAS domain [26, 88]. When heterologously expressed in HEK293 cells, the absence of a functional PAS domain in hERG1b triggers a roughly two-fold acceleration in the time course of activation, deactivation, and inactivation recovery in heteromeric hERG 1a/1b channels compared to homomeric hERG1a channels [131]. In cardiomyocytes derived from human induced pluripotent stem cells (hiPSC-CMs), silencing hERG1b by overexpressing a polypeptide that mimics the hERG1a PAS domain slows native I_{Kr} gating kinetics and reduces I_{Kr} magnitude, triggering increased action potential duration and early after depolarizations [89]. Conversely, disabling the hERG1a PAS domain using PAS-targeting antibodies accelerates I_{Kr} gating, increases I_{Kr} magnitude, and hastens cardiac repolarization [31].

Extracellular acidosis is a major inhibitor of I_{Kr} [133], and occurs in a variety of pathological situations associated with cardiac dysfunction, including SIDS and myocardial ischemia [134-136]. Consequently, a large body of work has explored the impact of extracellular protons on

hERG1 [133, 137-143]. Briefly, reduced extracellular pH reduces hERG1 channel conductance, depolarizes channel voltage dependence of activation, and accelerates channel deactivation [137, 139, 140, 144]. The pro-arrhythmic effects of reduced pH on hERG1 are two-fold, pore block by protons slows cardiac repolarization whereas the accelerated deactivation impairs hERG1's ability to protect the heart from premature stimulation [133, 145, 146]. Interestingly, it was demonstrated that the inhibitory effect of extracellular protons is enhanced in hERG1b-containing channels [147, 148].

Several studies suggest that hERG1 subunit abundance is dynamically regulated *in vivo* [129, 149-154]. However, the mechanisms that determine hERG1 subunit abundance and the impact of altered subunit abundance on the susceptibility of arrhythmia are poorly understood. LQTS mutations in the hERG1a PAS domain were shown to disrupt hERG1b trafficking to the membrane [155]. In murine tissue, targeted mERG1b deletion abolishes I_{Kr} in adult mice but only reduces I_{Kr} magnitude by roughly 50% in neonates, compared to wildtype littermate controls [156]. These data suggest that mERG1a is selectively downregulated during maturation of the murine heart. In the human heart, hERG1a mRNA transcripts are upregulated and hERG1b transcripts downregulated in adult ventricular tissue compared to fetal cardiac tissue [7]. Similarly, the relative abundance of hERG1a to hERG1b protein was reduced in failing cardiac tissue compared to non-diseased donor controls [157].

In this study, we used *in vitro* maturation of hiPSC-CMs to probe the impact of hERG1 subunit dynamics on proton modulation of native cardiac I_{Kr}. The data presented herein demonstrate that

increased hERG1a and reduced hERG1b in matured hiPSC-CMs diminish I_{Kr} sensitivity to extracellular protons compared to I_{Kr} recorded from immature hiPSC-CMs.

Results

Protons decrease hERG1 current amplitude and accelerate the time course of hERG1 deactivation [133, 137, 139, 140, 143, 158]. However, the specific effects of extracellular acidosis can vary across expression systems. For example, the impact of protons on the voltage dependence of activation is not consistently reported. These variations across systems suggest that other unidentified factors contribute to the response of hERG1 to protons [139, 141-143, 145, 158, 159]. Subunit abundance is one factor that may explain the different acidosis sensitivities. To determine the impact of hERG1 subunit abundance on native I_{Kr} sensitivity, we cultured hiPSC-CMs on two different matrices to promote distinct stages of maturation and corresponding shifts in hERG1 subunit expression.

Extracellular matrix mediates hiPSC-CM maturation

Culturing hiPSC-CMs on a pliable substrate promotes hiPSC-CM maturation, although the "matured" hiPSC-CMs still retain features of immaturity including irregular shape and absence of t-tubules [118, 160, 161]. We cultured hiPSC-CMs on either a pliable substrate (polydimethylsiloxane, PDMS) or a stiff substrate (glass). All substrates were coated with Matrigel® prior to hiPSC-CM plating. Previous reports using PDMS as a substrate, hiPSC-CMs have more mature electrophysiological features (e.g., increased I_{Na} and I_{K1}, faster upstroke velocity and faster conduction velocity, hyperpolarized RMP, etc.) compared to hiPSC-CMs plated on a

hard substrate [118]. Here, we found that hiPSC-CMs cultured on Matrigel-coated PDMS displayed electrophysiological characteristics consistent with enhanced maturation compared to hiPSC-CMs cultured on Matrigel-coated glass coverlips (Fig. 1). Action potentials recorded from hiPSC-CMs cultured on PDMS displayed hyperpolarized resting membrane potentials and larger action potential amplitudes compared to action potentials recorded from hiPSC-CMs cultured on glass (Table 1, Fig. 1A–C). Additionally, E-4031-sensitive currents, which are indicative of native I_{Kr}, showed a trend to be increased in PDMS-cultured hiPSC-CMs compared to glass-cultured hiPSC-CMs. Steady-state I_{Kr} density, measured at the end of a three second step pulse, was increased from 1.3 ± 0.1 pA/pF in glass-cultured hiPSC-CMs to 1.9 ± 0.3 pA/pF in PDMS-cultured hiPSC-CMs (Table 1, Fig.1D–F). Tail I_{Kr} was similarly increased, from 1.4 ± 0.1 pA/pF in glass-cultured hiPSC-CMs to 2.3 ± 0.3 pA/pF in PDMS-culture hiPSC-CMs (Table 1, Fig. 1D,G,H). hiPSC-CM maturation had no effect on the voltage dependence of I_{Kr} activation (Fig. 1I). There was no significant difference in cell capacitance between immature and matured cells (Fig. 1J).

We also investigated the impact of hiPSC-CM maturation on I_{Kr} kinetics. We fit the decay of tail currents at -40 mV with a bi-exponential equation (Equation 2). The fits yielded fast (τ_{fast}) and slow (τ_{slow}) time constants that were similar in matured (118.4 ± 10 ms and 1,173 ± 216 ms for τ_{fast} and τ_{slow}, respectively) compared to immature hiPSC-CMs (110 ± 15 ms and 1313.5 ± 174 ms for τ_{fast} and τ_{slow}, respectively) (Fig. 2A,B). We also recorded I_{Kr} during a voltage command designed to mimic a human ventricular action potential (Fig. 2C). We integrated E-4031-sensitive currents elicited during the AP waveform and normalized the resultant charge to cell capacitance. Surprisingly, despite the substantial increase in tail I_{Kr} density, there was no significant difference in I_{Kr} charge densities recorded from immature and matured hiPSC-CMs (Fig. 2D). To test if

additional changes in I_{Kr} kinetics could be present in matured hiPSC-CMs, we normalized the I_{Kr} charge recorded during the AP waveform to the peak tail I_{Kr} recorded from the same cell. Like I_{Kr} deactivation, relative repolarizing charge in matured hiPSC-CMs trended to a reduction compared to immature hiPSC-CMs, but the difference was not statistically significant (P = 0.22, Fig. 2E). This may indicate differences in gating kinetics, where channel activation is slowed, or inactivation stabilized.

External acidosis differentially impacts I_{Kr} recorded from mature and immature hiPSC-CMs.

Acidosis has complex electrophysiological effects on hERG1 channels that lead to altered electrical activity. The effects of acidosis on I_{Kr} have been studied previously, revealing changes in the voltage-dependence of activation when the pH was adjusted from 7.4 to 6.3 [133]. Fleet et al., 1985, reported that acidosis in pig myocardium can drive extracellular pH to as low as pH 6.3 [162]. Also, pH 6.3 was previously used to highlight differential proton sensitivity of hERG1a and hERG1b channels in CHO cells [145, 148]. Here, we studied the impact of extracellular acidosis on native I_{Kr} recorded from either immature or matured hiPSC-CMs (Table 1, Fig. 3). Figure 3A depicts representative paired I_{Kr} traces, recorded first in bath solution titrated to pH 7.4 then bath solution titrated to pH 6.3. For I_{Kr} recorded from either immature or matured hiPSC-CMs, pH 6.3 decreased the step pulse and tail pulse current density by ~50% (Table 1, Fig. 3B–E), depolarized the voltage-dependence of activation by ~12 mV (Fig. 3F), and dramatically accelerated the time course of deactivation (Fig. 3G).

Next, we normalized the magnitude of I_{Kr} at pH 6.3 to the maximum I_{Kr} magnitude recorded at pH 7.4 for the same cell (Table 1, Fig. 3B–E). Steady-state I_{Kr} from immature hiPSC-CMs was significantly more sensitive to extracellular acidosis than steady-state I_{Kr} in matured hiPSC-CMs. Tail I_{Kr}, however, displayed a similar trend between immature and PDMS-matured hiPSC-CMs, but it was not statistically significant at -10 mV ($p = 0.73$) (Table 1, Fig. 3B,C, & E). Steady-state I_{Kr} displayed a roughly two-fold increase in inhibition in immature cells compared to matured cells at 0 through +20 mV (Table 1, Fig. 3B,C). Similar to our initial recordings (Fig. 2B), there is a trend that the time course of I_{Kr} deactivation recorded from immature hiPSC-CMs display smaller time constants (117 ± 23 ms at pH 7.4 and 41 ± 11 ms at pH 6.3) than I_{Kr} recorded from matured hiPSC-CMs (195 ± 72 ms at pH 7.4 and 80 ± 35 at pH 6.3), Figure 3G. I_{Kr} deactivation at pH 6.3 does not have a slow component of decay.

These results confirm the experimental observations of previous studies on the impact of protons on hERG1 channel activity. And given the distinct deactivation kinetics and proton sensitivities of I_{Kr} recorded from immature vs matured hiPSC-CMs, these data also suggest that shifts in hERG1 subunit abundance may mediate the response of native I_{Kr} to extracellular acidosis.

hERG1a and hERG1b expression is dependent upon hiPSC-CM maturation.

hERG1 subunit expression is dynamic, varying with development, cell cycle, maturation, and disease states [151, 163-167]. The slowing of I_{Kr} deactivation with maturation suggests an increase in hERG1a relative to hERG1b. The diminished proton sensitivity of I_{Kr} in matured cells also suggests that hERG1a is upregulated, as hERG1a was shown to be less sensitive to protons, compared to hERG1b, in CHO cells [148]. To examine the expression of the hERG1a and hERG1b

subunits in mature and immature hiPSC-CMs, we measured subunit-specific immunofluorescence and mRNA expression levels by qRT-PCR from monolayers cultured on glass or PDMS (Table 2, Fig. 4).

Consistent with our hypothesis, we found that hERG1a immunofluorescence was significantly increased in matured hiPSC-CM monolayers (4.8 ± 0.4 A.U.) compared to immature hiPSC-CM monolayers (3.7 ± 0.3 A.U.) (Table 2, Fig. 4A,B). In contrast, hERG1b immunofluorescence was significantly decreased in matured monolayers (3.0 ± 0.3 A.U.) compared to immature monolayers (5.5 ± 0.5 A.U.) (Table 2, Fig. 4C,D). hERG1a and hERG1b mRNA levels were similarly affected in matured hiPSC-CMs compared to immature hiPSC-CMs (1.5 ± 0.2-fold change and 0.7 ± 0.07-fold change in matured cells for hERG1a and hERG1b mRNA levels, respectively), as shown in Figure 4E. These data demonstrate that hiPSC-CM maturation increases hERG1a expression while decreasing hERG1b expression. These data also further support the hypothesis that hERG1 subunit abundance determines I_{Kr} proton sensitivity in hiPSC-CMs.

PAS expression reduces I_{Kr} proton sensitivity in immature hiPSC-CMs.

Defining the regulatory elements of hERG1 subunits as they pertain to responses to acidosis is a necessary step toward understanding the functional adaptation and impairment of native cardiomyocytes during developmental and pathological processes. Our study revealed that proton inhibition of I_{Kr} is enhanced in immature hiPSC-CMs, where hERG1b expression is upregulated. These data suggest that hERG1b expression promotes proton inhibition of I_{Kr}. To test this hypothesis, we overexpressed a polypeptide identical to the hERG1a PAS domain in immature hiPSC-CMs (Table 3, Fig. 5). This technique has been used in heterologous expression systems

[98, 168] and hiPSC-CMs [89] to mask the impact of hERG1b on heteromeric channel gating. When overexpressed, the PAS polypeptide fills the open receptor site left by the abbreviated hERG1b N-terminal domain [98, 168], and thereby transforms heteromeric hERG1a/1b channel gating to a phenotype indistinguishable from homomeric hERG1a channels.

To validate that the PAS polypeptide was appropriately modifying native hERG1 channel function, we first quantified the magnitude of rectification of GFP and PAS-transduced cells. The hERG1a PAS domain promotes inactivation and thereby enhances rectification [98, 131], thus I_{Kr} recorded from PAS-transduced cells should display increased rectification. We normalized steady-state currents to the maximum peak tail current recorded from the same cell to quantify the magnitude of current inhibition at positive potentials (rectification). As predicted, PAS-transduced cells displayed enhanced rectification of steady-state currents at both pH 7.4 and pH 6.3, compared to GFP-transduced controls (Table 3, Fig. 5B,C). These data demonstrate that the overexpressed PAS domain is modifying the function of the extant hERG1 channels at both pH 7.4 and pH 6.3. Remarkably, the degree of rectification observed in immature hiPSC-CMs expressing PAS was comparable to that seen in matured hiPSC-CMs (Fig. 5D).

As expected, pH 6.3 significantly inhibited I_{Kr} magnitude (Table 3, Fig. 5A,E–H), accelerated I_{Kr} deactivation (Table 3, Fig. 5I), and depolarized the voltage-dependence of I_{Kr} activation (Table 3, Fig. 5J) in both PAS-transduced and GFP-transduced controls. Consistent with our hypothesis, PAS polypeptide overexpression significantly reduced I_{Kr} inhibition by protons, compared to GFP controls (Fig. 5A,E–H). At pH 6.3, normalized steady-state I_{Kr} was reduced by only 40 ± 6% in PAS-transduced cells compared to 65 ± 9% in GFP-transduced cells, at -10 mV (Table 3, Fig. 5E

& F). Tail I_{Kr} was reduced by 44 ± 8% and 54 ± 8% for PAS and GFP-transduced cells, respectively (Table 3, Fig. 5G & H). In fact, the magnitude of proton inhibition of I_{Kr} in PAS-transduced cells was comparable to that observed in our matured hiPSC-CMs (cf. Fig. 3B–E). Together, our findings shed light on how the hERG1a PAS domain, in addition to modulating the kinetic properties of channel gating, plays an important role in the response of hERG1 channels to extracellular acidosis. Finally, these data also demonstrate that the relative abundance of hERG1a and hERG1b subunits influences the magnitude of I_{Kr} inhibition by extracellular protons.

Discussion

The present study investigates the impact of extracellular acidosis on native I_{Kr} recorded from hiPSC-CMs. First, as demonstrated by others [118], the data presented herein validate that hiPSC-CMs cultured on a soft Matrigel-coated PDMS substrate displayed electrophysiological features consistent with enhanced cardiac maturation, including hyperpolarized resting membrane potentials and increased action potential amplitude, when compared to cells plated on Matrigel-coated glass. Additionally, I_{Kr} recorded from PDMS-matured hiPSC-CMs was less sensitive to extracellular protons compared I_{Kr} recorded from immature hiPSC-CMs. Finally, the decrease in proton sensitivity between immature and matured cells was mediated by an increase in the relative abundance of hERG1a and hERG1b subunits at the cell surface membrane.

Proton Modulation of hERG1

The impact of external protons on hERG1a has been well-described in heterologous expression systems, with distinct effects on single channel conductance and gating [137, 139, 140, 143, 147].

Surprisingly, the impact of protons on native I_{Kr} is poorly described. This is of particular importance because native cardiac hERG1 channels comprise both hERG1a and hERG1b subunits [26, 89, 129], and are modulated by other potential accessory subunits (e.g. KCNE1 and KCNE2) and interacting proteins (e.g. KvLQT1) [169-172].

Here we demonstrated that reduced extracellular pH inhibited current density and depolarized the voltage dependence of I_{Kr} recorded from hiPSC-CMs. These data are consistent with other work on native I_{Kr} [133, 173]. Interestingly, our study demonstrated that the degree of I_{Kr} inhibition by protons correlated with the relative abundance of the hERG1b subunit. Work in CHO cells has also demonstrated that inhibition of hERG1 conductance by protons is more pronounced in channels that contain the hERG1b subunit, compared hERG1a homomeric channels [148]. In this study, proton inhibition of I_{Kr} was greatest in immature hiPSC-cardiomyocytes, where hERG1b was upregulated. The enhanced inhibition by protons was then abolished by increasing the number of PAS domains per channel, effectively transforming hERG1b subunits into hERG1a subunits. Importantly, the time course of deactivation is an additional marker of PAS activity, where PAS-deficient heteromeric hERG1a/1b channels display faster deactivation compared to homomeric hERG1a channels. However, because of the dramatic accelerating effects of protons on deactivation, it is not a reliable marker of PAS action at reduced pH. Accordingly, our data demonstrate that hERG1 subunit stoichiometry mediates proton inhibition of I_{Kr} in hiPSC-CMs.

It is unclear how hERG1b selectively enhances proton inhibition of channel conductance without altering the impact of protons on channel gating. This is somewhat surprising given the pronounced

accelerating effects that hERG1b has on hERG1 channel gating, particularly deactivation [26, 88, 131]. hERG1 has proton binding sites at the pore and voltage-sensing domains that modulate conductance and gating, respectively, with different pH sensitivities (Fig. 6) [137, 139, 140, 143, 147, 174]. At the voltage sensing domain, mutating a trio of aspartates to alanines (D456A/D460A/D509A) disrupts proton modulation of channel gating [139, 174, 175]. Proton block, however, is critically dependent upon residues E575 and H578 at the hERG1 pore turret, where the combined mutations E575Q and H578N abolish proton block without affecting proton modulation of deactivation [147]. Although they are located on the outer circumference of the hERG1 pore, these proton binding sites (at least E575 and H578) alter the electrostatic environments in and around the selectivity filter [147]. It was proposed that the outer hERG pore near the selectivity filter is somewhat flexible [18, 176, 177], underlying inactivation and possibly providing a mechanism to transmit protonation of E575 and H578 to changes in hERG1 channel conductance and open time [18, 147, 178]. Nonetheless, this must be approached with caution because only the E575 side chain was shown in the hERG1 cryo-EM structure to directly interact with residues that connect to the selectivity filter [18]. Because the residues involved in proton sensitivity are found in both hERG1a and hERG1b, it is possible that based on the cryo-EM structure, the greater effect we observed on cells preferentially expressing hERG1b was due to indirect/allosteric consequences of the unique hERG1b N-terminus that favor exposure of E575 and H578 to protons. Another possibility is that the residues H578 and H587, which are found in a relatively disordered channel region (Fig. 6) [18], may be involved in the removal of the proton block of the pore because they are in a more flexible region of the channel and may interact with other residues (e.g., D580) that can modulate the channel's proton sensitivity indirectly, adding to the possibility of distinct conformations during gating and/or channel composition . Finally,

intracellular acidosis does not affect hERG1a homomeric channels [144], but we cannot rule out that the short hERG 1b N-terminus may expose intracellular proton binding sites, otherwise occluded by the hERG1a PAS domain.

Protons in I_{Kr}-Mediated Cardiac Dysfunction

Cardiac acidosis occurs under a number of physiological and pathophysiological conditions. Two conditions, ischemic heart disease and sudden infant death syndrome (SIDS), are particularly affiliated with hERG1 dysfunction. In chronic cardiac dysfunction, i.e. heart failure, native I_{Kr} is significantly downregulated [179, 180] and the relative abundance of hERG1b to hERG1a is increased [157]. These changes in I_{Kr} occur alongside the downregulation of other major K^+ currents: I_{Ks}, I_{to}, and I_{K1} [181-183]. The reduced I_K contributes collectively to the reduced repolarization reserve, prolonged action potential duration, and overall heightened arrhythmogenic potential in the failing myocardium. Our data suggest that a relative increase in hERG1b in the failing heart would also enhance I_{Kr} sensitivity to protons during ischemic events. And although hERG1b homomeric channels may not exist in adult hearts – hERG1b subunits preferentially associate with hERG1a – [184, 185], the relative expression of hERG1a and hERG1b subunits appears heterogeneous in cardiac tissue [128, 154, 186]. In this regard, regional variation in hERG1 isoform abundances could facilitate heterogeneity of repolarization and arrhythmogenesis during acidosis.

hERG1 subunits in neonatal and fetal demise

KCNH2 variants have long been linked with sudden infant death syndrome (SIDS) [7, 8, 122]. Respiratory acidosis is one hypothesis proposed to explain the association of stomach sleeping with SIDS [123, 187]. Interestingly, hERG1a mRNA is upregulated and hERG1b mRNA is downregulated in adult human cardiac tissue compared to fetal cardiac tissue [7]. These molecular data combined with our electrophysiological data suggest that upregulated hERG1b in the immature heart could promote proton inhibition of I_{Kr} during respiratory acidosis, and thereby contribute to SIDS. The shifts in subunit abundance during maturation also predict that the pathophysiological impact of hERG1b-specific mutations would be greatest in the immature heart and vice versa for hERG1a-specific mutations. Indeed, the only two hERG1b-specific mutations identified to date were a case of intrauterine fetal death, R25W, [7] and an 8-year old girl, A8V, [131]. Interestingly, similarly to other mutations found in SIDS cases (R273Q and R954C/K897T), the mutation R25W generates a profound reduction in current density when expressed as heterotetramers with the hERG1a subunit [7, 10, 124].

For normal heart function, these two hERG1 subunits must be functionally expressed. Changes in the abundance of hERG1a or hERG1b can cause proarrhythmic events [89, 131, 152]. Clearly, there is a link between LQTS2 and intrauterine fetal death [7, 188-190]. hERG1 channel variants that have been solely linked with SIDS have the potential to be LQTS variants. And it is possible that LQTS cases are being disguised under the SIDS umbrella, setting a precedent for future research into the role of cardiac channelopathies.

Subunit-Selective Modulators

Protons are not the only factor shown to differentially modulate homomeric and heteromeric hERG1 channels. Several studies have demonstrated that subunit abundance, and its impact on gating, mediates the channel's response to a subset of clinically relevant drugs [131, 191, 192]. Additionally, ANP and cGMP perfusion were both shown to selectively inhibit hERG1b-containing channels heterologously expressed in HEK293 cells [193]. In the same study, the authors demonstrated that cGMP inhibited I_{Kr} recorded from atrial but not ventricular murine myocytes, suggesting that mERG1b (mouse ERG1b) was more expressed in atrial than in ventricular murine tissue [193]. Assuming that mERG1b is primarily expressed in the atria, and based on findings from computational modelling indicating that the gain-of-function mutations L532P and N588K cause a higher and earlier peak of I_{Kr} during atrial APs and lead to rotor formation [194], we postulate that ERG1b subunit expression may play a key role in atrial fibrillation [195]. In contrast, hERG1b shows a protective effect against oxidative inhibition, presumably by regulating access to a key residue in the channel's C-linker domain C723 (hERG1a numbering). Roughly two thirds of the protective effect from hERG1b was attributable to the subunit's acceleration of channel deactivation [196].

The fact that hERG1b is upregulated in "immature" hiPSC-cardiomyocytes underscores the need for increased understanding of mechanisms regulating hERG1 subunit abundance. Drugs that preferentially target hERG1 isoforms may be one approach to overcome obstacles in treating disorders in the heart and other tissues where hERG1 is a contributing factor. The two hERG1 isoforms are expressed in distinct ratios and contribute differently to the maintenance of hERG1 currents in tissues where hERG1 is functional. For example, while hERG1b is expressed at lower

levels in the human heart, it is the predominant isoform in tumor cells [197]. In B-cells and T-cell lineage, while hERG1b is upregulated, the other isoform, hERG1a, is downregulated [198]. Therefore, identifying the mechanisms that control hERG1 subunit abundance could improve clinical therapies in diseases throughout the body.

Conclusion

The experimental data presented herein show for the first time the effects of extracellular acidosis on native I_{Kr} recorded from hiPSC-cardiomyocytes following shifts in hERG1 subunit abundance. And although the exact tetrameric conformation of native hERG1 channels remains elusive, these findings provide insight into the response of adult and immature cardiomyocytes to an acidic environment.

Limitations

Here, we report data from experiments conducted in immature and matured hiPSC-CMs. While our studies demonstrate the impact of extracellular acidosis in a human cardiomyocyte model, hiPSC-CMs still cannot recapitulate the chamber-specific or layer-specific electrical phenotypes of intact cardiac tissue. And though tools to enhance hiPSC-CM maturation have improved, the "PDMS-matured" hiPSC-CMs used in this study still display significant markers of immaturity, including irregular shape, disorganized contractile machinery, and spontaneous action potential firing. Thus, the PDMS-matured hiPSC-CMs are not an accurate model of an adult ventricular cardiomyocyte, and comparison of the effects observed in this manuscript with the adult myocardium should be done with caution. Additionally, native I_{Kr} magnitudes are relatively small,

particularly at pH 6.3, which increases experimental variability. Nonetheless, these data provide important insight into the triggers of I_{Kr} dysfunction during extracellular acidosis.

Materials and Methods

Stem Cell Culture and Cardiac Differentiation

DF19-9-11 human iPS cells were obtained from the WiCell Research Institute (Madison, WI). Cells were cultured and differentiated into cardiomyocytes using the GiWi protocol, as described [199]. Stem cells were seeded on Matrigel-coated plasticware with iPS-brew medium. Spontaneous differentiation was removed, and cells were passed at 70% confluence. At the day of cell passage, cells were re-seeded to continue the line, or to grow monolayers for cardiac-directed differentiation. 4×10^5 cells were plated into each well of a 6-well plate and cultured to ~80% confluence for treatment with GSK3 inhibitor and induction of mesodermal differentiation (day 0). Following mesodermal differentiation, cells were treated with a Wnt inhibitor for induction of cardiac mesoderm (day 2). On day 4, Wnt inhibitor was removed to direct the cells into cardiac progenitor cells. hiPSC-cardiomyocytes with autonomous contractility emerged eight to ten days after initiation of cardiac-directed differentiation. The hiPSC-cardiomyocytes were cultured until 20 days after initiation of differentiation and purified using by magnetic-beads assisted isolation with an hiPSC-Derived Cardiomyocyte Isolation Kit, human (Miltenyi Biotec, USA). Purified hiPSC-cardiomyocytes were then plated on either Matrigel-coated glass coverslips (immature cells) or Matrigel-coated polydimethylsiloxane (matured cells) for seven days before completing experiments. hiPSC-CMs cultured on glass display electrical characteristics consistent with embryonic/early fetal cardiomyocytes including depolarized resting membrane potential, reduced action potential upstroke velocity, and reduced action potential amplitude [200, 201]. hiPSC-CMs cultured on PDMS display characteristics consistent with enhanced maturation, similar to late fetal/neonatal electrophysiology including: hyperpolarized resting membrane potentials, increased action potential amplitude and

upstroke velocity, increased expression of mature sarcolemma components (e.g., SCN5A, Kir2.1, and Cx43), as well as myofilament markers (cTnI), and faster conduction velocities [118, 161].

Adenovirus transduction of hiPSC-CMs

hiPSC-CMs were replated at a low density onto Matrigel-coated glass coverslips in a 6-well plate and maintained at 37°C in 5% CO_2 for at least 72 h before transduction. hiPSC-CMs were then transduced for 48 h and then refreshed with RPMI/B27+ media. hiPSC-CMs were transduced with either GFP-encoded adenovirus or the scFv2.10-CFP encoded adenovirus (University of Michigan Viral Vector Core). Fluorescence was monitored after 24 h to verify successful transduction. Contracting fluorescent hiPSC-CMs were used for electrophysiology experiments 48 h after transduction.

RT-qPCR

For quantitative evaluation of the steady-state mRNA expression in hiPSC-CM cultures, total RNA was prepared using the RNeasy Mini Kit (Qiagen), including DNAse treatment. 300 ng of RNA were reverse transcribed and converted to cDNA with oligo$(dT)_{12–18}$ primers using reverse transcriptase according to the manufacturer's specifications, M-MLV Reverse transcriptase (Cat # 28025-013, Invitrogen). Quantitative PCR was performed using IDT Mastermix (Cat # 1055772, ThermoFisher) and TaqMan assay primers (Cat # 4331182 and 43513752, 10 µM; ThermoFisher) for *KCNH2*, 1a and 1b isoforms. The PCR condition consisted of 95°C for 30 secs, followed by

39 cycles of 95°C for 3 secs and 60°C for 20 secs, followed by melting-curve analysis to verify the correctness of the amplicon.

The samples were analyzed in technical triplicates using the primers included in the TaqMan Assay system (Invitrogen) and run in a Biorad C1000 Touch Thermal Cycle CFX96 (Applied Biosystems). The expression of the mRNA of the gene of interest relative to the internal control GAPDH in samples from immature and matured hiPSC-CMs was calculated by the ΔΔCT method, based on the threshold cycle (CT), as fold change = 2^−(ΔΔCT), where $\Delta CT = CT_{\text{gene of interest}} - CT_{GAPDH}$ and $\Delta\Delta CT = \Delta CT_{\text{Matured hiPSC-CMs}} - \Delta CT_{\text{Immatured hiPSC-CMs.}}$ From each experiment, the cDNA of 3 cell culture wells were measured as biological replicates of each cell maturation state. Each cell culture well was measured from at least 3 separate cardiomyocyte differentiation.

Immunocytochemistry

hiPSC-CMs were seeded either on glass or PDMS and fixed with 4% paraformaldehyde/PBS for 15 min. Then, hiPSC-CMs were washed 5 min with PBS and blocked with block solution (PBS + 1% BSA + 0.5% Triton X + 10% Goat Serum secondary antibodies) for 1 h. Incubation with primary antibodies was done in block solution for overnight at 4°C. The next day, to washout the excess of primary antibody, hiPSC-CMs were washed 3×5min with PBS. Next, secondary antibodies in block solution (without Triton X) were added to each slip and incubated for 1 h in the dark at room temperature. hiPSC-CMs were kept in dark, washed with PBS 3×5 min, and mounted with ProLong Gold antifade reagent (Thermo Fisher) and a coverslip. Both primary and secondary antibodies were diluted in block solution (without Triton-X).

Differentiated cardiac lines were validated using immunocytochemistry targeting actin (phalloidin, cat #A12379 ThermoFisher) to display the cardiac sarcomeric organization, and patch clamp electrophysiology measuring cardiac I_{Kr}, indicative of hERG1 expression. Phalloidin-488 comes with a fluorophore conjugated so no secondary Ab incubation was needed. To target the hERG1a isoform, hiPSC-cardiomyocytes were immunolabeled with a 1:200 dilution of the primary antibody #ALX-215-050-R100 (Enzo Life Sciences). To target the hERG1b isoform, the primary antibody #ALX-215-051-R100 was used in a 1:200 dilution (Enzo Life Sciences). In both cases, a 1:250 dilution of secondary antibody goat anti-rabbit Alexa Fluor 647 (#4050-31, Southern Biotec) was used. The nuclei were labeled using 1:1000 dilution of DAPI (1µg/ml) for 15 minutes (ThermoScientific, Cat. #62248). Immunostained preparations were analyzed by confocal microscopy, using a confocal microscope (Zeiss 880) to determine protein localization. Images were analyzed using FIJI where we measured mean hERG immunofluorescence intensity in the cytoplasmic region of the cell from matured or immature hiPSC-CMs.

Electrophysiology

Standard patch-clamp techniques were used to measure both action potential clamp waveform and I_{Kr}. All recordings were completed at physiological temperature (37 ± 1°C) using whole-cell patch clamp with an IPA® Integrated Patch Amplifier run by SutterPatch® (Sutter Instrument) and Igor Pro 8 (Wavemetrics). Leak subtraction was performed off-line based on measured current observed at potentials negative to I_{Kr} activation. The inter-pulse duration for all recordings was 10 seconds where cells were at -40 mV.

Data were sampled at 5 kHz and low-pass filtered at 1 kHz. Cells were perfused with extracellular solution containing (in mM): 150 NaCl, 5.4 KCl, 1.8 $CaCl_2$, 1 $MgCl_2$, 15 glucose, 10 HEPES, 1 Na-pyruvate, and titrated to pH 6.3 and pH 7.4 using NaOH. Fleet et al., 1985, reported that acidosis in pig myocardium can drive extracellular pH to as low as pH 6.3 [162]. Also, pH 6.3 was previously used to highlight differential proton sensitivity of hERG1a and hERG1b channels in CHO cells [145, 148]. Recording pipettes had resistances of 2–5 MΩ when backfilled with intracellular solution containing (in mM): 5 NaCl, 150 KCl, 2 $CaCl_2$, 5 EGTA, 10 HEPES, 5 MgATP and titrated to pH 7.2 using KOH. Intracellular solution aliquots were kept frozen until the day of recording. We kept the intracellular solution on ice during recordings and discarded it 2–3 hours post-thaw.

To isolate I_{Kr}, all protocols were completed before and after extracellular perfusion of 2 μM of the I_{Kr}-specific blocker, E-4031. To inactivate sodium currents, a 100-ms step to -40 mV was applied before the any I_{Kr} recordings. To assess the voltage dependence of I_{Kr} activation, cells were stepped from a holding potential of -40 mV to a three second pre-pulse between -50 and +50 mV in 10 mV increments. Tail currents were then measured during a -40 mV, 3 second test pulse. Peak tail current was normalized to cellular capacitance, plotted as a function of pre-pulse potential, and fitted with the following Boltzmann equation:

$$\textit{Equation 1:} \quad y = \left[\frac{A_1 - A_2}{1 + e^{(V - V_0)/k}}\right] + A_2,$$

where A_1 and A_2 represent the maximum and minimums of the fit, respectively, V is the membrane potential, V_0 is the midpoint, and k is the slope factor. The time course of I_{Kr} deactivation was assessed by fitting current decay during the test pulse with a double exponential function:

$$\textit{Equation 2:} \quad y = Y_0 + A_1 e^{-t/\tau_1} + A_2 e^{-t/\tau_2},$$

where Y_0 is the asymptote, A_1 and A_2 are the relative components of the fast and slow time constants τ_1 and τ_2, respectively. The magnitude of I_{Kr} rectification was quantified by dividing the average I_{Kr} during the final 10 ms of each step pulse by the maximum peak outward tail current evoked at -40 mV. Repolarizing charge was calculated by integrating I_{Kr} recorded during a voltage protocol that mimics a human ventricular action potential[202].

Statistical Analysis

Analysis was completed using Prism 8 (GraphPad) and Igor Pro 8 (Wavemetrics). Values were first tested for normality (Shapiro-Wilk test) and for outlier identification (ROUT and Grubbs' tests) before statistical evaluation. All data are reported as mean ± SD and were compared using a non-parametric Mann-Whitney test or 2-way ANOVA with a Bonferroni post-hoc test, where applicable. Statistical significance was taken at $p < 0.05$. Data points greater than two times the standard deviation were termed outliers and excluded from analysis. The fraction of excluded data was no more than the 10% of each data set. Unless stated otherwise, the number *n* of observations indicated reflects the number of hiPSC-CMs recorded from each cell line from at least 3 differentiations. All experiments were performed as a single-blind study to avoid sources of bias.

Figures

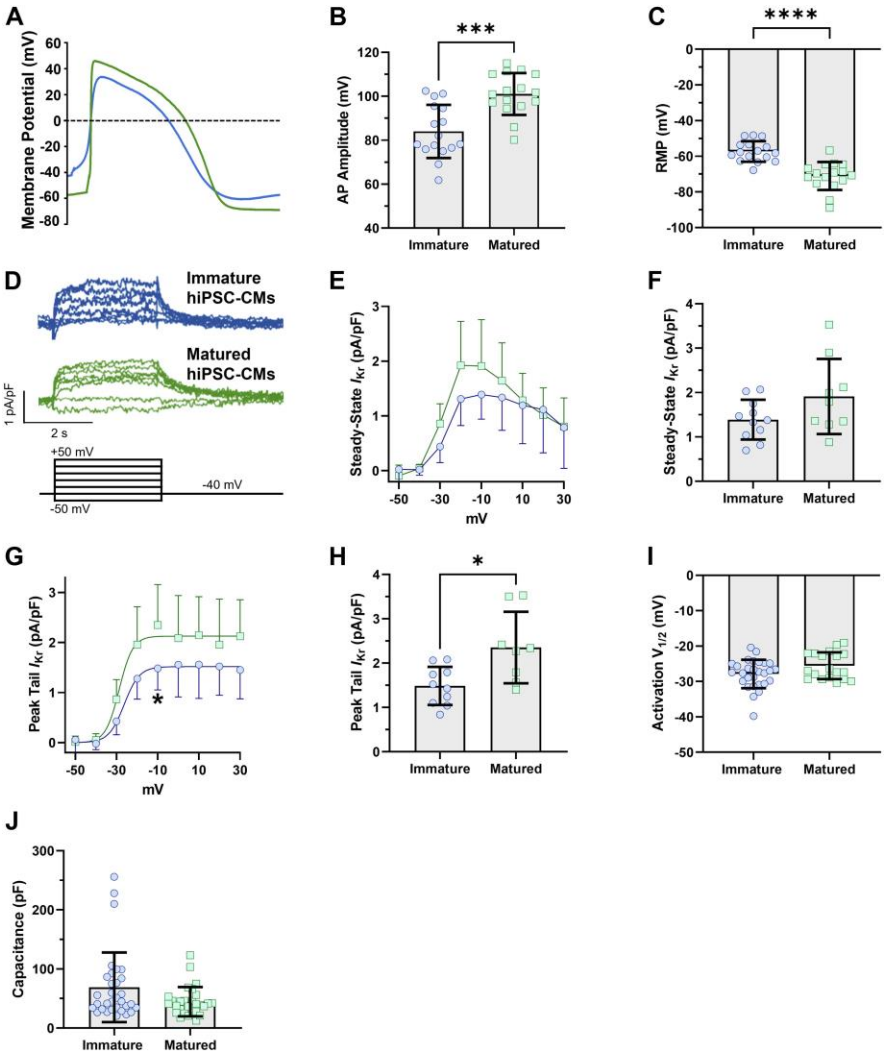

Figure 3.1 hiPSC-CM maturation with PDMS hyperpolarizes the AP and increases I_{Kr} density

A) Action potential recordings from cells cultured on glass (blue) and PDMS (green). B–C) AP parameters. Cells plated on PDMS demonstrated more hyperpolarized resting membrane potential and greater action potential amplitude than cells plated on glass. D) Representative I_{Kr} traces elicited by the protocol at bottom. E) Steady-State I_{Kr} measured at the end of the step pulse, recorded from immature and matured hiPSC-CMs. F) Steady-State current densities at -10 mV.

G) Tail I_{Kr} in immature and matured hiPSC-CMs. H) Tail current densities at -10 mV. hiPSC-CMs plated on PDMS had larger ERG currents than hiPSC-CMs plated on glass. I) There was no significant difference in the voltage dependence ($V_{1/2}$) of I_{Kr} activation recorded from immature hiPSC-CMs versus matured hiPSC-CMs. J) There was no statistically significant difference in the cellular capacitance between immature and matured hiPSC-CMs. Data were compared using a two-way ANOVA test and a two-tailed Mann-Whitney test where appropriate. Errors bars represent mean ± SD. N-value = 3, n-value ≥ 8. ****$P < 0.0001$, ***$P = 0.0002$, and *$P < 0.05$.

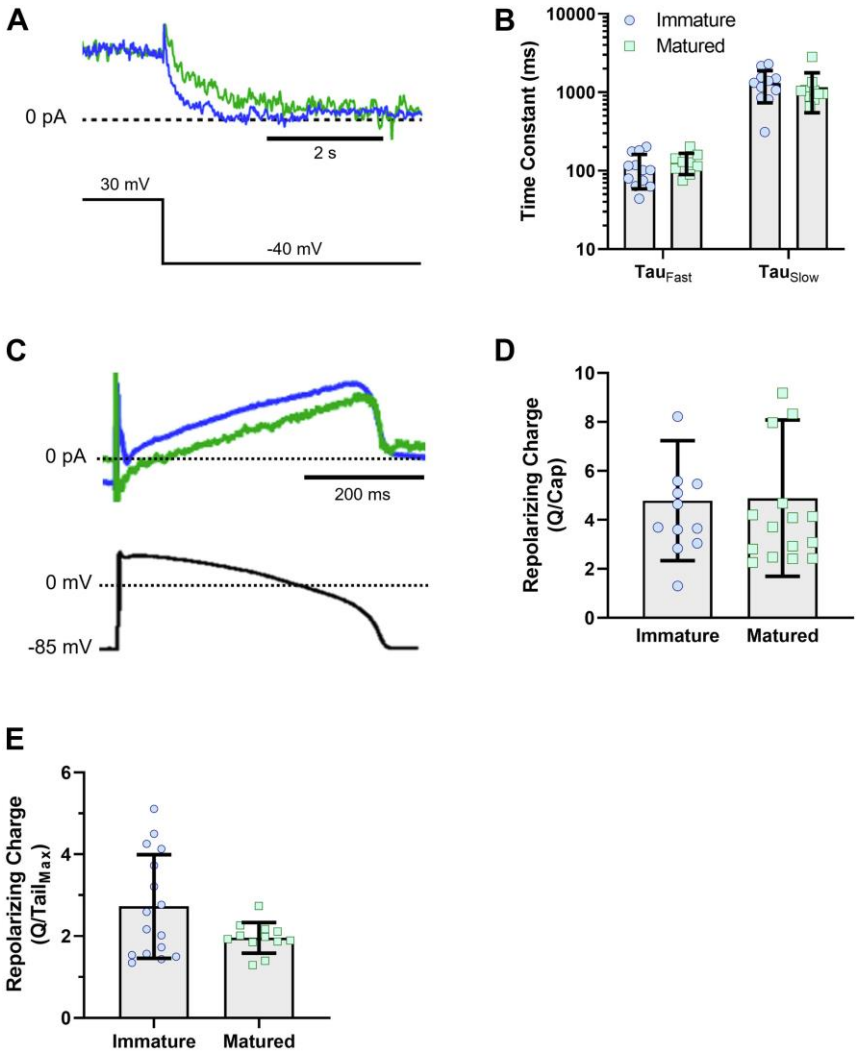

Figure 3.2 Effect of cell maturation on I_{Kr} deactivation

A) Tail I_{Kr} traces recorded from immature (blue) and matured (green) hiPSC-CMs at -40 mV. B) Corresponding deactivation time constants for I_{Kr} recorded from hiPSC-CMs cultured on glass (immature) versus PDMS (matured). C) Representative I_{Kr} traces recorded from immature (blue) and matured (green) hiPSC-CMs using a ventricular AP clamp protocol. D) Repolarizing charge normalized to the cell capacitance in matured and immature hiPSC-CMs. E) Repolarizing charge normalized to the peak-tail I_{Kr} of the same cell recorded from matured and immature hiPSC-CMs. Two-tailed Mann-Whitney test. Errors bars represent mean ± SD. N-value = 3, n-value $\geq$10.

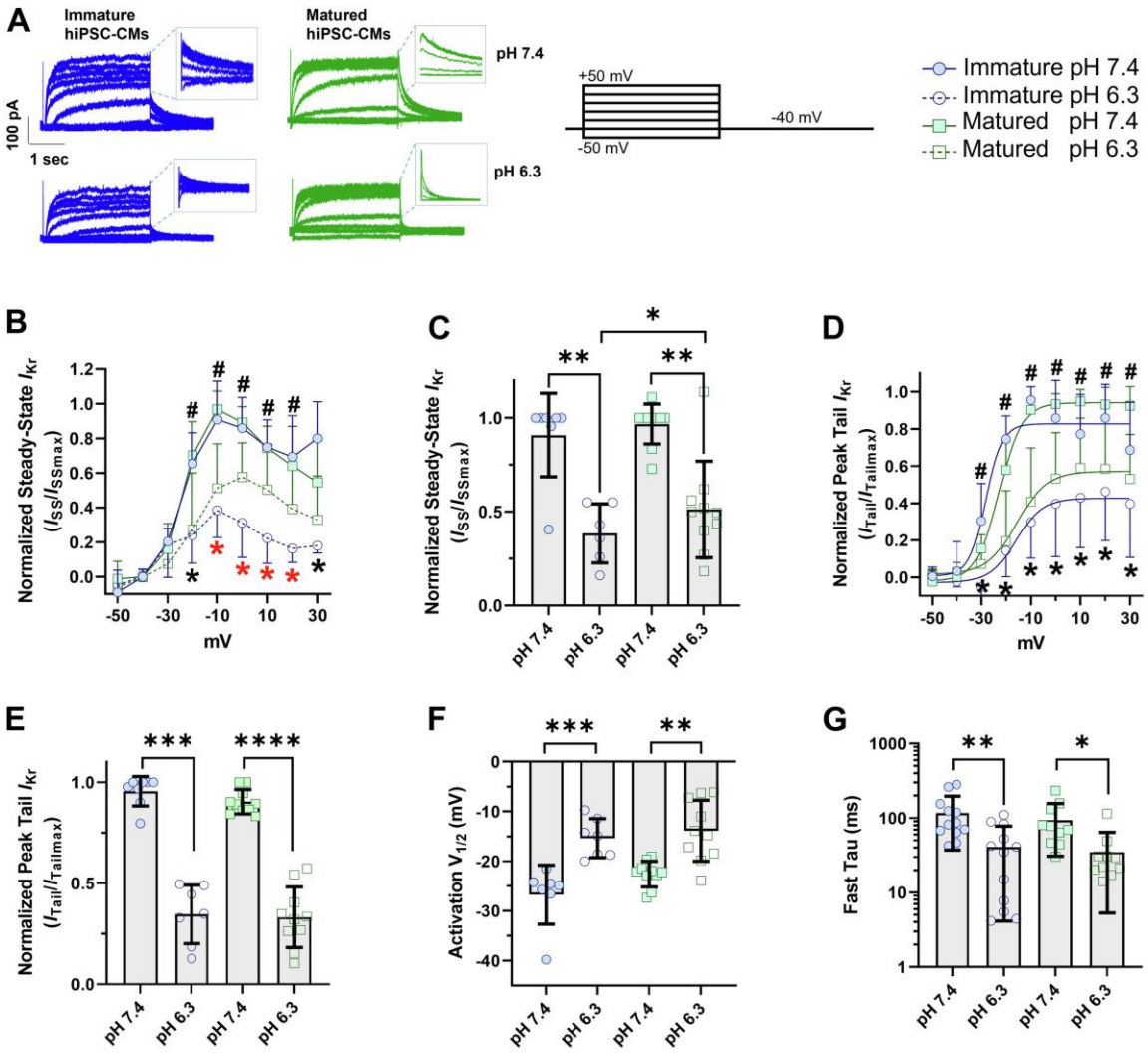

Figure 3.3 Proton sensitivity of native I_{Kr} corresponds with hiPSC-CM maturation

A) Representative I_{Kr} traces elicited by the protocol below from matured and immature hiPSC-CMs at pH 7.4 and pH 6.3. B) Steady-state I_{Kr} density in immature and matured hiPSC-CMs at pH 7.4 and pH 6.3. C) Normalized Steady-State current densities at -10 mV. D) Peak-tail I_{Kr} density in immature and matured hiPSC-CMs in control and acidic environment. E) Normalized peak-tail I_{Kr} densities at -10 mV. The symbols * (black and red) and # represent the statistical significance of normalized Peak tail and Steady-State I_{Kr} at pH 7.4 vs pH 6.3 in immature and matured hiPSC-

CMs, respectively. The symbol * (red only) denotes significant difference between immature and matured hiPSC-CMs at pH 6.3. F) Voltage-dependence of activation ($V_{1/2}$) for I_{Kr} from immature and matured hiPSC-CMs in control and acidic environment. G) Time constants of I_{Kr} deactivation recorded from immature and matured hiPSC-CMs at pH 7.4 and acidic pH 6.3. Data were compared using a two-way ANOVA and a two-tailed Mann-Whitney test. Errors bars represent mean ± SD. N-value = 3, n-value ≥ 9. ****$P < 0.0001$, ***$P = 0.0008$, **$P = 0.0024$, and *$P < 0.05$.

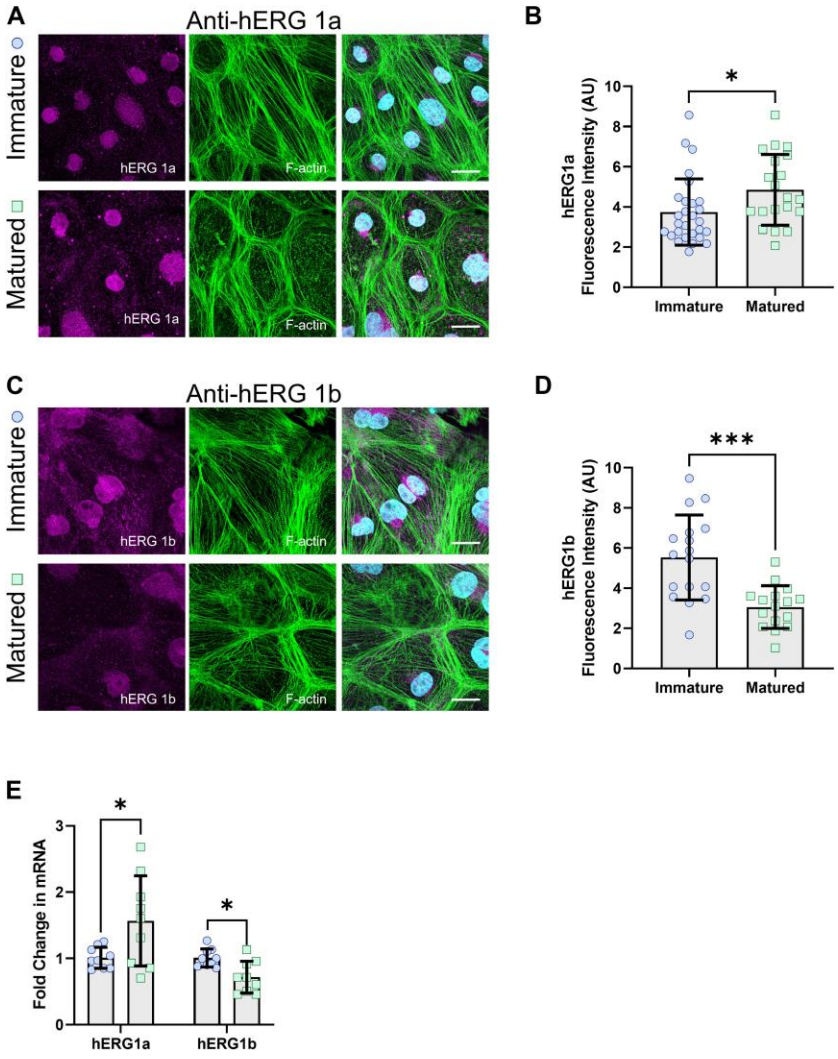

Figure 3.4 hERG1 subunit abundance in matured and immature hiPSC-CMs

A) Representative immunostainings for hERG1a and F-actin. B) Quantification of mean hERG1a immunofluorescence from matured and immature hiPSC-CMs. C) Representative immunostainings for hERG1b and F-actin. D) Quantification of mean hERG1b immunofluorescence from matured and immature hiPSC-CMs. E) hERG1a and hERG1b mRNA levels in matured and immature hiPSC-CMs. Data were compared using a two-tailed Mann-Whitney test. Errors bars represent mean ± SD. N-value = 3, n-value ≥ 8. ****P* = 0.0002, and **P* < 0.05. Scale bars indicate 25 µM.

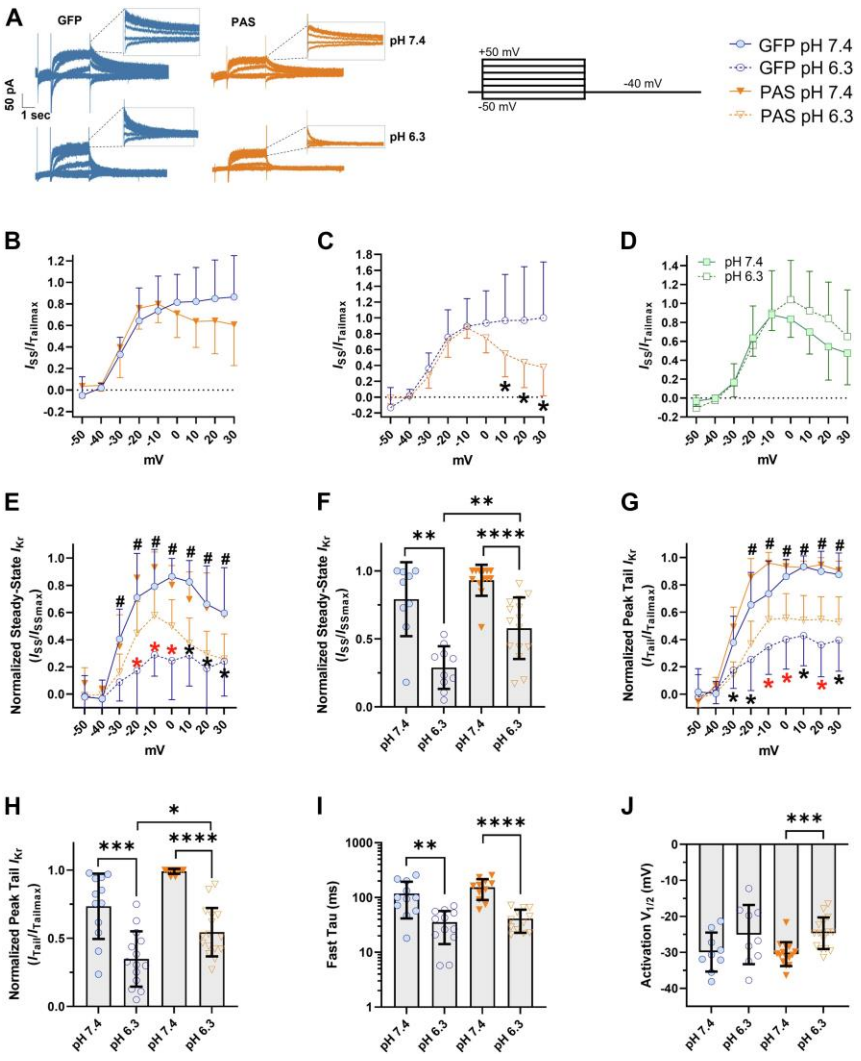

Figure 3.5 PAS domain expression diminishes I_{Kr} proton sensitivity in immature hiPSC CMs

A) Representative I_{Kr} traces elicited by the protocol below from PAS (orange) and GFP (blue)-transduced hiPSC-CMs at pH 7.4 and pH 6.3. B–C) Steady-state I-V relationships normalized to the maximum peak tail I_{Kr} from immature hiPSC-CMs expressing either GFP or PAS, at pH 7.4 and 6.3, respectively. D) Steady-state I-V relationships normalized to the maximum peak tail I_{Kr} recorded from the same cell for matured hiPSC-CMs at pH 7.4 (solid symbols) and 6.3 (open symbols), respectively. E) Steady-state I_{Kr} at pH 7.4 and 6.3 in immature hiPSC-CMs

overexpressing PAS or GFP. F) Normalized steady-state current densities at -10 mV. G) Peak-tail I_{Kr} levels measured at pH 7.4 and 6.3 in immature hiPSC-CMs overexpressing PAS (orange) or GFP (blue). H) Normalized tail current densities at -10 mV. I) Deactivation kinetics from GFP and PAS-expressing hiPSC-CMs. J) Voltage-dependence of activation ($V_{1/2}$) in immature and matured hiPSC-CMs at pH 7.4 and pH 6.3. The symbols * (black and red) and # represent the statistical significance of normalized Peak tail and Steady-State I_{Kr} at pH 7.4 vs pH 6.3 in GFP and PAS-transduced hiPSC-CMs, respectively. The symbol * (in red) represent statistical differences between PAS and GFP-transduced hiPSC-CMs at pH 6.3. Data were compared using a two-way ANOVA and a two-tailed Mann-Whitney test. Errors bars represent mean ± SD. N-value = 3, n-value ≥ 10. ****$P < 0.0001$, ***$P = 0.0008$, **$P < 0.0036$, and *$P < 0.05$.

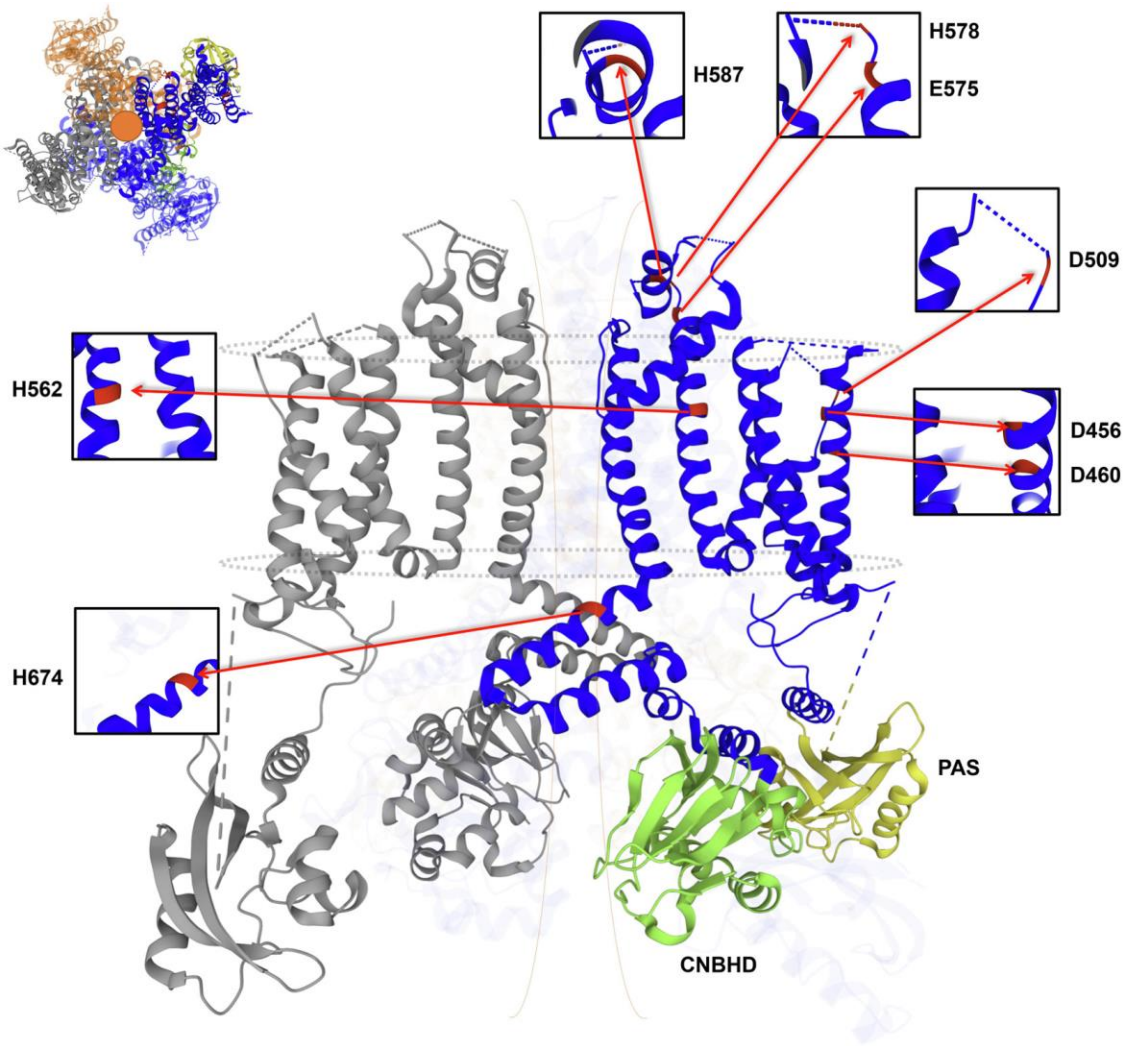

Figure 3.6 Cryo-EM structure of the hERG1a channel with predicted locations of residues identified as proton sensors

Predicted pronatable amino acids modelled on the hERG1a cryo-EM structure (PBD: 5VA1) using the RCSB PBD (rcsb.org) [140, 147, 174, 175, 203, 204]. Eight residues are highlighted: E575, H578, and H587 in the pore turret, D509 in the S3 helix, D456 and D460 in the S2 helix, H562 in the S5 helix, and H674 in the S6 helix/CNBHD linker. Black boxes depict expanded view of each residue position. The CNBHD and PAS are highlighted in green and yellow, respectively. Dashed

blue lines represent regions unresolved in the cryo-EM structure. Inset depicts a top-down view of the tetrameric subunit arrangement of the hERG1a channel cryo-EM structure.

Tables

		Immature	SD	*n*	Matured	SD	*n*
APA (mV)		84**	12.08	16	101.03	9.54	16
RMP (mV)		-57.29****	5.75	16	-71.04	7.86	16
Steady-state I_{Kr} at -10 mV (pA/pF)		1.39	0.44	11	1.91	0.84	9
Peak tail I_{Kr} at -10 mV (pA/pF)		1.48*	0.43	10	2.35	0.8	8
Steady-state I_{Kr} at -10 mV (pA/pF)	pH 7.4	1.47***	0.47	7	1.91**	0.84	10
	pH 6.3	0.3*	0.27	6	0.93	0.52	10
Peak tail I_{Kr} at -10 mV (pA/pF)	pH 7.4	0.78*	0.61	8	1.61***	0.61	10
	pH 6.3	0.36	0.4	7	0.65	0.4	10
Relative Steady-state I_{Kr} at -10 mV (I_{SS}/I_{SSMAX})	pH 7.4	0.9**	0.22	7	0.96**	0.1	10
	pH 6.3	0.38*	0.15	6	0.51	0.25	10
Relative Peak tail I_{Kr} at -10 mV ($I_{Tail}/I_{TailMAX}$)	pH 7.4	0.95***	0.07	8	0.9****	0.06	10
	pH 6.3	0.34	0.14	7	0.33	0.14	10
$V_{1/2}$ (mV)	pH 7.4	-26.74***	5.95	7	-22.58**	2.57	10
	pH 6.3	-15.39	3.92	7	-13.88	6.13	10
Fast Tau (ms)	pH 7.4	117.04**	79.84	12	194.83*	249.35	12
	pH 6.3	40.96	36.82	12	80.45	122.93	12

APA: Action Potential Amplitude, RMP: Resting Membrane Potential. Two-tailed Mann-Whitney test. N-value = 3, n-value ≥ 6. *****$P < 0.0001$, ***$P \leq 0.0008$, **$P = 0.0024$, and *$P < 0.05$.

Table 3.1 Biophysical parameters of immature and matured hiPSC-CMs.

	Immature	SD	*n*	Matured	SD	*n*
hERG1a fluorescence intensity (AU)	3.74*	1.65	28	4.85	1.76	20
hERG1b fluorescence intensity (AU)	5.53***	2.11	17	3.05	1.06	16
hERG1a mRNA levels (AU)	1.01*	0.15	9	1.5	0.67	9
hERG1b mRNA levels (AU)	1*	0.13	9	0.71	0.23	9

Two-tailed Mann-Whitney test. N-value = 3, n-value ≥ 9. ***$P = 0.0002$ and *$P < 0.05$.

Table 3.2 hERG1a and hERG1b expression in immature and matured hiPSC-CMs.

		GFP-transduced	SD	*n*	PAS-transduced	SD	*n*
Steady-state I_{Kr} at -10 mV (I_{SS}/I_{SSMAX})	pH 7.4	0.79**	0.27	9	0.93****	0.11	13
	pH 6.3	0.28**	0.15	10	0.57	0.22	15
Peak tail IKr at -10 mV ($I_{Tail}/I_{TailMAX}$)	pH 7.4	0.73***	0.23	12	0.99****	0.01	13
	pH 6.3	0.34*	0.2	14	0.54	0.17	16
Steady-state I_{Kr} at -10 mV (pA/pF)	pH 7.4	2.23*	2.12	9	2.19**	1.75	13
	pH 6.3	1.22	0.84	10	1.49	1.18	15
Peak tail I_{Kr} at -10 mV (pA/pF)	pH 7.4	2.18*	1.77	12	2.72*	2.27	13
	pH 6.3	0.94*	0.68	14	1.58	1.12	16
$V_{1/2}$ (mV)	pH 7.4	-29.93***	5.41	9	-30.49	3.32	15
	pH 6.3	-25.06	8.2	9	-24.68	4.39	15
Fast Tau (ms)	pH 7.4	118.13**	76.66	11	153.44****	62.86	11
	pH 6.3	35.5	21.36	12	41.42	18.64	12

Two-tailed Mann-Whitney test. N-value = 3, n-value ≥ 9. *****P < 0.0001, ***P = 0.0008, **P < 0.0036, and *P < 0.05.

Table 3.3 Biophysical parameters of GFP and PAS-transduced hiPSC-CMs.

Chapter 4 Discussion and Future Directions

Summary

hERG1 is a major regulator of cardiac repolarization. When I_{Kr} is disrupted, cardiac electrical signaling becomes unstable, promoting arrhythmia and sudden cardiac death. Loss-of-function *KCNH2* variants and off-target pharmacological drug interactions that inhibit hERG1 function can cause LQTS2 and acquired LQTS, respectively, which predispose individuals to *torsades de pointes*, an often-lethal ventricular tachycardia, and sudden cardiac death [2, 6-11]. I_{Kr} is also downregulated during heart failure [179, 180]. Understanding the regulatory mechanisms of hERG1 to avoid off-target hERG1 block and identify new antiarrhythmic therapeutics is a priority in academia and the pharmaceutical industry. To this end, this body of work investigated the role of hERG1's N-terminal regulatory PAS domain in modulating I_{Kr} magnitude, kinetics, and response to external acidosis, as well as the PAS domain's potential as an antiarrhythmic drug target.

First, we found that selectively disabling the hERG1a PAS domain with the PAS-targeting scFv2.10, which disables its interaction with the CNBHD, reduces the incidence of proarrhythmia in hiPSC-CMs derived from a patient with Jervell and Lange-Nielsen syndrome (JLNS) (Chapter 2). scFv2.10 transduction increased I_{Kr} magnitude, shortened APD, reduced AP beat-to-beat variability, and reduced the number of EADs in JLN hiPSC-CMs compared to GFP transduced controls. Notably, the effects on I_{Kr} were exclusive to JLN hiPSC-CMs as scFv2.10 transduction in control hiPSC-CMs had no effect on I_{Kr}. Our data demonstrate that enhancing I_{Kr} by disabling the hERG1a PAS domain may be a viable strategy for treating diseases of cardiac excitability.

Next, we investigated the role of hERG1 subunit abundance in modulating I_{Kr}. We discovered that the relative abundance of hERG1a and hERG1b is dictated by the maturation state of hiPSC-CMs and also modulates I_{Kr} sensitivity to external protons. For both mRNA and protein levels, immature hiPSC-CMs display increased hERG1b and reduced hERG1a, whereas matured hiPSC-CMs display increased hERG1a and reduced hERG1b (Chapter 3). hERG1b is elevated in the developing heart and protons have a greater inhibitory effect on hERG1b relative to hERG1a. In agreement with these findings, we demonstrated that immature hiPSC-CMs are more sensitive to proton block compared to matured hiPSC-CMs and that transforming hERG1b subunits with PAS domain overexpression abolished this effect [94].

hERG1b is upregulated relative to hERG1a during heart failure [157] and selective downregulation of hERG1b is proarrhythmic in healthy hiPSC-CMs [89]. If hERG1b expression is in fact elevated in the infant heart, this would predispose the infant to arrhythmia during respiratory or metabolic acidosis. Given that respiratory acidosis is proposed to be a contributing factor in SIDS, the change in hERG1 subunit abundance could be an underlying trigger of SIDS [187]. In this context, a developing heart would be more susceptible to cardiac acidosis due to increased hERG1b abundance. Additionally, upregulated hERG1b could promote cardiac arrhythmia in the context of heart failure and ischemic heart disease. These findings underscore the critical role of PAS expression, dictated by hERG1 subunit abundance, in hERG1 function and cardiac pathophysiology.

Future Directions

Acute vs. chronic scFv expression

The data in Chapter 2 demonstrates that targeted PAS-disruption by scFv2.10 increases I_{Kr} magnitude and protects against proarrhythmic behavior in JLN hiPSC-CMs. However, the mechanism by which scFv2.10 modulates hERG1 function depends on the expression system and mode of delivery. At room temperature, lentiviral delivery of scFv2.10 accelerates deactivation and reduces tail current density in HEK293 cell stably expressing hERG1a, as was reported by intracellular delivery through the patch pipette [31]. In contrast, transfecting cells with scFv2.10 has no effect on hERG1 gating or current magnitude. It is possible that transient transfection with scFv2.10 does not express sufficient scFv2.10 levels to produce a measurable effect on hERG1 current. Interestingly, whether scFv2.10 is delivered through the recording pipette or a lentivirus, it has no effect on hERG1 current at physiological temperature (Figure 4.1).

To determine how short-term vs. long-term scFv2.10 expression affects the mechanism of scFv2.10-mediated PAS disruption, one could characterize scFv2.12 in HEK 293 cells stably expressing hERG1a and control hiPSC-CMs using transfection and lentiviral delivery. scFv2.12 also binds to and disables the PAS domain but recognizes a epitope distinct from that of scFv2.10. Comparing both delivery methods with scFv2.12 may recapitulate the effects we observed with scFv2.10, where acute expression modifies channel kinetics and chronic expression modifies channel trafficking.

hERG1a/1b assembly is mediated through N-terminal interactions at the transcript and protein levels [185]. scFv2.10 binds the most distal component of the hERG1 N-terminal domain, the PAS cap, and may outcompete hERG1b to associate with hERG1a during transcription and disrupt heteromeric channel assembly. On the other hand, when acutely expressed, scFv2.10 may

only act on channels that are already present at the membrane limiting its effects to channel kinetics.

To test this, one could transduce hiPSC-CMs with scFv2.10 or a GFP control and coimmunoprecipitate *hERG1a* and *hERG1b* transcripts using a hERG1a specific antibody. A hERG1a specific antibody coimmunoprecipitates *hERG1a* and *hERG1b* transcripts when in complex with each other [109, 205]. If scFv2.10 is indeed disrupting *hERG1a/1b* transcript association, we would expect scFv2.10 expression to increase *hERG1a* transcript and reduce *hERG1b* transcript levels when coimmunoprecipitated with hERG1a. Any changes in mRNA can also be quantified using qRT-PCR.

The effects of other scFvs from the source library on hERG1 functions could be characterized as well. It is worth exploring whether CNBHD-targeting scFvs could similarly also disrupt the PAS-CNBHD interaction and enhance I_{Kr} magnitude. The CNBHD could also be an alternative small molecule target. Relatedly, hERG1b-selective scFvs could determine unique contributions of the 1b N-terminus as well. Additionally, scFvs that target binding sites of known small molecule hERG1 activators may be more effective at correcting cardiac repolarization in LQTS, assuming they retain their hERG1 selectivity. One could design and test scFvs that target hERG1 residues 620-640. This region encompasses key molecular determinants of activity of both hERG1 activators and hERG1 blockers and is positioned extracellularly as opposed to the intracellular scfv2.10 epitope (Figure 1.1, Figure 1.2).

hERG1 modulation in HEK293 and hiPSC-CMs

The mechanism of scFv2.10 differed between *in vitro* expression systems. (Figure 4.1). Chronic scFv2.10 expression increased I_{Kr} density and slowed the time course of deactivation in

JLN hiPSC-CMs at 37°C and but had no effect on control hiPSC-CMs. In Chapter 2 we show that scFv2.10 increases hERG1a subunit abundance. In HEK293 cells stably expressing hERG1a, chronic scFv2.10 expression had no effect on hERG1a current at 37°C. At RT, scFv2.10 accelerated gating and reduced steady-state and tail current density (Chapter 2). Of scFv2.10's multiple actions on hERG1 kinetics, accelerating inactivation recovery and increasing hERG1 density at the surface membrane are most functionally important as both increase I_{Kr} during a ventricular action potential.

hiPSC-CMs better recapitulate intact human cardiac physiology than HEK293 cells and highlight the importance of testing biologics across multiple relevant systems. To this end, scFvs must also be tested in a multicellular context such as recording APD from cardiac monolayers using optical mapping (Figure 2.9). To confirm scFv2.10's selectivity, it is imperative to demonstrate that it does not affect other cardiac ion channels. We must also consider that *KCNQ1* knockdown in the JLNS background likely affects the expression and activity of multiple cardiac proteins that may play a role in the mechanism of hERG1 activation.

hERG1b may be involved in scFv2.10-mediated hERG1 activation. To test this one could record hERG1 deactivation in HEK293 cells expressing hERG1a and hERG1b, transduced with scFv2.10 or GFP. We know that, compared to GFP controls, scFv2.10 expression does not alter hERG1 gating at RT or 37°C in HEK 293 cells stably expressing hERG1a. Thus, if we observe a change in the time course of deactivation in HEK 293 cells expressing hERG1a and hERG1b transduced with scFv2.10 compared to GFP controls, this suggests that hERG1b plays an indirect role in scFv2.10's mechanism of action. hERG1 expression at the surface membrane should also be measured in both groups to determine if scFv2.10 differentially impacts hERG1 trafficking compared to GFP controls. scFv2.10 reduces hERG1 current density in HEK 293 cells stably

expressing hERG1a. It would be interesting to see how current density is altered when both hERG1a and hERG1b are expressed.

In this work, the CMV promoter drove scFv2.10 expression and we did not quantitatively measure scFv2.10 expression in our studies. Excess scFv2.10 expression could trigger short QT syndrome and increase the risk for arrhythmia and sudden cardiac death. Thus, it is important to determine a therapeutic index of scFv2.10 prior to leveraging it as a therapeutic. We assume that scFv2.10 and PAS – which were expressed using lentiviral and adenoviruses, respectively, – are in excess (Chapter 2-3). However, we cannot exclude the possibility that maximal expression was not achieved. It may be worth exploring scFv2.10 expression under other promoters such as SV40 which results in more stable transgene expression albeit with lower expression levels than the CMV promoter to determine how different expression levels impact hERG1 current [206].

scFv2.10 as a hERG1 chaperone

Our data suggest that KCNQ1 deficiency is requisite for scFv2.10-dependent increase in hERG1 expression. KCNQ1 knockdown reduces *KCNH2* expression and disrupting KCNQ1 trafficking impairs hERG1 membrane localization. In this context KCNQ1 acts as a hERG1 chaperone. KCNQ1 and hERG1 are proposed to interact via their C-terminal domains which may be regulated by cyclic AMP [112, 169, 207]. In agreement with these studies, we found that I_{Kr} magnitude in JLN hiPSC-CMs is about half that of control hiPSC-CMs (Chapter 2). It is important to note that we did not generate an isogenic control for the JLN hiPSC-CMs given the complexity of the mutation - a premature stop codon in one allele and *exon3* deletion in the other. In this KCNQ1-deficient background, scFv2.10 may act as a substitute chaperone that promotes hERG1 trafficking. This could be tested by expressing KCNQ1 in JLN hiPSC-CMs followed by scFv2.10

transduction. If KCNQ1 overexpression disrupts the ability of scFv2.10 to increase I_{Kr} density, this might suggest that the hERG1a PAS domain is occluded in such a way that scFv2.10 cannot bind to recruit additional channels. There may also be compensatory mechanisms that dictate maximal hERG1 expression at the surface membrane. Alternatively, if disrupting KCNQ1 expression with a KCNQ1 targeting shRNA in control hiPSC-CMs allows for an scFv2.10-mediated increase in I_{Kr} density, this would also support the hypothesis that scFv2.10 is working as a KCNQ1 surrogate chaperone.

scFv2.10 binds to the hERG1 N-terminal PAS-cap domain, but KCNQ1 is reported to exert its chaperone effect through the hERG1 C-terminal domain. It is possible that scFv2.10 binding induces a conformational change that promotes forward hERG1a trafficking, comparable to what might occur when KCNQ1 is present. When KCNQ1 is present, assuming it acts as a hERG1 chaperone, perhaps scFv2.10 is unable to exert its effects. We also cannot rule out the possibility that scFv2.10 does not bind the PAS domain in control hiPSC-CMs as we did not observe any measurable effects of its activity.

hiPSC-CMs cultured on glass have an immature phenotype. Immature cardiomyocytes express elevated levels of hERG1b mRNA and protein. As such, I_{Kr} recorded from immature hiPSC-CMs is more susceptible to proton block. Transducing hERG1a PAS into immature hiPSC-CMs significantly reduced the magnitude of proton block, which demonstrated that the hERG1a PAS domain modulates proton sensitivity. With this in mind, we should test if PAS expression recapitulates the antiarrhythmic effects of scFv2.10 in JLN hiPSC-CMs. If it does, this would suggest that PAS can also act as a chaperone, presumably by converting hERG1b to hERG1a channels and enhancing their trafficking to the surface membrane. Another consideration is that

hERG1 activating therapeutics might be useful in conjunction with hERG1 blocking drugs to mitigate off-target effects from hERG1 block.

Preliminary optical mapping data show that scFv2.1 shortens APD_{80} in control hiPSC-CMs (Figure 2.9). However, these data need to be repeated with appropriate fluorophore tags to reduce signal-to-noise measurements. Additional optical mapping experiments should be done with other hERG1 blockers (E-4031, terfenadine, astemizole, etc.) to determine whether chronic scFv2.10 expression might be ineffective in drug induced LQTS models with no *KCNQ1* deficiency.

hERG1 isoforms

The stoichiometry of heteromeric hERG1 channels remains unknown, but substantial evidence has emerged supporting that the relative abundance of hERG1a to hERG1b is dynamic and changes through development and during chronic cardiac dysfunction [7, 94, 156, 157]. A hERG1a/1b and hERG1b structure would provide important structural insights to develop new hERG1 modulators, especially subunit specific modulators. In some cancers, hERG1b is elevated and proposed to be a potential cancer biomarker [208]. A hERG1b-specific modulator that reduces the relative abundance of hERG1b might be therapeutic in this context. LQTS PAS mutations that cause trafficking defects could be offset with modulators that selectively increase hERG1a trafficking, like scFv2.10.

Preparing for the clinic

To our knowledge, the are no FDA approved scFv therapies whereas there are a plethora of antibody drug conjugates and bispecific antibodies in clinical development. FDA guidelines

typically require biologic candidates to be above 75 kDa for approval. Biologics below this threshold, such as scFvs which are typically ~25 kDa have poor clearance times [209, 210]. This may be why scFv-based therapies have been unsuccessful in clinical development. To stay a few steps ahead, we should consider testing bispecific antibodies and antibody drug conjugates. Perhaps attaching scFv to an antibody or developing a standard monoclonal antibody would increase the chance for scFv entering a clinical pipeline.

Limitations

There are several limitations associated with developing an anti-hERG1 scFv for clinical use. Off-target hERG1 block is a major liability in drug development. Thus, pharmaceutical industries may be hesitant to invest in a hERG1-targeting therapy for arrhythmia. There are at least two FDA approved lentiviral gene therapies, one for Beta thalassemia and one for cerebral adrenoleukodystrophy. Both therapies act by expressing functional polypeptides of the deficient proteins whose absence causes disease. that are essential for hemoglobin development and removal of very long chain fatty acid build up in the brain, respectively. Other viral delivery methods can be explored – such as adeno-associated virus (AAV) or adenovirus – but only a few AV/AAV therapies are FDA approved [211-213]. Another challenge is that scFvs typically have a short-half life that makes them undesirable for clinical use. Immune responses that degrade foreign antibodies and viral vectors is also a concern [209].

Translating hERG1 biophysical properties and the effects of hERG1 modulators across different systems are highly variable. Chapters 2 and 3 demonstrate that hERG1 modulators often do not impact hERG1 currents in HEK293 cells as they do I_{Kr} in hiPSC-CMs. For example, PAS slows hERG1 deactivation in HEK293 cells and this effect is sometimes diminished in hiPSC-

CMs [89, 94, 99]. This is likely a consequence of multifactorial regulation of signaling pathways that are not present in HEK293. Thus, hERG1 modulators may have differing effects *in vivo*. Another important factor is that I_{Kr} in hiPSC-CMs is significantly smaller than hERG1 current in HEK 293 cells, making it more difficult to resolve changes in current kinetics and current density. It is possible that many regulatory elements present in hiPSC-CMs (e.g., auxiliary subunits, secondary messengers, kinases, etc.) enhance or diminish our markers of activity.

Furthermore, hiPSC-CMs are not a complete model of the adult human heart. Although we can promote maturation, ventricular hiPSC-CMs used in this work still showed spontaneous activity and irregular morphology, two definitive markers of immaturity. Additionally, single cell AP data does not fully reflect AP activity in multicellular systems. Cellular diversity of cells throughout the heart are difficult to reproduce in hiPSC-CM derived systems. We did attempt to record AP from JLN cardiac monolayers but were unable to generate enough cells needed for the experiment. Using advanced animal models, such as rabbit, dogs, or guinea pigs, should better recapitulate human cardiac physiology and be a better model to assess the efficacy of scFv2.10 to correcting abnormal cardiac repolarization [214].

Final Remarks

This body of work demonstrates that the PAS domain serves as a master regulator of hERG1 function and could be a promising antiarrhythmic drug target. Disabling the hERG1 PAS domain mitigates disrupted repolarization caused by LQTS1. We also show that the PAS domain diminishes susceptibility to cardiac acidosis. While I propose several follow up studies, the most important work will be to determine how hERG1 modulation translates *in vivo*, elucidate the

molecular mechanisms between acute and chronic expression scFv2.10 delivery, and determine if scFv development is a viable strategy for enhancing selective protein targeting.

References

1. Trudeau, M.C., et al., *HERG, a human inward rectifier in the voltage-gated potassium channel family.* Science, 1995. **269**(5220): p. 92-5.
2. Curran, M.E., et al., *A molecular basis for cardiac arrhythmia: HERG mutations cause long QT syndrome.* Cell, 1995. **80**(5): p. 795-803.
3. Fink, M., et al., *Contributions of HERG K+ current to repolarization of the human ventricular action potential.* Prog Biophys Mol Biol, 2008. **96**(1-3): p. 357-76.
4. Warmke, J.W. and B. Ganetzky, *A family of potassium channel genes related to eag in Drosophila and mammals.* Proc Natl Acad Sci U S A, 1994. **91**(8): p. 3438-42.
5. Sanguinetti, M.C., et al., *A mechanistic link between an inherited and an acquired cardiac arrhythmia: HERG encodes the IKr potassium channel.* Cell, 1995. **81**(2): p. 299-307.
6. Jones, D.K., et al., *Dominant negative consequences of a hERG 1b-specific mutation associated with intrauterine fetal death.* Prog Biophys Mol Biol, 2016. **120**(1-3): p. 67-76.
7. Crotti, L., et al., *Long QT syndrome-associated mutations in intrauterine fetal death.* JAMA, 2013. **309**(14): p. 1473-82.
8. Christiansen, M., et al., *Mutations in the HERG K+-ion channel: a novel link between long QT syndrome and sudden infant death syndrome.* Am J Cardiol, 2005. **95**(3): p. 433-4.
9. Tester, D.J., et al., *Cardiac channel molecular autopsy: insights from 173 consecutive cases of autopsy-negative sudden unexplained death referred for postmortem genetic testing.* Mayo Clin Proc, 2012. **87**(6): p. 524-39.
10. Arnestad, M., et al., *Prevalence of long-QT syndrome gene variants in sudden infant death syndrome.* Circulation, 2007. **115**(3): p. 361-7.
11. Schwartz, P.J., *Stillbirths, sudden infant deaths, and long-QT syndrome: puzzle or mosaic, the pieces of the Jigsaw are being fitted together.* Circulation, 2004. **109**(24): p. 2930-2.
12. Vincent, G.M., J.A. Abildskov, and M.J. Burgess, *Q-T interval syndromes.* Prog Cardiovasc Dis, 1974. **16**(6): p. 523-30.
13. Schwartz, P.J., M. Periti, and A. Malliani, *The long Q-T syndrome.* Am Heart J, 1975. **89**(3): p. 378-90.
14. Schewe, M., et al., *A pharmacological master key mechanism that unlocks the selectivity filter gate in K(+) channels.* Science, 2019. **363**(6429): p. 875-880.
15. Bentzen, B.H., et al., *Pharmacological activation of Kv11.1 in transgenic long QT-1 rabbits.* J Cardiovasc Pharmacol, 2011. **57**(2): p. 223-30.
16. O'Hare, B.J., et al., *Promise and Potential Peril With Lumacaftor for the Trafficking Defective Type 2 Long-QT Syndrome-Causative Variants, p.G604S, p.N633S, and p.R685P, Using Patient-Specific Re-Engineered Cardiomyocytes.* Circ Genom Precis Med, 2020. **13**(5): p. 466-475.
17. Morais Cabral, J.H., et al., *Crystal structure and functional analysis of the HERG potassium channel N terminus: a eukaryotic PAS domain.* Cell, 1998. **95**(5): p. 649-55.
18. Wang, W. and R. MacKinnon, *Cryo-EM Structure of the Open Human Ether-a-go-go-Related K(+) Channel hERG.* Cell, 2017. **169**(3): p. 422-430 e10.
19. Farid, R., et al., *New insights about HERG blockade obtained from protein modeling, potential energy mapping, and docking studies.* Bioorg Med Chem, 2006. **14**(9): p. 3160-73.
20. Masetti, M., A. Cavalli, and M. Recanatini, *Modeling the hERG potassium channel in a phospholipid bilayer: Molecular dynamics and drug docking studies.* J Comput Chem, 2008. **29**(5): p. 795-808.

21. Osterberg, F. and J. Aqvist, *Exploring blocker binding to a homology model of the open hERG K+ channel using docking and molecular dynamics methods.* FEBS Lett, 2005. **579**(13): p. 2939-44.
22. Bari, V., et al., *Time, frequency and information domain analysis of heart period and QT variability in asymptomatic long QT syndrome type 2 patients.* Annu Int Conf IEEE Eng Med Biol Soc, 2015. **2015**: p. 294-7.
23. Spector, P.S., et al., *Fast inactivation causes rectification of the IKr channel.* J Gen Physiol, 1996. **107**(5): p. 611-9.
24. Smith, P.L., T. Baukrowitz, and G. Yellen, *The inward rectification mechanism of the HERG cardiac potassium channel.* Nature, 1996. **379**(6568): p. 833-6.
25. Shi, Y.P., et al., *The hERG channel activator, RPR260243, enhances protective I(Kr) current early in the refractory period reducing arrhythmogenicity in zebrafish hearts.* Am J Physiol Heart Circ Physiol, 2020. **319**(2): p. H251-H261.
26. London, B., et al., *Two isoforms of the mouse ether-a-go-go-related gene coassemble to form channels with properties similar to the rapidly activating component of the cardiac delayed rectifier K+ current.* Circ Res, 1997. **81**(5): p. 870-8.
27. Kupershmidt, S., et al., *A K+ channel splice variant common in human heart lacks a C-terminal domain required for expression of rapidly activating delayed rectifier current.* J Biol Chem, 1998. **273**(42): p. 27231-5.
28. Li, Q., et al., *NMR solution structure of the N-terminal domain of hERG and its interaction with the S4-S5 linker.* Biochem Biophys Res Commun, 2010. **403**(1): p. 126-32.
29. Gustina, A.S. and M.C. Trudeau, *hERG potassium channel gating is mediated by N- and C-terminal region interactions.* J Gen Physiol, 2011. **137**(3): p. 315-25.
30. Moglich, A., R.A. Ayers, and K. Moffat, *Structure and signaling mechanism of Per-ARNT-Sim domains.* Structure, 2009. **17**(10): p. 1282-94.
31. Harley, C.A., et al., *Enhancement of hERG channel activity by scFv antibody fragments targeted to the PAS domain.* Proc Natl Acad Sci U S A, 2016. **113**(35): p. 9916-21.
32. LeesMiller, J.P., et al., *Electrophysiological characterization of an alternatively processed ERG K+ channel in mouse and human hearts.* Circulation Research, 1997. **81**(5): p. 719-726.
33. Sale, H., et al., *Physiological properties of hERG 1a/1b heteromeric currents and a hERG 1b-specific mutation associated with Long-QT syndrome.* Circ Res, 2008. **103**(7): p. e81-95.
34. Hay, M., et al., *Clinical development success rates for investigational drugs.* Nat Biotechnol, 2014. **32**(1): p. 40-51.
35. Dickson, M. and J.P. Gagnon, *Key factors in the rising cost of new drug discovery and development.* Nat Rev Drug Discov, 2004. **3**(5): p. 417-29.
36. Kalyaanamoorthy, S. and K.H. Barakat, *Development of Safe Drugs: The hERG Challenge.* Med Res Rev, 2018. **38**(2): p. 525-555.
37. Hishigaki, H. and S. Kuhara, *hERGAPDbase: a database documenting hERG channel inhibitory potentials and APD-prolongation activities of chemical compounds.* Database (Oxford), 2011. **2011**: p. bar017.
38. Onakpoya, I.J., C.J. Heneghan, and J.K. Aronson, *Post-marketing withdrawal of 462 medicinal products because of adverse drug reactions: a systematic review of the world literature.* BMC Med, 2016. **14**: p. 10.

39. Creanza, T.M., et al., *Structure-Based Prediction of hERG-Related Cardiotoxicity: A Benchmark Study.* J Chem Inf Model, 2021. **61**(9): p. 4758-4770.
40. Meyer, T., et al., *Micro-electrode arrays in cardiac safety pharmacology: a novel tool to study QT interval prolongation.* Drug Saf, 2004. **27**(11): p. 763-72.
41. Asai, T., et al., *Cryo-EM Structure of K(+)-Bound hERG Channel Complexed with the Blocker Astemizole.* Structure, 2021. **29**(3): p. 203-212 e4.
42. Kamiya, K., et al., *Molecular determinants of HERG channel block.* Mol Pharmacol, 2006. **69**(5): p. 1709-16.
43. Perrin, M.J., et al., *Drug binding to the inactivated state is necessary but not sufficient for high-affinity binding to human ether-a-go-go-related gene channels.* Mol Pharmacol, 2008. **74**(5): p. 1443-52.
44. Herzberg, I.M., M.C. Trudeau, and G.A. Robertson, *Transfer of rapid inactivation and sensitivity to the class III antiarrhythmic drug E-4031 from HERG to M-eag channels.* J Physiol, 1998. **511 (Pt 1)**(Pt 1): p. 3-14.
45. Ficker, E., W. Jarolimek, and A.M. Brown, *Molecular determinants of inactivation and dofetilide block in ether a-go-go (EAG) channels and EAG-related K(+) channels.* Mol Pharmacol, 2001. **60**(6): p. 1343-8.
46. Garg, V., F.B. Sachse, and M.C. Sanguinetti, *Tuning of EAG K(+) channel inactivation: molecular determinants of amplification by mutations and a small molecule.* J Gen Physiol, 2012. **140**(3): p. 307-24.
47. Perry, M., et al., *PD-118057 contacts the pore helix of hERG1 channels to attenuate inactivation and enhance K+ conductance.* Proceedings of the National Academy of Sciences of the United States of America, 2009. **106**(47): p. 20075-20080.
48. Zhang, S.T., et al., *Mechanism of block and identification of the verapamil binding domain to HERG potassium channels.* Circulation Research, 1999. **84**(9): p. 989-998.
49. Thurner, P., et al., *Mechanism of hERG channel block by the psychoactive indole alkaloid ibogaine.* J Pharmacol Exp Ther, 2014. **348**(2): p. 346-58.
50. Fernandez, D., et al., *Physicochemical features of the HERG channel drug binding site.* J Biol Chem, 2004. **279**(11): p. 10120-7.
51. Huang, F.D., et al., *Long-QT syndrome-associated missense mutations in the pore helix of the HERG potassium channel.* Circulation, 2001. **104**(9): p. 1071-5.
52. Helliwell, M.V., et al., *Structural implications of hERG K(+) channel block by a high-affinity minimally structured blocker.* J Biol Chem, 2018. **293**(18): p. 7040-7057.
53. Witchel, H.J., et al., *The low-potency, voltage-dependent HERG blocker propafenone - Molecular determinants and drug trapping.* Molecular Pharmacology, 2004. **66**(5): p. 1201-1212.
54. Alexandrou, A.J., et al., *Mechanism of hERG K+ channel blockade by the fluoroquinolone antibiotic moxifloxacin.* British Journal of Pharmacology, 2006. **147**(8): p. 905-916.
55. Choe, H., et al., *A novel hypothesis for the binding mode of HERG channel blockers.* Biochem Biophys Res Commun, 2006. **344**(1): p. 72-8.
56. Imai, Y.N., S. Ryu, and S. Oiki, *Docking model of drug binding to the human ether-a-go-go potassium channel guided by tandem dimer mutant patch-clamp data: a synergic approach.* J Med Chem, 2009. **52**(6): p. 1630-8.
57. Ferrer, T., et al., *The S4-S5 linker directly couples voltage sensor movement to the activation gate in the human ether-a'-go-go-related gene (hERG) K+ channel.* J Biol Chem, 2006. **281**(18): p. 12858-64.

58. Zhou, J., et al., *Novel potent human ether-a-go-go-related gene (hERG) potassium channel enhancers and their in vitro antiarrhythmic activity.* Molecular Pharmacology, 2005. **68**(3): p. 876-884.
59. Mitcheson, J.S. and J.C. Hancox, *Modulation of hERG potassium channels by a novel small molecule activator.* British Journal of Pharmacology, 2017. **174**(20): p. 3669-3671.
60. Mao, H.Y., et al., *Pharmacologic Approach to Defective Protein Trafficking in the E637K-hERG Mutant with PD-118057 and Thapsigargin.* Plos One, 2013. **8**(6).
61. Kamiya, K., et al., *Molecular determinants of hERG channel block by terfenadine and cisapride.* J Pharmacol Sci, 2008. **108**(3): p. 301-7.
62. Asayama, M., et al., *Effects of an hERG activator, ICA-105574, on electrophysiological properties of canine hearts.* J Pharmacol Sci, 2013. **121**(1): p. 1-8.
63. Zangerl-Plessl, E.M., et al., *Toward a Structural View of hERG Activation by the Small-Molecule Activator ICA-105574.* J Chem Inf Model, 2020. **60**(1): p. 360-371.
64. Mannikko, R., et al., *Pharmacological and electrophysiological characterization of AZSMO-23, an activator of the hERG K(+) channel.* Br J Pharmacol, 2015. **172**(12): p. 3112-25.
65. El Harchi, A. and O. Brincourt, *Pharmacological activation of the hERG K(+) channel for the management of the long QT syndrome: A review.* J Arrhythm, 2022. **38**(4): p. 554-569.
66. Abu-Zeitone, A., et al., *Efficacy of different beta-blockers in the treatment of long QT syndrome.* J Am Coll Cardiol, 2014. **64**(13): p. 1352-8.
67. Lewis, A.M., et al., *Mexiletine in human blood and breast milk.* Postgrad Med J, 1981. **57**(671): p. 546-7.
68. Mason, J.W., *A comparison of seven antiarrhythmic drugs in patients with ventricular tachyarrhythmias. Electrophysiologic Study versus Electrocardiographic Monitoring Investigators.* N Engl J Med, 1993. **329**(7): p. 452-8.
69. Schwartz, P.J., et al., *Genotype-phenotype correlation in the long-QT syndrome: gene-specific triggers for life-threatening arrhythmias.* Circulation, 2001. **103**(1): p. 89-95.
70. Zareba, W., et al., *Implantable cardioverter defibrillator in high-risk long QT syndrome patients.* J Cardiovasc Electrophysiol, 2003. **14**(4): p. 337-41.
71. Lu, H.R., et al., *Predicting drug-induced changes in QT interval and arrhythmias: QT-shortening drugs point to gaps in the ICHS7B Guidelines.* British Journal of Pharmacology, 2008. **154**(7): p. 1427-1438.
72. Hansen, R.S., et al., *In vivo effects of the IKr agonist NS3623 on cardiac electrophysiology of the guinea pig.* J Cardiovasc Pharmacol, 2008. **52**(1): p. 35-41.
73. Diness, T.G., et al., *Antiarrhythmic properties of a rapid delayed-rectifier current activator in rabbit models of acquired long QT syndrome.* Cardiovasc Res, 2008. **79**(1): p. 61-9.
74. Choi, S.H., et al., *Ginsenoside Rg3 activates human KCNQ1 K+ channel currents through interacting with the K318 and V319 residues: a role of KCNE1 subunit.* Eur J Pharmacol, 2010. **637**(1-3): p. 138-47.
75. Choi, S.H., et al., *Differential effects of ginsenoside metabolites on HERG k channel currents.* J Ginseng Res, 2011. **35**(2): p. 191-9.
76. Zeng, H.Y., et al., *Mallotoxin is a novel human Ether-a-go-go-related gene (hERG) potassium channel activator.* Journal of Pharmacology and Experimental Therapeutics, 2006. **319**(2): p. 957-962.

77. Cholon, D.M., C.R. Esther, Jr., and M. Gentzsch, *Efficacy of lumacaftor-ivacaftor for the treatment of cystic fibrosis patients homozygous for the F508del-CFTR mutation.* Expert Rev Precis Med Drug Dev, 2016. **1**(3): p. 235-243.
78. Fiedorczuk, K. and J. Chen, *Mechanism of CFTR correction by type I folding correctors.* Cell, 2022. **185**(1): p. 158-168 e11.
79. El Harchi, A. and O. Brincourt, *Pharmacological activation of the hERG K+ channel for the management of the long QT syndrome: A review.* Journal of Arrhythmia, 2022. **38**(4): p. 554-569.
80. Jones, D.K., *Hysteretic hERG channel gating current recorded at physiological temperature.* Sci Rep, 2022. **12**(1): p. 5950.
81. Harley, C.A., et al., *Conformation-sensitive antibody reveals an altered cytosolic PAS/CNBh assembly during hERG channel gating.* Proc Natl Acad Sci U S A, 2021. **118**(44).
82. Jervell, A. and F. Langenielsen, *Congenital Deaf-Mutism, Functional Heart Disease with Prolongation of the Q-T Interval, and Sudden Death.* American Heart Journal, 1957. **54**(1): p. 59-68.
83. Mitcheson, J.S., *Drug binding to HERG channels: evidence for a 'non-aromatic' binding site for fluvoxamine.* Br J Pharmacol, 2003. **139**(5): p. 883-4.
84. Jost, N., et al., *Ionic mechanisms limiting cardiac repolarization reserve in humans compared to dogs.* J Physiol, 2013. **591**(17): p. 4189-206.
85. Wymore, R.S., et al., *Tissue and species distribution of mRNA for the IKr-like K+ channel, erg.* Circ Res, 1997. **80**(2): p. 261-8.
86. Calloe, K., et al., *A dual potassium channel activator improves repolarization reserve and normalizes ventricular action potentials.* Biochem Pharmacol, 2016. **108**: p. 36-46.
87. Jones, E.M., et al., *Cardiac IKr channels minimally comprise hERG 1a and 1b subunits.* J Biol Chem, 2004. **279**(43): p. 44690-4.
88. Lees-Miller, J.P., et al., *Electrophysiological characterization of an alternatively processed ERG K+ channel in mouse and human hearts.* Circ Res, 1997. **81**(5): p. 719-26.
89. Jones, D.K., et al., *hERG 1b is critical for human cardiac repolarization.* Proc Natl Acad Sci U S A, 2014. **111**(50): p. 18073-7.
90. Codding, S.J. and M.C. Trudeau, *The hERG potassium channel intrinsic ligand regulates N- and C-terminal interactions and channel closure.* J Gen Physiol, 2019. **151**(4): p. 478-488.
91. Gianulis, E.C., Q. Liu, and M.C. Trudeau, *Direct interaction of eag domains and cyclic nucleotide-binding homology domains regulate deactivation gating in hERG channels.* J Gen Physiol, 2013. **142**(4): p. 351-66.
92. Wu, J., W.G. Ding, and M. Horie, *Molecular pathogenesis of long QT syndrome type 1.* J Arrhythm, 2016. **32**(5): p. 381-388.
93. Jervell, A. and F. Lange-Nielsen, *Congenital deaf-mutism, functional heart disease with prolongation of the Q-T interval and sudden death.* Am Heart J, 1957. **54**(1): p. 59-68.
94. Ukachukwu, C.U., et al., *hERG1 channel subunit composition mediates proton inhibition of rapid delayed rectifier potassium current (I(Kr)) in cardiomyocytes derived from hiPSCs.* J Biol Chem, 2022: p. 102778.
95. Jain, A., et al., *KCNH2 encodes a nuclear-targeted polypeptide that mediates hERG1 channel gating and expression.* Proc Natl Acad Sci U S A, 2023. **120**(3): p. e2214700120.

96. Ukachukwu, C.U., et al., *hERG1 channel subunit composition mediates proton inhibition of rapid delayed rectifier potassium current (I(Kr)) in cardiomyocytes derived from hiPSCs.* J Biol Chem, 2023. **299**(2): p. 102778.
97. Wu, J., et al., *A trafficking-deficient KCNQ1 mutation, T587M, causes a severe phenotype of long QT syndrome by interfering with intracellular hERG transport.* J Cardiol, 2019. **73**(5): p. 343-350.
98. Trudeau, M.C., et al., *hERG1a N-terminal eag domain-containing polypeptides regulate homomeric hERG1b and heteromeric hERG1a/hERG1b channels: a possible mechanism for long QT syndrome.* J Gen Physiol, 2011. **138**(6): p. 581-92.
99. Gustina, A.S. and M.C. Trudeau, *A recombinant N-terminal domain fully restores deactivation gating in N-truncated and long QT syndrome mutant hERG potassium channels.* Proc Natl Acad Sci U S A, 2009. **106**(31): p. 13082-7.
100. Magyar, J., et al., *Role of gap junction channel in the development of beat-to-beat action potential repolarization variability and arrhythmias.* Curr Pharm Des, 2015. **21**(8): p. 1042-52.
101. January, C.T., V. Chau, and J.C. Makielski, *Triggered activity in the heart: cellular mechanisms of early after-depolarizations.* Eur Heart J, 1991. **12 Suppl F**: p. 4-9.
102. Meng, J., et al., *Compound ICA-105574 prevents arrhythmias induced by cardiac delayed repolarization.* Eur J Pharmacol, 2013. **718**(1-3): p. 87-97.
103. Larsen, A.P., et al., *Pharmacological activation of IKr impairs conduction in guinea pig hearts.* J Cardiovasc Electrophysiol, 2010. **21**(8): p. 923-9.
104. Zeng, H., et al., *Mallotoxin is a novel human ether-a-go-go-related gene (hERG) potassium channel activator.* J Pharmacol Exp Ther, 2006. **319**(2): p. 957-62.
105. Soderback, E., et al., *The redox- and fixed nitrogen-responsive regulatory protein NIFL from Azotobacter vinelandii comprises discrete flavin and nucleotide-binding domains.* Mol Microbiol, 1998. **28**(1): p. 179-92.
106. Huang, Z.J., I. Edery, and M. Rosbash, *PAS is a dimerization domain common to Drosophila period and several transcription factors.* Nature, 1993. **364**(6434): p. 259-62.
107. Nambu, J.R., et al., *The Drosophila single-minded gene encodes a helix-loop-helix protein that acts as a master regulator of CNS midline development.* Cell, 1991. **67**(6): p. 1157-67.
108. Fernandes, A.S., J.H. Morais-Cabral, and C.A. Harley, *Screening for Non-Pore-Binding Modulators of EAG K+ Channels.* J Biomol Screen, 2016. **21**(7): p. 758-65.
109. Phartiyal, P., E.M.C. Jones, and G.A. Robertson, *Heteromeric assembly of human ether-a-go-go-related gene (hERG) 1a/1b channels occurs cotranslationally via N-terminal interactions.* J Biol Chem, 2007. **282**(13): p. 9874-9882.
110. Zhou, Z.F., Q.M. Gong, and C.T. January, *Correction of defective protein trafficking of a mutant HERG potassium channel in human long QT syndrome - Pharmacological and temperature effects.* Journal of Biological Chemistry, 1999. **274**(44): p. 31123-31126.
111. Onohara, T., et al., *Molecular mechanisms underlying the pilsicainide-induced stabilization of hERG proteins in transfected mammalian cells.* J Arrhythm, 2017. **33**(3): p. 226-233.
112. Biliczki, P., et al., *Trafficking-deficient long QT syndrome mutation KCNQ1-T587M confers severe clinical phenotype by impairment of KCNH2 membrane localization: evidence for clinically significant IKr-IKs alpha-subunit interaction.* Heart Rhythm, 2009. **6**(12): p. 1792-801.

113. Locatelli, F., et al., *Betibeglogene Autotemcel Gene Therapy for Non-beta(0)/beta(0) Genotype beta-Thalassemia.* N Engl J Med, 2022. **386**(5): p. 415-427.
114. Thakkar, S., et al., *Affinity improvement of a therapeutic antibody to methamphetamine and amphetamine through structure-based antibody engineering.* Sci Rep, 2014. **4**: p. 3673.
115. Duan, L., et al., *Exosome-mediated delivery of gene vectors for gene therapy.* Nanoscale, 2021. **13**(3): p. 1387-1397.
116. Rybakova, Y., et al., *mRNA Delivery for Therapeutic Anti-HER2 Antibody Expression In Vivo.* Mol Ther, 2019. **27**(8): p. 1415-1423.
117. Schledermann, W., et al., *Modulation of rat erg1, erg2, erg3 and HERG K+ currents by thyrotropin-releasing hormone in anterior pituitary cells via the native signal cascade.* J Physiol, 2001. **532**(Pt 1): p. 143-63.
118. Herron, T.J., et al., *Extracellular Matrix-Mediated Maturation of Human Pluripotent Stem Cell-Derived Cardiac Monolayer Structure and Electrophysiological Function.* Circ Arrhythm Electrophysiol, 2016. **9**(4): p. e003638.
119. Huo, J., et al., *Evaluation of Batch Variations in Induced Pluripotent Stem Cell-Derived Human Cardiomyocytes from 2 Major Suppliers.* Toxicol Sci, 2017. **156**(1): p. 25-38.
120. Rae, J., et al., *Low access resistance perforated patch recordings using amphotericin B.* J Neurosci Methods, 1991. **37**(1): p. 15-26.
121. Miller, T.E., et al., *Recurrent third-trimester fetal loss and maternal mosaicism for long-QT syndrome.* Circulation, 2004. **109**(24): p. 3029-34.
122. Kato, K., et al., *Cardiac channelopathies associated with infantile fatal ventricular arrhythmias: from the cradle to the bench.* J Cardiovasc Electrophysiol, 2014. **25**(1): p. 66-73.
123. Adams, S.M., C.E. Ward, and K.L. Garcia, *Sudden infant death syndrome.* Am Fam Physician, 2015. **91**(11): p. 778-83.
124. Rhodes, T.E., et al., *Cardiac potassium channel dysfunction in sudden infant death syndrome.* J Mol Cell Cardiol, 2008. **44**(3): p. 571-81.
125. Wedekind, H., et al., *Sudden infant death syndrome and long QT syndrome: an epidemiological and genetic study.* Int J Legal Med, 2006. **120**(3): p. 129-37.
126. Tester, D.J. and M.J. Ackerman, *Sudden infant death syndrome: how significant are the cardiac channelopathies?* Cardiovasc Res, 2005. **67**(3): p. 388-96.
127. Schwartz, P.J., et al., *Molecular diagnosis in a child with sudden infant death syndrome.* Lancet, 2001. **358**(9290): p. 1342-3.
128. Jones, E.M.C., et al., *Cardiac IKr Channels Minimally Comprise hERG 1a and 1b Subunits.* Journal of Biological Chemistry, 2004. **279**(43): p. 44690-44694.
129. Pond, A.L., et al., *Expression of distinct ERG proteins in rat, mouse, and human heart. Relation to functional I(Kr) channels.* J Biol Chem, 2000. **275**(8): p. 5997-6006.
130. Anderson, C.L., et al., *Large-scale mutational analysis of Kv11.1 reveals molecular insights into type 2 long QT syndrome.* Nat Commun, 2014. **5**: p. 5535.
131. Sale, H., et al., *Physiological properties of hERG 1a/1b heteromeric currents and a hERG 1b-specific mutation associated with Long-QT syndrome.* Circulation research, 2008. **103**(7): p. e81-e95.
132. Ng, C.A., et al., *The S4-S5 linker acts as a signal integrator for HERG K+ channel activation and deactivation gating.* PLoS One, 2012. **7**(2): p. e31640.

133. Vereecke, J. and E. Carmeliet, *The effect of external pH on the delayed rectifying K+ current in cardiac ventricular myocytes.* Pflugers Arch, 2000. **439**(6): p. 739-51.
134. Benzing, H., G. Gebert, and M. Strohm, *Extracellular acid-base changes in the dog myocardium during hypoxia and local ischemia, measured by means of glass micro-electrodes.* Cardiology, 1971. **56**(1): p. 85-8.
135. Makielski, J.C., *SIDS: genetic and environmental influences may cause arrhythmia in this silent killer.* J Clin Invest, 2006. **116**(2): p. 297-9.
136. Ravindran, C.R., et al., *Intracellular acidosis and pH regulation in central respiratory chemoreceptors.* J Health Care Poor Underserved, 2011. **22**(4 Suppl): p. 174-86.
137. Bett, G.C. and R.L. Rasmusson, *Functionally-distinct proton-binding in HERG suggests the presence of two binding sites.* Cell Biochem Biophys, 2003. **39**(3): p. 183-93.
138. Zhou, Q. and G.C. Bett, *Regulation of the voltage-insensitive step of HERG activation by extracellular pH.* Am J Physiol Heart Circ Physiol, 2010. **298**(6): p. H1710-8.
139. Shi, Y.P., et al., *External protons destabilize the activated voltage sensor in hERG channels.* European Biophysics Journal, 2013. **43**(2-3): p. 59-69.
140. Van Slyke, A.C., et al., *Proton block of the pore underlies the inhibition of hERG cardiac K+ channels during acidosis.* Am J Physiol Cell Physiol, 2012. **302**(12): p. C1797-806.
141. Jiang, M., W. Dun, and G.N. Tseng, *Mechanism for the effects of extracellular acidification on HERG-channel function.* Am J Physiol, 1999. **277**(4): p. H1283-92.
142. Berube, J., M. Chahine, and P. Daleau, *Modulation of HERG potassium channel properties by external pH.* Pflugers Arch, 1999. **438**(3): p. 419-22.
143. Anumonwo, J.M., et al., *Proton and zinc effects on HERG currents.* Biophysical journal, 1999. **77**(1): p. 282-298.
144. Du, C.Y., et al., *Pharmacological inhibition of the hERG potassium channel is modulated by extracellular but not intracellular acidosis.* J Cardiovasc Electrophysiol, 2011. **22**(10): p. 1163-70.
145. Du, C.Y., et al., *Acidosis impairs the protective role of hERG K(+) channels against premature stimulation.* J Cardiovasc Electrophysiol, 2010. **21**(10): p. 1160-9.
146. Lu, Y., et al., *Effects of premature stimulation on HERG K(+) channels.* J Physiol, 2001. **537**(Pt 3): p. 843-51.
147. Wilson, S.L., et al., *Identification of a proton sensor that regulates conductance and open time of single hERG channels.* Sci Rep, 2019. **9**(1): p. 19825.
148. Du, C.Y., et al., *Enhanced inhibitory effect of acidosis on hERG potassium channels that incorporate the hERG1b isoform.* Biochem Biophys Res Commun, 2011. **405**(2): p. 222-7.
149. Larsen, A.P., *Role of ERG1 isoforms in modulation of ERG1 channel trafficking and function.* Pflugers Arch, 2010. **460**(5): p. 803-12.
150. Larsen, A.P. and S.-P. Olesen, *Differential expression of hERG1 channel isoforms reproduces properties of native I(Kr) and modulates cardiac action potential characteristics.* PloS one, 2010. **5**(2): p. e9021-e9021.
151. Luo, X., et al., *Genomic structure, transcriptional control, and tissue distribution of HERG1 and KCNQ1 genes.* Am J Physiol Heart Circ Physiol, 2008. **294**(3): p. H1371-80.
152. McNally, B.A., Z.D. Pendon, and M.C. Trudeau, *hERG1a and hERG1b potassium channel subunits directly interact and preferentially form heteromeric channels.* J Biol Chem, 2017. **292**(52): p. 21548-21557.

153. Perissinotti, L.L., et al., *Determinants of Isoform-Specific Gating Kinetics of hERG1 Channel: Combined Experimental and Simulation Study.* Front Physiol, 2018. **9**: p. 207.
154. Larsen, A.P., et al., *Characterization of hERG1a and hERG1b potassium channels—a possible role for hERG1b in the I Kr current.* Pflügers Archiv - European Journal of Physiology, 2008. **456**(6): p. 1137-1148.
155. Harley, C.A., et al., *Changes in channel trafficking and protein stability caused by LQT2 mutations in the PAS domain of the HERG channel.* PLoS One, 2012. **7**(3): p. e32654.
156. Lees-Miller, J.P., et al., *Selective knockout of mouse ERG1 B potassium channel eliminates I(Kr) in adult ventricular myocytes and elicits episodes of abrupt sinus bradycardia.* Mol Cell Biol, 2003. **23**(6): p. 1856-62.
157. Holzem, K.M., et al., *Reduced response to IKr blockade and altered hERG1a/1b stoichiometry in human heart failure.* J Mol Cell Cardiol, 2016. **96**: p. 82-92.
158. Terai, T., et al., *Effects of External Acidosis on HERG Current Expressed in Xenopus Oocytes.* Journal of Molecular and Cellular Cardiology, 2000. **32**(1): p. 11-21.
159. Jo, S.-H., et al., *Blockade of HERG channels expressed in Xenopus oocytes by external H +.* Pfl�gers Archiv European Journal of Physiology, 1999. **438**(1): p. 23-29.
160. da Rocha, A.M., et al., *hiPSC-CM Monolayer Maturation State Determines Drug Responsiveness in High Throughput Pro-Arrhythmia Screen.* Sci Rep, 2017. **7**(1): p. 13834.
161. Dhahri, W., et al., *In Vitro Matured Human Pluripotent Stem Cell-Derived Cardiomyocytes Form Grafts With Enhanced Structure and Function in Injured Hearts.* Circulation, 2022. **145**(18): p. 1412-1426.
162. Fleet, W.F., et al., *Effect of serial brief ischemic episodes on extracellular K+, pH, and activation in the pig.* Circulation, 1985. **72**(4): p. 922-932.
163. Wang, L. and H.J. Duff, *Identification and characteristics of delayed rectifier K+ current in fetal mouse ventricular myocytes.* Am J Physiol, 1996. **270**(6 Pt 2): p. H2088-93.
164. Wang, L., et al., *Developmental changes in the delayed rectifier K+ channels in mouse heart.* Circ Res, 1996. **79**(1): p. 79-85.
165. Yang, T., D.J. Snyders, and D.M. Roden, *Rapid inactivation determines the rectification and [K+]o dependence of the rapid component of the delayed rectifier K+ current in cardiac cells.* Circ Res, 1997. **80**(6): p. 782-9.
166. Arcangeli, A., et al., *HERG- and IRK-like inward rectifier currents are sequentially expressed during neuronal development of neural crest cells and their derivatives.* Eur J Neurosci, 1997. **9**(12): p. 2596-604.
167. Conti, M., *Targeting K+ channels for cancer therapy.* J Exp Ther Oncol, 2004. **4**(2): p. 161-6.
168. Gianulis, E.C. and M.C. Trudeau, *Rescue of aberrant gating by a genetically encoded PAS (Per-Arnt-Sim) domain in several long QT syndrome mutant human ether-a-go-go-related gene potassium channels.* J Biol Chem, 2011. **286**(25): p. 22160-9.
169. Ehrlich, J.R., et al., *KvLQT1 modulates the distribution and biophysical properties of HERG. A novel alpha-subunit interaction between delayed rectifier currents.* J Biol Chem, 2004. **279**(2): p. 1233-41.
170. Abbott, G.W., X. Xu, and T.K. Roepke, *Impact of ancillary subunits on ventricular repolarization.* J Electrocardiol, 2007. **40**(6 Suppl): p. S42-6.
171. Um, S.Y. and T.V. McDonald, *Differential association between HERG and KCNE1 or KCNE2.* PLoS One, 2007. **2**(9): p. e933.

172. Du, C., et al., *Modification by KCNE1 variants of the hERG potassium channel response to premature stimulation and to pharmacological inhibition.* Physiological reports, 2013. **1**(6): p. e00175-e00175.
173. Komukai, K., et al., *Electrophysiological response of rat ventricular myocytes to acidosis.* Am J Physiol Heart Circ Physiol, 2002. **283**(1): p. H412-22.
174. Shi, Y.P., et al., *Extracellular protons accelerate hERG channel deactivation by destabilizing voltage sensor relaxation.* J Gen Physiol, 2019. **151**(2): p. 231-246.
175. Kazmierczak, M., et al., *External pH modulates EAG superfamily K+ channels through EAG-specific acidic residues in the voltage sensor.* The Journal of general physiology, 2013. **141**(6): p. 721-735.
176. Cordeiro, J.M., et al., *Modulation of I(Kr) inactivation by mutation N588K in KCNH2: a link to arrhythmogenesis in short QT syndrome.* Cardiovasc Res, 2005. **67**(3): p. 498-509.
177. Satler, C.A., et al., *Multiple different missense mutations in the pore region of HERG in patients with long QT syndrome.* Hum Genet, 1998. **102**(3): p. 265-72.
178. McPate, M.J., et al., *The N588K-HERG K+ channel mutation in the 'short QT syndrome': Mechanism of gain-in-function determined at 37°C.* Biochemical and Biophysical Research Communications, 2005. **334**(2): p. 441-449.
179. Tsuji, Y., et al., *Pacing-induced heart failure causes a reduction of delayed rectifier potassium currents along with decreases in calcium and transient outward currents in rabbit ventricle.* Cardiovasc Res, 2000. **48**(2): p. 300-9.
180. Kääb, S., et al., *Ionic mechanism of action potential prolongation in ventricular myocytes from dogs with pacing-induced heart failure.* Circ Res, 1996. **78**(2): p. 262-73.
181. Johnson, E.K., et al., *Differential Expression and Remodeling of Transient Outward Potassium Currents in Human Left Ventricles.* Circ Arrhythm Electrophysiol, 2018. **11**(1): p. e005914.
182. Kääb, S., et al., *Molecular basis of transient outward potassium current downregulation in human heart failure: a decrease in Kv4.3 mRNA correlates with a reduction in current density.* Circulation, 1998. **98**(14): p. 1383-93.
183. Li, G.R., et al., *Ionic current abnormalities associated with prolonged action potentials in cardiomyocytes from diseased human right ventricles.* Heart Rhythm, 2004. **1**(4): p. 460-8.
184. Phartiyal, P., et al., *Endoplasmic reticulum retention and rescue by heteromeric assembly regulate human ERG 1a/1b surface channel composition.* J Biol Chem, 2008. **283**(7): p. 3702-7.
185. Phartiyal, P., E.M. Jones, and G.A. Robertson, *Heteromeric assembly of human ether-a-go-go-related gene (hERG) 1a/1b channels occurs cotranslationally via N-terminal interactions.* J Biol Chem, 2007. **282**(13): p. 9874-82.
186. Gintant, G.A., *Characterization and functional consequences of delayed rectifier current transient in ventricular repolarization.* American Journal of Physiology-Heart and Circulatory Physiology, 2000. **278**(3): p. H806-H817.
187. Kahn, A., et al., *Sudden infant deaths: stress, arousal and SIDS.* Early Hum Dev, 2003. **75 Suppl**: p. S147-66.
188. Ishikawa, S., et al., *Fetal presentation of long QT syndrome--evaluation of prenatal risk factors: a systematic review.* Fetal Diagn Ther, 2013. **33**(1): p. 1-7.
189. Nof, E., et al., *A common single nucleotide polymorphism can exacerbate long-QT type 2 syndrome leading to sudden infant death.* Circ Cardiovasc Genet, 2010. **3**(2): p. 199-206.

190. Bhuiyan, Z.A., et al., *Recurrent intrauterine fetal loss due to near absence of HERG: clinical and functional characterization of a homozygous nonsense HERG Q1070X mutation.* Heart Rhythm, 2008. **5**(4): p. 553-61.
191. Abi-Gerges, N., et al., *hERG subunit composition determines differential drug sensitivity.* British journal of pharmacology, 2011. **164**(2b): p. 419-432.
192. El Harchi A, M.D., Zhang H, Hancox JC. , *Investigation of hERG1b Influence on hERG Channel Pharmacology at Physiological Temperature.* J Pharmacol Pharmacother, 2018. **9**: p. 92-103.
193. Mewe, M., et al., *Modulation of cardiac ERG1 K(+) channels by cGMP signaling.* J Mol Cell Cardiol, 2010. **49**(1): p. 48-57.
194. Loewe, A., et al., *Arrhythmic potency of human ether-a-go-go-related gene mutations L532P and N588K in a computational model of human atrial myocytes.* Europace, 2014. **16**(3): p. 435-43.
195. Krummen, D.E., V. Swarup, and S.M. Narayan, *The role of rotors in atrial fibrillation.* J Thorac Dis, 2015. **7**(2): p. 142-51.
196. Kolbe, K., et al., *Cysteine 723 in the C-linker segment confers oxidative inhibition of hERG1 potassium channels.* J Physiol, 2010. **588**(Pt 16): p. 2999-3009.
197. Crociani, O., et al., *Cell Cycle-dependent Expression of HERG1 and HERG1B Isoforms in Tumor Cells.* Journal of Biological Chemistry, 2003. **278**(5): p. 2947-2955.
198. Pillozzi, S., et al., *Differential expression of hERG1A and hERG1B genes in pediatric acute lymphoblastic leukemia identifies different prognostic subgroups.* Leukemia, 2014. **28**(6): p. 1352-5.
199. Block, T., et al., *Human perinatal stem cell derived extracellular matrix enables rapid maturation of hiPSC-CM structural and functional phenotypes.* Sci Rep, 2020. **10**(1): p. 19071.
200. Ma, J., et al., *High purity human-induced pluripotent stem cell-derived cardiomyocytes: electrophysiological properties of action potentials and ionic currents.* Am J Physiol Heart Circ Physiol, 2011. **301**(5): p. H2006-17.
201. Zhao, Z., et al., *Ion Channel Expression and Characterization in Human Induced Pluripotent Stem Cell-Derived Cardiomyocytes.* Stem Cells Int, 2018. **2018**: p. 6067096.
202. Zhou, Z., et al., *Properties of HERG channels stably expressed in HEK 293 cells studied at physiological temperature.* Biophys J, 1998. **74**(1): p. 230-41.
203. Bett, G.C.L., M. Liu, and R.L. Rasmusson, *Histidine 562 on S5 is a pH Sensor for HERG Gating.* Biophysical Journal, 2011. **100**(3): p. 426a.
204. Shi, Y.P., et al., *External protons destabilize the activated voltage sensor in hERG channels.* Eur Biophys J, 2014. **43**(2-3): p. 59-69.
205. Liu, F., et al., *Cotranslational association of mRNA encoding subunits of heteromeric ion channels.* Proc Natl Acad Sci U S A, 2016. **113**(17): p. 4859-64.
206. Wang, X.Y., et al., *Impact of Different Promoters on Episomal Vectors Harbouring Characteristic Motifs of Matrix Attachment Regions.* Sci Rep, 2016. **6**: p. 26446.
207. Organ-Darling, L.E., et al., *Interactions between hERG and KCNQ1 alpha-subunits are mediated by their COOH termini and modulated by cAMP.* Am J Physiol Heart Circ Physiol, 2013. **304**(4): p. H589-99.
208. Lastraioli, E., et al., *hERG1 behaves as biomarker of progression to adenocarcinoma in Barrett's esophagus and can be exploited for a novel endoscopic surveillance.* Oncotarget, 2016. **7**(37): p. 59535-59547.

209. Ahmad, Z.A., et al., *scFv antibody: principles and clinical application.* Clin Dev Immunol, 2012. **2012**: p. 980250.
210. Winthrop, M.D., et al., *Selection and characterization of anti-MUC-1 scFvs intended for targeted therapy.* Clin Cancer Res, 2003. **9**(10 Pt 2): p. 3845S-53S.
211. Li, C. and R.J. Samulski, *Engineering adeno-associated virus vectors for gene therapy.* Nat Rev Genet, 2020. **21**(4): p. 255-272.
212. Zhang, W.W., et al., *The First Approved Gene Therapy Product for Cancer Ad-p53 (Gendicine): 12 Years in the Clinic.* Hum Gene Ther, 2018. **29**(2): p. 160-179.
213. Ghanaat, M., et al., *Virus against virus: strategies for using adenovirus vectors in the treatment of HPV-induced cervical cancer.* Acta Pharmacol Sin, 2021. **42**(12): p. 1981-1990.
214. Cesarovic, N., et al., *Animals in cardiovascular research.* Eur Heart J, 2020. **41**(2): p. 200-203.